

EFFECTS OF VEHICLE SPEED AND ENGINE LOAD ON DIESEL EXHAUST PARTICULATES

LIM JAEHYUN

**NATIONAL UNIVERSITY OF SINGAPORE
2008**

**EFFECTS OF VEHICLE SPEED AND ENGINE LOAD
ON DIESEL EXHAUST PARTICULATES**

LIM JAEHYUN
(M. ENG., KONKUK UNIVERSITY)

**A THESIS SUBMITTED
FOR THE DEGREE OF DOCTOR OF PHILOSOPHY
DEPARTMENT OF CHEMICAL AND
BIOMOLECULAR ENGINEERING
NATIONAL UNIVERSITY OF SINGAPORE
2008**

ACKNOWLEDGEMENTS

This work was supported by National University of Singapore (grant no.: R-288-000-026-133), the Korean government fellowship program for overseas study (grant no.: 2003-S-20) and Transportation Pollution Research Center (TPRC) at National Institute of Environmental Research (NIER) of Korea Ministry of Environment.

First of all, I would like to give my deepest gratitude to Professor Liya Yu for her brilliant guidance during my graduate studies. God helped me to meet her and then I could have the opportunity to work with her, who introduced me to the fields of aerosol chemistry and diesel combustion. Her advice, critical evaluation, suggestion and open-minded discussion encourage me to pursue excellence, in addition to completing my thesis work.

Moreover, I thank my committee members: Professor Matthias Roth, Professor Neoh Koon Gee, Professor Hidajat Kus and Professor Kawi Sibudjing; they generously shared their knowledge of aerosol chemistry and diesel combustion along with their constructive criticism and comments. I am also indebted to Dr. Iouri Kostetski, who helped me to conduct various measurements of free radicals via electric paramagnetic resonance (EPR).

I would also like to express my appreciation to the other students in Professor Yu's research group (Dr. Yang Liming, Mr. Zhou Hu, Mr. Singh Avinash, Mr. Gao Yonggang, Ms. Pal Amrita and Mr. Balasubramanian Suresh Kumar) for their support,

help and the valuable discussions. In particular, Dr. Yang Liming and his wife always cheered me and stood by my side as friends.

Without the kind help from the people listed below, I will not be able to conduct my experimental work smoothly; my thanks go to Mdm. Li Xiang, Mdm. Susan, Ms. Mary, Dr. Raja, Ms. Choon Yen, Mdm. Fengmei, Mr. Suki, Mr. Sidek, Mdm. Jamie and Mr. Ng.

I also special thank to God and Korean friends in Nasum church and Hwapung church including members of Peace, New Light, Jesus Fragrance and Nest home church, such as Mr. Hong, Mr. Choi, Mr. Soan and Mr. Jung. They always prayed for me and my family with deepest heart. I can not to forget their warm mind and help including love of my Lord.

Last but not the least, I wish to thank Mr. Lee Hahyung and Dr. Lim Cheolsoo, who have shown me what is the real friendship, my parents, younger brother, mother-in-law and brother-in-law including his family for their love, understanding and encouragement. I would like to express the greatest appreciation to my wife and two daughters (Tiffany and Amy), for their patience and love to me which is always making me smile especially even during the hard time of my experimental progress and writing thesis.

TABLE OF CONTENTS

ACKNOWLEDGEMENTS.....	i
TABLE OF CONTENTS.....	iii
SUMMARY.....	vi
LIST OF TABLES.....	xi
LIST OF FIGURES.....	xii
NOMENCLATURE.....	xiv
CHAPTER 1 INTRODUCTION.....	1
1.1 Environmental and Health Effects.....	1
1.2 Diesel Exhaust Particles and Mitigation Strategies.....	4
1.2.1 Concentrations of DEPs.....	4
1.2.2 Metals in DEPs.....	6
1.2.3 Organic compounds in DEPs.....	7
1.3 Objectives.....	9
1.4 Organization.....	10
CHAPTER 2 EXPERIMENTAL.....	11
2.1 Sampling and measurements.....	11
2.2 Total Carbon (TC)/Elemental Carbon (EC) Analyses.....	15
2.3 Analysis of Persistent Free Radicals.....	17
2.4 Analysis of Metal Contents in DEPs.....	17
2.5 Analysis of Organic Compounds in DEPs.....	19

2.6	Analysis of Nitrogen-Containing Compounds in DEPs.....	21
CHAPTER 3	RESULTS AND DISCUSSION.....	23
3.1	Effect of Driving Conditions on Number Concentration, EC, OC and Persistent Free Radicals in DEPs.....	23
3.1.1	Diesel exhaust particulates (DEPs) distribution of 13-mode....	23
3.1.2	Size distribution of DEPs	26
3.1.3	Persistent free radicals and carbon content in DEPs	31
3.1.4	Size segregated EC and OC in DEPs	36
3.2	Effect of Driving Conditions on Metal Contents in DEPs.....	40
3.2.1	Effects of driving conditions, diesel fuel, and lubricants on metals in DEPs	40
3.2.2	Metal contents in size segregated DEPs	44
3.2.3	Comparison of metals-to-iron ratio with other studies	51
3.3	Effect of Driving Conditions on Organic Compounds in DEPs....	54
3.3.1	Effects of driving conditions on identified organic compounds in DEPs	54
3.3.2	Effects of driving conditions on alkanes in DEPs.....	64
3.3.3	Effects of driving conditions on polycyclic aromatic hydrocarbons (PAHs) in DEPs.....	67
3.3.4	Effects of driving conditions on nitrogen-containing polycyclic aromatic compounds (NPACs) in DEPs.....	70
CHAPTER 4	CONCLUSIONS AND FUTURE WORK.....	75
4.1	Conclusions.....	75
4.2	Recommended Further Work.....	82
BIBLIOGRAPHY		84

APPENDICES.....	99
Appendix A.....	99
Appendix B.....	109
Appendix C.....	118
Appendix D.....	119
Appendix E.....	120
Appendix F.....	122
Appendix G.....	125

SUMMARY

Diesel exhaust particles (DEPs) are one of the important airborne pollutants responsible for degrading atmospheric environment and causing adverse health effects, and systematic and characterization of DEPs are needed to comprehensively provide reference of DEP properties (both physical and chemical ones) to evaluate efficiencies of mitigation devices and to explore cost-effective control strategies. Direct contribution of this work to develop cost-effective control strategies is the finding that reducing engine loads can significantly decrease number concentrations, amounts of persistent free radicals and ultrafine-mode metals as well as carbonaceous materials in diesel exhaust particulates. Indirect contribution is providing base knowledge of characteristics of chemical and physical properties of DEPs in order to evaluate efficiencies of aftertreatment devices to be retrofitted in the future. Four driving modes, which consisted of two engine loads (60% and 100%) and two engine speed (1800 and 3000 rpm) and could represent real on-road conditions were examined to characterize how operating speeds and loads of a medium-duty diesel engine affect resultant diesel exhaust particulates (DEPs) in terms of number concentrations (≤ 400 nm), size distribution, persistent free radicals, elemental carbon (EC), organic carbon (OC), metal contents and organic species.

At the medium engine load (60%), DEPs of 40–70 nm exhibited the largest number concentration. DEPs under the full engine load (100%) showed a distinctive bimodal distribution with a large population in 30–50 nm and 100–400 nm. When the

engine load decreased from 100% to the medium level (60%), the significant changes in DEPs include (i) DEPs in ultrafine size (≤ 100 nm) and 100–400 nm decreased for at least 1.4 times ($5.6\text{--}4.0\times 10^8$ #/cm³) and more than 3 times ($2.7\text{--}0.8\times 10^8$ #/cm³), respectively; (ii) persistent free radicals in DEPs were decreased for up to ~30 times ($123\text{--}4\times 10^{16}$ #spin/g); and (iii) both EC and OC in total DEPs were concurrently reduced for around 2 times, from 27.3–13.9 mg/m³ and 17.6–9.2 mg/m³, respectively. Under the full engine load, EC and OC in DEPs smaller than 1 μm consistently peaked at 170–330 nm under an engine speed of 1800 rpm, indicating prominent nucleation during DEP formation. On the other hand, the surge of EC and OC at 94–170 nm under an engine speed of 3000 rpm may reflect dominant cluster-cluster agglomeration and condensation involving existing DEPs. Decreasing the engine load from 100% to 60% reduced EC and OC in DEPs (smaller than 1 μm) for at least 3 times (0.6 down to 0.2 mg/m³) and 2 times (0.4 down to 0.2 mg/m³), respectively.

Eighteen metals in DEPs of 6 size ranges between 34 and 1000 nm were quantified with a total concentration ranging from 6.1–7.7 $\mu\text{g}/\text{m}^3$, which increased with increasing engine speeds or engine loads. Among the four driving conditions, DEPs in ultrafine size (<100 nm) and in accumulation mode carried up to 40% and 76% of the total quantified metals, respectively. An increase in the engine load from 60% to 100% enhanced metal content (from 1.5–3.1 $\mu\text{g}/\text{m}^3$) mainly in ultrafine DEPs and peaked at DEP < 66 nm, while moderately affected metals in accumulation-mode DEPs (by around 10%), suggesting that increasing the engine load may encourage metals to undergo nucleation during combustion. Under the maximum engine load, metal contents showed an opposite trend to EC, providing the first tailpipe evidence

that metals may catalyze oxidation of DEPs during engine operation. Among the identified metals, Fe ($2.3\text{--}3.9\ \mu\text{g}/\text{m}^3$) is the most abundant component ($> 38\%$) followed by Li, Cr, V, and Pb, which could be mainly contributed from diesel fuel and through engine wear. An increase in the engine load enhanced the averaged cumulative fraction of the five most abundant metals (Fe, Li, Cr, V and Pb) in ultrafine DEPs for 1.4–1.9 times, changing from 24–34% (for engine speed of 1800 rpm) and 22–42% (for engine speed of 3000 rpm). A Cr-to-Fe ratio of DEPs, ranging between 0.08–0.29, can be at least 2 times higher than that of gasoline-exhaust particles, suggesting that the Cr-to-Fe ratio can be employed as a fingerprint differentiating diesel- vs. gasoline-origin particulates at locations mainly under traffic influence.

Concentration of the identifiable organic compounds in DEPs ($<1\ \mu\text{m}$) ranged from 12.4 to around $20\ \mu\text{g}/\text{m}^3$, which accounts for 2–10% of the total organic compounds. When the engine speed and load increased from 1800 rpm/60% to 3000 rpm/100%, the fraction of identifiable organic compounds in DEPs ($<1\ \mu\text{m}$) reduced for > 3 times, indicating stronger formation of unresolved organic compounds (such as humic like substances) under more fuel injection, higher combustion temperature and larger pyrolysis zone in diesel engines.

For all four driving conditions, concentration of identifiable organic compounds in DEPs ultrafine (34–94 nm) and accumulation (94–1000 nm) modes ranged from $2.9\text{--}5.7\ \mu\text{g}/\text{m}^3$ and $9.5\text{--}16.4\ \mu\text{g}/\text{m}^3$, respectively; a larger amount (70–83%) of total identifiable organics in DEPs ($<1\ \mu\text{m}$) were allocated in accumulation-mode DEPs.

The identified organic compounds in DEPs (<1 μm) were classified into eleven classes: alkanes, alkenes, alkynes, aromatic hydrocarbons, carboxylic acids, esters, ketones, alcohols, ethers, nitrogen-containing compounds, and sulfur-containing compounds. For all driving conditions, alkane class consistently showed the highest concentration (8.3 $\mu\text{g}/\text{m}^3$ to 18.0 $\mu\text{g}/\text{m}^3$) among the identified organic classes in DEPs, followed by carboxylic acids, esters, ketones and alcohols. The concentration of alkanes also accounted for more than 60% (or up to 95%) of identified organics in DEPs (<1 μm). The amount of alkanes in DEPs (<1 μm) generally peaked between C19–C25. Among the 17 alkane species identified in DEPs (<1 μm), C19 exhibited the highest concentration for all driving conditions, except that with the highest engine speed and load, which peaked at C21.

Twelve polycyclic aromatic hydrocarbons (PAHs) in DEPs (<1 μm) were identified with a total concentration ranging from 37.9–174.8 ng/m^3 . When the engine load increased from 60% to 100%, more than 2 times of increase in the PAHs in DEPs (<1 μm) could result from stronger pyrosynthesis in diesel engines. Similar to the alkane class, quantified PAHs were mainly distributed in the accumulation-mode DEPs; in the ultrafine and accumulation-mode DEPs, the concentration of PAHs ranged from 10.8–23.2 ng/m^3 and 16.3–119.0 ng/m^3 , respectively. When the engine load was increased to the maximum, phenanthrene exhibited the highest concentration along with most substantial increase (up to 10 times). The concurrent increase in elemental carbon (relevant to soot) in DEPs (<1 μm) supports that phenanthrene is an important intermediate for PAHs growth and soot formation

Nine NPACs were identified in DEPs (<1 μm) with a total concentration ranging from 7.0–10.3 ng/m^3 . Similar to the trend in quantified PAHs, the identified NPACs are more abundant in accumulation-mode DEPs of driving conditions, in particular, under the full engine load. The identified NPACs are most abundant (6.4–7.5 ng/m^3) in accumulation-mode DEPs from driving condition under the maximum engine load, which could encourage formation of NPACs through pyrosynthesis of PAHs and NO_x .

The nine identified NPACs comprise four aza arenes and five nitroarenes with a respective concentration of 5.4–7.3 and 1.3–3.1 ng/m^3 . For all driving conditions, 7,8-benzoquinoline (7,8-BQ) showed the highest concentration, 5.1–6.0 ng/m^3 , or 59–72% of the quantified NPACs. The concentration of 7,8-BQ increased with increasing engine loads with the highest concentration under the most demanding driving condition (3000 rpm/100%). 7,8-BQ was responsible for 66 and 63% of quantified NPACs in ultrafine and accumulation mode DEPs, respectively. Since the most abundant PAH (phenanthrene) and NPACs (7,8-benzoquinoline and 3-nitrophenanthrene) comprise a similar molecular (3 aromatic-ring) structure, which could evidence the formation of aza arenes (7,8-benzoquinoline) and nitro-PAHs (3-nitrophenanthrene) through respective pyrosynthesis and nitration between PAHs radicals and NO_x radicals under the highest engine speed and engine load (3000 rpm/100% load).

LIST OF TABLES

Table 3.1	Metal-to-iron ratios of particulates in vehicle emissions	52
Table 3.2	Identifiable organic compounds in ultrafine and accumulation-mode DEPs	57
Table 3.3	Identifiable organic compounds in diesel fuel and lubricant employed in this study	61

LIST OF FIGURES

Fig. 2.1	Driving condition of 13-mode test.	11
Fig. 2.2	Schematic system for DEP monitoring and sampling.	13
Fig. 2.3	Experimental analyses involved for DEP filter samples.	14
Fig. 3.1	Ultrafine number concentration of 13-mode.	23
Fig. 3.2	Number-based size distributions for idling conditions of 13-mode. All data points represent an average of triplicate measurements with a standard deviation of cold idle $(0.13\text{--}205)\times 10^4 \text{ \#/cm}^3$, warm idle-1 $(0.15\text{--}349)\times 10^4 \text{ \#/cm}^3$, and warm-idle-2 $(0.05\text{--}525)\times 10^4 \text{ \#/cm}^3$.	25
Fig. 3.3	Concentrations of exhaust gases (CO, HC, and NO _x) and temperature (corresponding to the secondary y-axis) for individual driving conditions with corresponding fuel-to-air ratio (secondary x-axis). All data points represent an average of four measurements with a standard deviation of CO (2–21) ppm, HC (0.5–24) ppm, NO _x (7–49) ppm and temperature (1–4) °C.	26
Fig. 3.4	Size distribution for individual driving conditions. All data points represent an average of twenty measurements with a standard deviation of (a) $(0.3\text{--}108)\times 10^4 \text{ \#/cm}^3$, (b) $(0.3\text{--}73)\times 10^4 \text{ \#/cm}^3$, (c) $(4\text{--}17)\times 10^4 \text{ \#/cm}^3$, and (d) $(5\text{--}28)\times 10^4 \text{ \#/cm}^3$.	28
Fig. 3.5	Concentrations of persistent free radicals in DEPs of individual driving conditions.	32
Fig. 3.6	Concentration of total DEPs (or total particulate matter, TPM), and EC, OC, and EC-OC ratio (shown in parentheses) in DEPs of individual driving conditions, with corresponding fuel-to-air ratio (the top x-axis). Each data point represents the average of triplicate measurements with corresponding standard deviations of 0.090–0.203 mg/m ³ for OC and 0.090–0.235 mg/m ³ for EC.	34

Fig. 3.7	Size distribution of EC, OC, and EC-OC ratios of DEPs (34–1000 nm). All data points represent an average of triplicate measurements with a standard deviation of <math><0.01\text{--}0.15\text{ mg/m}^3</math> for EC and <math><0.01\text{--}0.11\text{ mg/m}^3</math> for OC.	37
Fig. 3.8	Effect of driving conditions on metal contents in DEPs (34 nm–1 μm).	41
Fig. 3.9	Comparison of metal contents in DEPs (34 nm–1 μm) with diesel fuel and lubricant.	43
Fig. 3.10	Effect of driving conditions on size distribution of metal contents in DEPs.	45
Fig. 3.11	Size distribution of metal contents and elemental carbon in DEPs.	48
Fig. 3.12	Size distribution and cumulative fractions of 9 most abundant metals in DEPs.	50
Fig. 3.13	Effect of driving conditions on identified organic compounds in DEPs (<math><1\ \mu\text{m}</math>).	55
Fig. 3.14	Oxygen-containing and non-oxygen-containing organic compounds in (a) ultrafine DEPs and (b) accumulation-mode DEPs.	58
Fig. 3.15	Identified organic compound classes in DEPs (<math><1\ \mu\text{m}</math>) under four driving conditions. The concentration of non-alkane compound classes corresponds to the secondary y-axis.	60
Fig. 3.16	Identified alkane species in ultrafine and accumulation-mode DEPs.	65
Fig. 3.17	Identified PAHs in ultrafine and accumulation-mode DEPs.	68
Fig. 3.18	Identified NPACs in ultrafine and accumulation-mode DEPs.	71

NOMENCLATURE

Ace	Acenaphthene
Acr	Acridine
Acy	Acenaphthylene
Ag	Silver
Ant	Anthracene
As	Arsenic
BaA	Benzo(a)anthracene
BaP	Benzo(a)pyrene
BbFt	Benzo(b)fluoranthene
Be	Beryllium
BkFt	Benzo(k)fluor
7,8-BQ	7,8-Benzoquinoline
BSTFA	N,O-bis(trimethylsilyl) trifluoroacetamide
CCRT	Catalyzed continuous regeneration trap
Cd	Cadmium
CO	Carbon monoxide
Co	Cobalt
Cr	Chromium
CRT	Continuous regeneration trap
Cry	Chrysene
Cs	Cesium
Cu	Copper
DCM	Dichloromethane
DEPs	Diesel exhaust particles (or particulates)
DPF	Diesel particle filter
DOC	Diesel Oxidation Catalyst
EC	Elemental carbon

EPR	Electron paramagnetic resonance
Fe	Iron
FID	Flame-ionization detector
Flu	Ffluorene
Flt	Fluoranthene
FTA	Fuel-to-air
FT-IR	Fourier transform-infrared
FTP	Federal test procedure
GC-MS	Gas chromatograph- mass spectrometry
HACA	Hydrogen abstraction acetylene addition
HC	Hydrocarbon
ICP-MS	Inductively coupled plasma-mass spectrometry
In	Indium
Li	Lithium
LPI	Low pressure impactor
MDT	Mini dilution tunnel
3-MiQ	3-Methylisoquinoline
Mn	Manganese
Mo	Molybdenum
9-Nant	9-Nitroanthracene
7-NBaA	7-Nitrobenz[a]anthracene
Nbp	4-Nitrobiphenyl
6-NCry	6-Nitrochrysene
Ni	Nickel
NIER	National Institute of Environmental Research
NIST	National Institute of Standards and Technology
NOx	Nitrogen oxides
NPACs	Nitrogen-containing polycyclic aromatic compounds
3-Nphe	3-Nitrophenanthrene
OC	Organic Carbon
OM-OC	Organic mass-to-organic-carbon

PAHs	Polycyclic (or polynuclear) aromatic hydrocarbons
Pb	Lead
1-PD	1-phenyldodecane
Phd	Phenanthridine
Phe	Phenanthrene
Pyr	Pyrene
ROS	Reactive oxygen species
SIM	Selected ion monitoring
Sn	Tin
SMPS	Scanning mobility particle sizer
TC	Total carbon
THF	Tetrahydrofuran
Tl	Thallium
TPM	Total particulate matter
TPRC	Transporation pollution research center
UFPs	Ultrafine particles
ULSD	Ultra Low Sulfur Diesel
V	Vanadium

Chapter 1

INTRODUCTION

1.1 Environmental and Health Effects

The population of on-road diesel-powered vehicles has been increasing substantially in many countries because the higher power output (Dagel and Brady, 1998) and the better fuel economy compared to gasoline-powered cars (Sullivan et al., 2004). In Singapore, the number of on-road diesel-powered vehicles has been substantially increasing during the past 10 years (Singapore Customer Services Division of Land Transport Authority, 2007); the population of on-road diesel cars in 2006 is 63% more than that in 1996, with more than 70% of diesel vehicle serving for shipping goods and other purposes. Interestingly, diesel-powered taxis and buses in Singapore account for 15 and 8%, respectively. Republic of Korea and USA reported more than 62% and 80% increase of registered diesel vehicles during 2000–2006 (Korea Ministry of Environment, 2007) and 2002–2005 (US Diesel Technology Forum, 2006), respectively. For European countries such as France, Italy and Germany, at least 50% of all the produced vehicles during 2005 is diesel-powered (Comité des Constructeurs Français d'Automobiles, 2006).

The increasing numbers of diesel cars in operation receive more concerns on how diesel exhaust particles (DEPs) may adversely affect air quality and human health; in particular, DEPs have been associating with adverse health effects, including

cardiovascular diseases (Hirano et al., 2003), lung cancers (Kagawa, 2002; Sato et al., 2001) and asthma (Nygaard et al., 2005a, 2005b; Kadkhoda et al., 2004; Heo et al., 2001). DEPs can also impede atmospheric visibility (Ying et al., 2004; Litton, 2002) and affect global climate changes (Novakov et al., 2003; Jacobson, 2002). Although advanced technologies can reduce mass concentrations of DEPs, population (numbers) of ultrafine particles (UFPs, below 100 nm) can be consequently increased (Kwon et al., 2003; Kim et al., 2001; Abdul-Khalek et al., 1998). This can be worrisome because a larger population of UFPs provides more surface areas to carry toxic materials, which can cause serious health effects (Donaldson et al., 1998).

Transition metals in airborne particulates collected at urban areas and road sides, upon uptake, can participate in generation of reactive oxygen species (ROS) which can induce DNA damages in human cells and increase inflammation of respiratory systems (Dellinger et al., 2001; Molinelli et al., 2002; Wilson et al., 2002; Lingard et al., 2005). Many anthropogenic sources are responsible for metals in airborne particulates, such as emissions from power plants (Park et al., 2006; Reddy et al., 2005), municipal waste incinerators (Hu et al., 2003), and biomass burning (See et al., 2007; Lala et al., 2005). Of these emission sources, vehicle emission is one of the major contributors (Lin et al., 2005; Lough et al., 2005; Gillies et al., 2001), in particular diesel exhaust particulates (DEPs). For example, DEPs can contain metals, which are 10 times of emissions from coke ovens, or more than 220 folds of pollutants from electrical arc furnaces (Wang et al., 2003). However, regulations controlling metals in DEPs are yet to be established due to the needs of differentiating metals originating from diesel vs. gasoline emissions. This becomes particularly

challenging after the phase-out of leaded gasoline, making lead an ineffective tracer for gasoline exhausts (Zheng et al., 2004).

DEPs, a primary pollutant, can also contain organics causing higher cytotoxicity and oxidative stress than fine particles collected in urban atmospheres (Hirano et al., 2003). Pan et al. (2004) also reported that certain components in DEPs, which are resistant to solvent and acid extraction, could catalyze ROS generation, indicating an inherent toxicity of DEPs. While a higher engine load of diesel trucks appeared to emit more polycyclic aromatic compounds in DEPs causing greater endocrine disruption (Okamura et al., 2004), Shah et al. (2005) reported that around 8–18 times higher n-alkanes and polycyclic aromatic hydrocarbons (PAHs), potential carcinogens, were emitted from heavy-duty diesel engines under creep conditions (heavily congested traffic) than under cruise driving. This demonstrates that driving conditions can substantially affect amounts and compositions of chemicals in DEPs. Nevertheless, unlike emissions of total mass of DEPs and total hydrocarbons, which have been standardized in many countries, more data (such as number concentrations, organic speciation, metals, etc.) are needed to appropriately regulate undesired species in DEPs.

1.2 Diesel Exhaust Particles and Mitigation Strategies

1.2.1 Concentrations of DEPs

To better understand how DEPs may affect air quality, Kittleson et al. (2004) monitored size distribution and number concentrations of DEPs using a mobile emission laboratory traveling along highways, and compared with particle concentrations at residential areas upwind and downwind of the highways. Actual on-road measurements have advantages of monitoring DEPs from various traffic conditions, incorporating a real-world dilution and discriminating proper background interference. While such data improve our understandings of exposure to on-road DEPs, studies on how driving conditions affect DEPs are needed to provide specifications (such as speed limit) for regulation purposes.

A few studies have been devoted to investigate how DEP properties are affected by driving conditions; an increase in diesel engine loads and engine speeds appeared to substantially increase mass and number concentrations of DEPs during tests using a dynamometer and on-road mobile laboratory (Kim et al., 2001; Kittleson et al., 2004). However, based on tests of 11 on-road heavy-duty diesel trucks, changes in engine models substantially affected emission rates (mg/mile) of carbonaceous content in DEPs (Shah et al., 2004), indicating that existing literature data concerning heavy-duty diesel vehicles can be inapplicable to emissions from medium-duty diesel engines. Because on-road medium-duty diesel vehicles are increasingly popular in various countries (KAMA, 2005; U.S. Department of Transportation, 2006; ACEA, 2006), studies systematically characterizing DEPs of medium-duty diesel vehicles are in demand. Although Kleeman et al. (2000) and Schauer et al. (1999) measured

chemical species in DEPs from medium-duty diesel trucks using Federal Test Procedure (FTP), such transient driving conditions insufficiently represent real on-road situations. This is expected because Denis et al. (1994) and Kelly and Groblicki (1993) have shown that FTP tests are mainly for emission tests, while misrepresent actual on-road conditions. While Kwon et al. (2003) and Higgins et al. (2003) reported size distribution of several driving conditions of medium-duty diesel engines operating under constant engine loads, information of chemical composition of DEPs were excluded.

More stringent emission standards have encouraged development of various aftertreatments to reduce DEPs from heavy-duty trucks and buses, while a few challenges remain. Holmén and Ayala (2002) reported that continuous regenerating trap (CRT) reduced total DEP numbers for 10–100 times although optimization of operation procedures and understanding of background interference were needed. Mohr et al. (2006) compared DEPs from diesel powered passenger cars equipped with five different after-treatment systems. They found that although efficient diesel particle filters were capable of lowering DEPs to an amount fewer than emissions of gasoline powered vehicles, after trap regeneration, DEPs was > 10 times higher than before regeneration. This suggests that accumulated soot cakes could enhance DEP filtration efficiencies, which, however, could vary with different driving conditions, leading to inconclusive quantification of overall reduction in DEPs. Following the understanding that CRT can actually increase emissions of ultrafine particles and sulfate at high exhaust temperatures, Grose et al. (2006) provided experimental evidence that sulfate was one of the major chemical components of DEPs in size of

10–560 nm generating from a heavy-duty diesel engine equipped with a CRT and powered by low-sulfur (< 50 ppm) diesel fuel. A recent study reported that a catalyzed CRT (CCRT) could satisfactorily minimize both ultrafine and accumulation mode DEPs down to background level (Kittleson et al., 2006). However, Geller et al. (2006) reported that chemical (redox) activity of DEPs unnecessarily decreased when aftertreatment devices removed substantial amounts of DEPs, suggesting that toxicity of chemical species in DEPs requires independent assessment in detail.

1.2.2 Metals in DEPs

To better understand metals in DEPs, a few tailpipe measurements were conducted. Wang et al. (2003) tested a medium-duty diesel engine operating under a US-transient cycle and cruise conditions of three individual engine speeds; they identified 20 metal species and correlated metal content with engine speeds without consideration of effects of engine loads. On the other hand, by testing more than three engine loadings under a constant maximum engine speed (1800 rpm), metal content in DEPs generally decreased with an increase in engine loads (Dwivedi et al., 2006). While these two studies partially tested effects of engine speeds and engine loads on metal contents in DEPs, cross-comparison among published data is hindered by inconsistent units expression (such as on a basis of air volumes, driving distance, or particulate mass).

Attempts have been given to reduce metals in DEPs. Catalyzed diesel particle filters (DPF) significantly reduced 70–95% of metals (per kilometer driving mileage) from diesel vehicles operating under steady-state or transient-mode driving conditions

(Geller et al., 2006). However, DEPs in ultrafine mode were shown to escape from DPF (Mohr et al., 2006; Kittleson et al., 2006), which may explain why, after DPF, 9 out of 18 measured metals in DEPs showed a concentration comparable to gasoline-powered vehicle exhausts. In fact, the amount of iron, chromium, and titanium in DEPs could be even higher than that in gasoline exhausts (Geller et al., 2006); in particular, iron in DEPs after DPF was still two times higher than that in gasoline exhausts, indicating that additional reduction of metals in DEPs is needed. On the other hand, after replacing 20% of mineral diesel with biodiesel fuel, Dwivedi et al. (2006) reported that emission of Fe, Cr, Ni, Zn, and Mg were actually increased although Cd, Pb, Na, and Ni were less in DEPs, demonstrating that alternative fuels selectively increased emissions of some metals.

1.2.3 Organic compounds in DEPs

Most published studies up to date mainly measured aliphatics and PAHs in DEPs. Riddle et al. (2007) reported that diesel engines under idle or creep operation generate more PAHs in DEPs of 100–320 nm. Shah et al. (2005) also found that emissions of n-alkanes and PAHs in total DEPs from creep operation were at least 13 times higher than that from cruise driving conditions. DEPs, which are smaller than 320 nm and emitted from driving conditions under low engine loads, contained more PAHs of smaller molecular weight, while DEPs of 100–530 nm in emissions under heavier engine loads tend to carry PAHs of larger molecular weight (Zielinska et al., 2004a). Although gasoline-vehicle exhausts contained higher proportions of PAHs of larger molecular weight, and DEPs had more nitro-PAHs (Zielinska et al., 2004b),

differentiating emissions from diesel- vs. gasoline-powered vehicles based on identified PAHs and alkanes remains challenging.

Interestingly, organics containing hydroxyl and/or carbonyl substitutes in DEPs could cause more cytotoxicity, oxidative stress, and inflammatory response than aliphatics and PAHs (Shima et al., 2006; Xia et al., 2004). However, only two studies in published literature identified several carbonyl substituents in DEPs, such as n-alkanoic acids, n-alkenoic acids, benzoic acids, substituted benzaldehydes, polycyclic aromatic ketones and quinones from heavy-duty diesel trucks and n-alkanoic acids, alkanedioic acids, aromatic acids and aromatic ketones from medium-duty diesel trucks (Schauer et al., 1999; Rogge et al., 1993a). Although Shima et al. (2006) and Xia et al. (2004) correlated toxicity with hydroxyl functional groups in DEPs, the structure of the compounds containing hydroxyl substituents in DEPs remains to be identified.

Taken together, both physical (number concentration) and chemical properties (metal and organic composition) in detail of DEPs from different driving conditions are needed as a basis to (1) properly evaluate the efficiencies of any mitigation device, and (2) explore simple and direct approach to mitigate and control toxic emissions from diesel vehicles. In this study, four operation conditions that most frequently occur on roads were selected to evaluate how driving conditions (loads and speeds) could affect number concentrations (≤ 400 nm), size distributions, and size segregation of elemental carbon (EC), organic carbon (OC), metals as well as organic species of DEPs. Since persistent free radicals have been identified in combustion generated particles, and could cause respiratory problems (Cormier et al., 2006;

Dellinger et al., 2001; Squadrito et al., 2001; Valavanidis et al., 2005), effects of engine speeds and engine loads on the generated persistent free radicals were also investigated. To assess the effects of driving conditions, 18 metal species and 11 classes of organic compounds in DEPs were quantified under four driving conditions. Individual metals segregated in six size groups ranging from 34–1000 nm were analyzed. An attempt is also given to explore potential fingerprint based on metals and organics in DEPs to differentiate diesel- vs. gasoline-origin exhaust particulates.

1.3 Objectives

This study aims to characterize in detail how engine speeds and loads of a medium-duty engine affect both physical and chemical properties of DEPs. The specific objectives of this research work are to

- Characterize engine loads and engine speeds on number concentration and size distribution of DEPs;
- Investigate how elemental carbon and organic carbon alter in total concentration and size distribution in DEPs under four driving conditions;
- Examine impacts of engine loads and engine speeds on resultant persistent free radicals in DEPs;
- Correlate engine loads and engine speeds and resultant metals in DEPs as well as soot formation; and
- Identify changes in organic compositions of DEPs resulting from different engine loads and engine speeds.

1.4 Organization

This dissertation consists of four chapters. Following the introduction (Chapter 1), Chapter 2 describes the experimental setup (including monitoring and sampling system), approach, and analysis protocols. The results and discussion (Chapter 3) of this thesis are categorized into three sections: Section 1 examines the effects of driving conditions on number concentrations, and concentration of elemental carbon (EC), organic carbon (OC) as well as persistent free radicals in diesel exhaust particulates (DEPs). Section 2 focuses on the effects of driving conditions on contents and size distribution of metals in DEPs. Section 3 discusses the impacts of driving conditions on identified 11 classes of organic compounds including polycyclic aromatic hydrocarbons (PAHs) and nitrogen-containing polycyclic aromatic compounds (NPACs) in DEPs. Finally, Chapter 4 concludes the overall findings and recommends future studies.

Chapter 2

EXPERIMENTAL

2.1 Sampling and Measurements

DEPs in this study were collected at the Transportation Pollution Research Center (TPRC) of the National Institute of Environmental Research (NIER) in Korea. A medium-duty diesel engine (model: K6, displacement: 6,728 cc, maximum power: 171 Ps/3000 rpm, maximum torque: 44.5 kg-m/1800 rpm, combustion system: direct-injection, DAEWOO Co., Korea), which is equipped in most popular on-road diesel vehicles in Korea, was operated in a 13-mode process (Fig. 2.1) and four steady-state driving conditions using a dynamometer (APA DYNO, AVL Co., Austria).

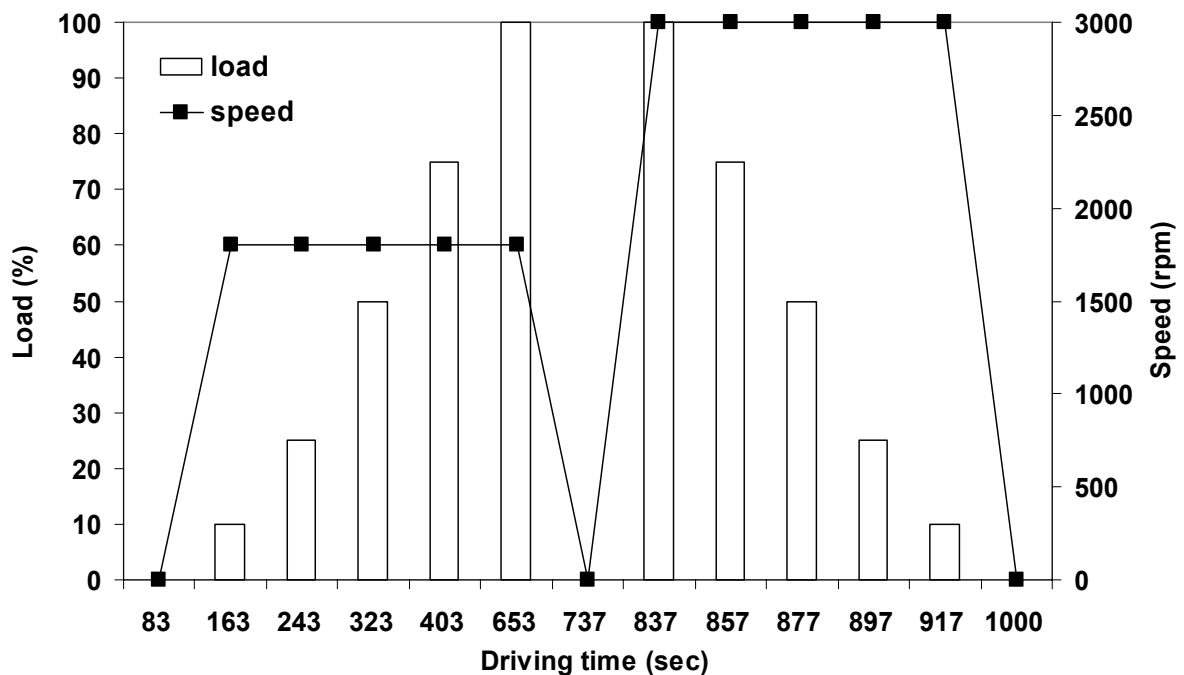


Fig. 2.1 Driving condition of 13-mode test.

By using a dynamometer, the diesel engine was operated following 13 driving conditions, composing of specific engine speed and load in 1000 seconds. Fig. 2.1 shows the 13 individual conditions as a function of elapse time (x-axis) with corresponding engine load (%) and engine speed (rpm) along primary and secondary y-axis, respectively. In detail, Fig. 2.1 shows the individual 13 modes of, in sequential order, (1) cold idle (for 83 seconds), (2) 1800 rpm/10% (for 80 seconds), (3) 1800 rpm/25% (for 80 seconds), (4) 1800 rpm/50% (for 80 seconds), (5) 1800 rpm/75% (for 80 seconds), (6) 1800 rpm/100% (for 250 seconds), (7) warm idle-1 (for 84 seconds), (8) 3000 rpm/100% (for 100 seconds), (9) 3000 rpm/75% (for 20 seconds), (10) 3000 rpm/50% (for 20 seconds), (11) 3000 rpm/25% (for 40 seconds), (12) 3000 rpm/10% (for 20 seconds) and (13) final warm idle-2 (for 83 seconds). The four steady-state driving modes comprised two engine speeds (1800 and 3000 rpm) under either medium (60%) or full (100%) engine load; the four steady-state driving conditions were selected for laboratory investigation in detail because they occurred on-road most frequently (or for longest duration) according to a survey of on-road driving patterns of medium-duty diesel trucks traveling between Seoul and Daejeon city in Korea for 29 trips (Eom et al., 2001). This survey was conducted based on five trips per day from Monday–Friday and two trips per day during Saturday and Sunday to evaluate actual on-road conditions involving high and low traffic. All trips consistently followed the same route of around 80 km, and lasted for more than one hour. Diesel fuel used in this study has an cetane number of 56 with a specific gravity of 830 kg/m³ (15°C), sulfur content of 0.02% (by wt), and 10% distillation residue of 0.01% (by wt). For aging effects of engine on DEPs, it is off concerns because the

mileage of the engine tested in this study was under 80,000 km, which is warranted by the manufacture for negligible deterioration (a common practice and test by vehicle manufactures world wide).

Fig. 2.2 shows schematic setup of sampling system of DEPs, which experienced a residence time of about 3 seconds from the engine outlet to points of monitoring or collection.

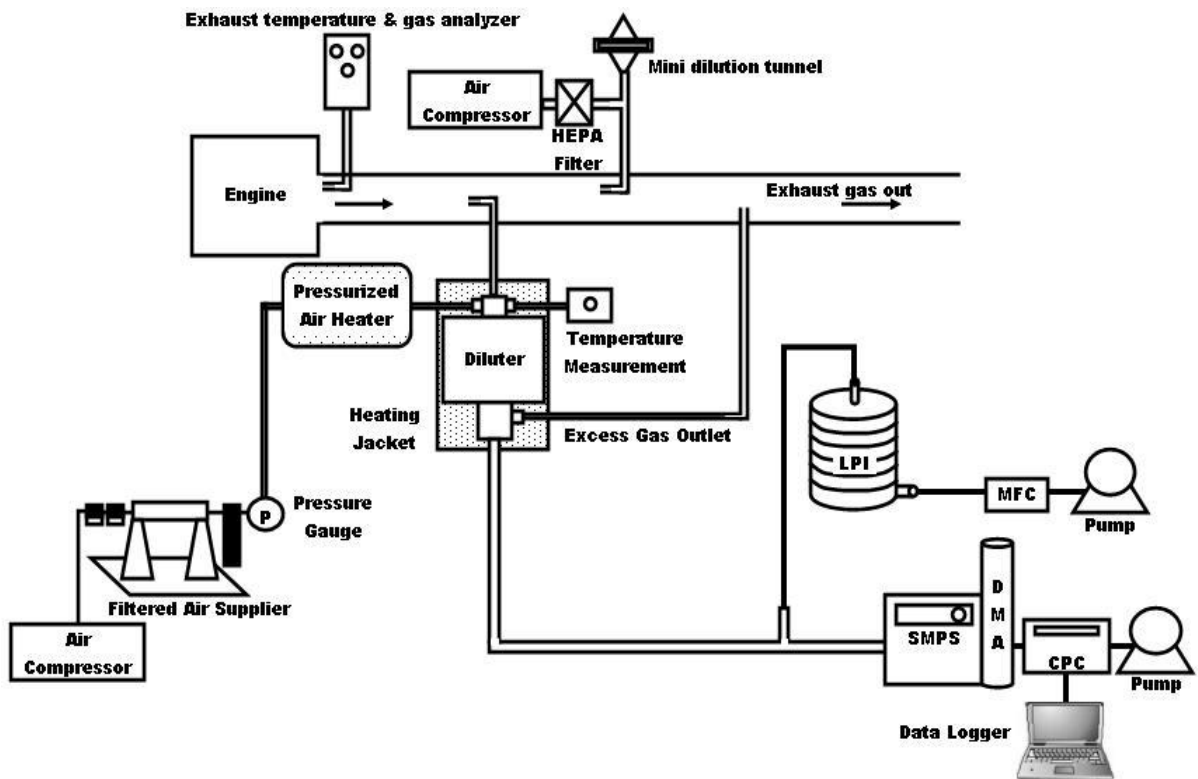
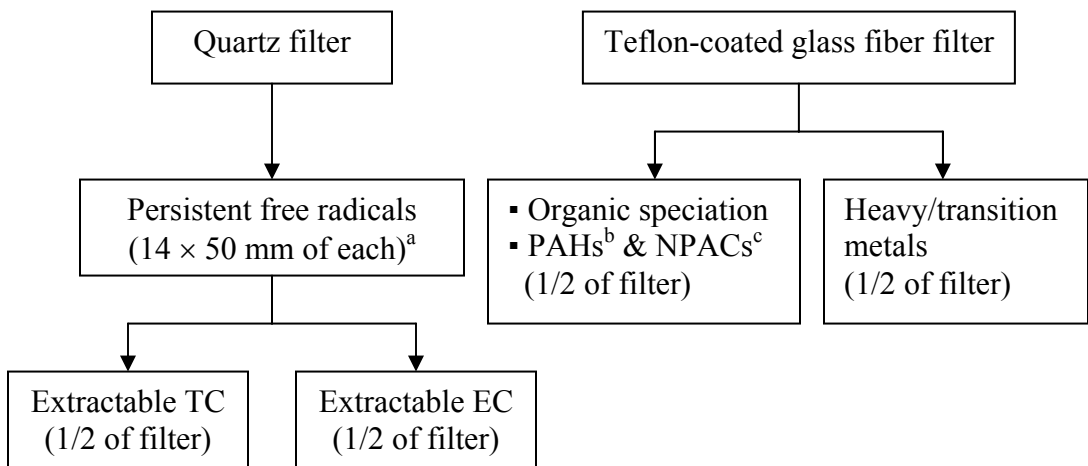


Fig. 2.2 Schematic system for DEP monitoring and sampling.

Fuel-to-air (FTA) ratio, CO, HC, NO_x and exhaust temperatures at the engine outlet were monitored throughout individual driving tests, and showed satisfactory reproducibility with a relative deviation of 0.4–10% (n = 4). For individual driving tests, exhaust stream was, in part, introduced through a mini dilution tunnel (MDT;

SPC 472, AVL Co, Austria) before total particulate matter (TPM) was collected (Fig. 2.2). An additional isokinetic sampling port directed exhaust through an ejector diluter (Dekati Ltd., Tampere, Finland) to monitor size distribution and number concentrations of DEPs using a scanning mobility particle sizer (SMPS; TSI 3936, MN, USA). In parallel, DEPs were collected using a low pressure impactor (LPI), which segregated DEPs into 6 groups with individual cut-off size of 34, 66, 94, 170, 330 and 550 nm for following gravimetric measurements and chemical speciation.

DEPs were collected onto two types of filters, 70-mm quartz filters (Whatman International Ltd., England) and 70-mm Teflon-coated glass fiber filters (Emfab™, Pallflex® , USA). The quartz-filter samples were for non-destructive measurements of persistent free radicals followed by analyses of extractable total carbon (TC) and elemental carbon (EC), while samples collected onto Teflon-coated glass fiber filters were to correct positive artifacts of the quartz filter samples and to analyze organic and metal compositions of DEPs (Fig. 2.3).



^a 14 × 50 mm filter is also used for next extraction step after persistent free radicals measurement

^b Polycyclic Aromatic Hydrocarbons (PAHs)

^c Nitrogen-containing Polycyclic Aromatic Compounds (NPACs)

Fig. 2.3. Experimental analyses involved for DEP filter samples

All filters and glass jars were cleaned prior to collection and storage of DEPs. To minimize background interference, Teflon-coated filters underwent sequential solvent cleaning, and quartz filters were annealed at 700°C for 2 hours prior to DEP sampling. To couple with the LPI, both pre-cleaned quartz filters and Teflon-coated glass-fiber filters were prepared in a “doughnut” shape. To obtain gravimetric data, quartz filters and Teflon-coated glass-fiber filters were weighed in a temperature- and humidity-controlled room ($20 \pm 2^\circ\text{C}$ and $47 \pm 5\%$) before and after DEP sampling. Before chemical analyses, all filter samples, including blank samples, were stored at -25°C under dark.

2.2 Total Carbon (TC)/Elemental Carbon (EC) Analyses

To measure extractable total carbon (TC), half of collected quartz filter samples underwent solvent extraction using tetrahydrofuran (THF) (Merck, Germany) followed by dichloromethane (DCM) (Merck, Germany) and hexane (Merck, Germany). The extracts were then transferred into a pre-cleaned and pre-weighed tin cup to evaporate solvents using a gentle nitrogen flow before CHNS (Perkin Elmer 2400 series II analyzer, Shelton, USA) measurements (Krivácsy et al., 2001). Cystine (Micro Analysis Limited, Devon, UK) was used to establish a calibration curve of carbon analyses. See Appendix B for calibration of total carbon and elemental carbon in detail. Replicate cystine standards were also tested between analyses to ensure accuracy and consistency among tests.

The remaining half of the quartz filter samples was put into a 340°C furnace for two hours to remove organic carbon (OC) before solvent extraction (Cachier et al., 1989). By applying the same CHNS measurements, extractable elemental carbons (EC) of the solvent extracts were obtained. Extractable OC was derived as difference between the extractable TC and EC (Chen et al., 1997).

To correct the organic vapors adsorbed onto the quartz filters, we analyzed mass ratios of total particulate matter (TPM) collected on quartz filters to that on Teflon-coated glass-fiber filters, which were larger than 1, indicating positive artifacts on the quartz filter samples; in particular, DEPs collected under a driving speed of 1800 rpm adsorbed 15–25% more materials (positive artifact) than that under an engine speed of 3000 rpm. To correct the positive artifact, organic carbon (OC) resulting from artifacts (additional organic vapors adsorbed onto the quartz filters) was estimated based on mass difference between quartz-filter samples and corresponding Teflon-coated glass-fiber filter samples, coupled with an organic-mass-to-organic-carbon (OM-OC) ratio of 1.2. Since volatile and semi-volatile organics in diesel exhausts contributing to artifacts were mostly composed of hydrocarbons such as alkanes (Tobias et al., 2001), adopting an OM-OC of 1.2 can reasonably correct overestimated OC. All discussions in following sections are based on corrected data.

2.3 Analysis of Persistent Free Radicals

Two pieces of samples (7×25 mm) were cut from each quartz filter, weighed, and placed on a standard Wilmad cell (Willmad Glass, NJ, USA) for free radical measurements via electron paramagnetic resonance (EPR). A Bruker Eleksys E500 spectrometer (Bruker Biospin GMBH, Germany) coupled with a rectangular (TE102) Super X cavity was operated at room temperature with a center field at 3497.6 G, and a field scan width at 110 G. Each scan lasted for 40 seconds using a microwave frequency at 9.80985 GHz coupled with a field modulation frequency and amplitude of 100 KHz and 3 G, respectively. The spin concentration was quantified along with a Mn^{2+} : MgO standard sample.

2.4 Analysis of Metal Contents in DEPs

Standard gold was selected as an ideal internal standard to monitor recovery of metal content throughout experiments because it is unlikely found in DEPs. Based on more than 30 tests, the metal analysis in this study rendered an averaged recovery efficiency of $88.5 \pm 3.5\%$. Prior to conducting microwave-assisted extraction via a digestion system (Milestone, Leutkirch, Germany), 200- μL standard gold solution in a concentration of 1 mg/L (Merck, Germany) was evenly spiked onto individual samples (including blank) followed by adding 1.5 mL of ultra-pure water, 2.0 mL of 69.5% HNO_3 (Fluka, Switzerland), and 1.5 mL of 30% H_2O_2 (Merck, Germany). To minimize undesired contaminants, before any usage, all apparatus were cleaned by soaking in 1% HNO_3 for 24 h, followed by rinsing with ultra-pure water three times.

To measure trace metals using an inductively coupled plasma-mass spectrometry (ICP-MS, Perkin Elmer, USA), aliquots of the digested solutions were further diluted to 20 mL using ultra-pure water. To identify and quantify metals in individual samples, triplicate measurements were obtained. Normal operating plasma in a dual detector mode (analog and pulse counts) was employed, while a cold plasma coupled with a pulse detector mode was adopted to measure iron content, least amounts of iron in samples were overestimated due to background ($40\text{Ar}^{16}\text{O}^+$) interference (Yang et al., 2007). Calibration curves of 18 standard metals, including silver (Ag), arsenic (As), beryllium(Be), cadmium (Cd), cobalt (Co), chromium (Cr), cesium (Cs), copper (Cu), iron (Fe), indium (In), lithium (Li), manganese (Mn), molybdenum (Mo), nickel (Ni), lead (Pb), tin (Sn), thallium (Tl) and vanadium (V), were established using ICP-multi element standard solutions VI (1000 mg/L, Merck, Germany) and individual standard solutions (1000 mg/L, Merck, Germany) in five concentrations (1, 10, 20, 50 and 100 $\mu\text{g/L}$) for quantification of metals in the DEPs samples. See Appendix B for calibration information of 18 metals in detail.

2.5 Analysis of Organic Compounds in DEPs

To monitor procedural loss of non-polar and polar compounds, two internal standards, perdeuterated tetracosane ($C_{24}D_{50}$, 31.25 μg) (Aldrich, USA) and perdeuterated succinic acid ($C_4D_6O_4$, 26.25 μg) (Cambridge Isotope Lab. Inc., USA) were spiked onto filter samples prior to solvent extraction. All filter samples were extracted successively using three types of solvents in the order of tetrahydrofuran (THF, 99.9%) (Merck, Germany), dichloromethane (99.8%, Merck, Germany), and hexane (98.5%, Merck, Germany). Each solvent ultrasonication lasted for 10 minutes. All the solvent extract was filtered through annealed quartz filters (Whatman QM-A, Whatman International Ltd., UK) and concentrated down to 0.5 mL using a TurboVap II workstation (Zymark Co., USA). Each extract was then transferred into a cleaned 2-mL vial and further dried using a microconcentrator (Pierce Inc., USA) then re-dissolved in THF up to 20 μL . All extracted samples were stored in a freezer (-25°C) in dark before following chemical analyses.

To successfully resolve polar compounds via a gas chromatograph coupled with mass spectrometer (GC-MS; Agilent Technologies, CA, USA), silylation was adopted to replace acidic hydrogens with non-polar trimethylsilyl groups. 10 μL of concentrated extracts was transferred into a 2-mL vial before 4- μL of N,O-bis(trimethylsilyl) trifluoroacetamide (BSTFA, Pierce, USA; 1% of trimethylsilyl) was added. After 20 to 30 min, 1–2 μL of derivatized extract was injected into GC-MS. 1-phenyldodecane (1-PD, 51.4 $\mu\text{g}/\text{mL}$ THF) (Aldrich, USA) was used as the co-injection standard to correct injection loss and to account for deviating performance of GC-MS. A GC-MS HP-5MS column (5% phenyl-methylpolysiloxane capillary

column of 30 m × 0.25 mm i.d. × 0.25 μm, Agilent Technologies, CA, USA) directed helium as carrier gas at a flow rate of 1 mL/min undergoing an initial temperature of 60°C for 3 min before an increase to 280°C at a rate of 8°C/min. Final oven temperature of 280°C was held for 15 min (Yang et al., 2007).

Individual compounds were identified based on spectrum reference provided by the National Institute of Standards and Technology (NIST) mass spectral library, or confirmed by comparing with mass fragmentation patterns and the elution time of authentic standards. Identified compounds were classified into two categories: (1) positive identification, when a compound was confirmed with authentic standards, or showed a mass spectrum matching against the library database for ≥ 70%, and (2) probable identification, when compounds showed a mass spectrum against library database between 50% and 70%. Identifiable compounds were quantified taking into account the response of co-injection standard (1-PD) and extraction recovery efficiencies, resulting in propagated errors of 7–13%. Blank analyses were conducted to examine background interference. To enhance detection sensitivity of polycyclic aromatic hydrocarbons (PAHs) in extracts, selected ion monitoring (SIM) was employed for separated GC-MS analyses, and were identified against a suite of 16 priority PAH standards (Supelco, PA, USA), which are recommended by US EPA.

2.6 Analysis of Nitrogen-Containing Compounds in DEPs

Nitrogen-containing organic compounds were separated using a HP-5MS capillary column in a GC (Shimadzu, Japan) equipped with dual detectors, flame-ionization detector (FID, Shimadzu, Japan) and chemiluminescence detector (Antek Inc., TX, USA). While adopting a temperature program same as the GC-MS measurements, the carrier gas, helium, was set at a constant flow rate of 3 mL/min. At the end of separation column, sample stream was introduced to a 10:1 split adaptor leading to FID and chemiluminescence detectors, respectively.

The chemiluminescence detector was operated at 950°C to pyrolyze samples, and ozone was generated to catalyze nitrogen-containing components to nitrogen dioxide at an excited state. When the excited nitrogen dioxide returned to ground state, chemiluminescence was released and recorded to quantify the amount of nitrogen-containing compounds (Yu et al., 1999).

Similar to the abovementioned approach of quality assurance for GC-MS measurements, each sample was co-injected with 1-PD (51.4 µg/mL, Aldrich, USA) and 50.0 µg/mL of N-nitrosodiphenylamine-d₆ (C₁₂H₄D₆N₂O, Cambridge Isotope Lab. Inc., USA) to monitor performance of flame-ionization and chemiluminescence detectors, respectively. To account for procedural loss, additional internal standards, 1,10-phenanthroline-d₈ (C₁₂D₈N₂, Aldrich, USA, 50.0 µg), perdeuterated tetracosane and perdeuterated succinic acid were spiked onto filter samples prior to solvent extraction. Calibration curves of 20 standard nitrogen-containing compounds in five concentrations were established to quantify detected nitrogen-containing compounds.

For calibration of 20 nitrogen-containing compounds, see Appendix B. The 20 standards were injected individually for five times (total 100 injections) and the injection of standard mixtures composed of these 20 standards were repeated 8 times to assess the reproducibility of elution behavior of these nitrogen-containing organic compounds. Each nitrogen-containing compound, whether injected individually or as a part of standard mixtures, exhibited an elution time satisfactorily consistent with a deviation of 0.004–0.021 seconds. Among the standard compounds tested, since the shortest time between the elution of any two standard compounds is at least 0.1 sec, much larger than the deviation of elution time of a single compound, identification of individual NPAC based on their GC elution behaviors can be acceptable. For every batch (day) analysis, an injection of the standard mixture was conducted before and after the analysis of actual samples to monitor how the instrument performs differently. Among the injections of 24 DEP samples, the largest difference between the eluted compounds and its presumably corresponding standard compounds is 0.092 second. In other words, any isomers or unknown NPAC eluted within 0.092 second may be inaccurately identified. To take into account the influence of instrument performance on elution behavior, for each batch of injection, calibration curves were established individually.

Chapter 3

RESULTS AND DISCUSSION

3.1 Effect of Driving Conditions on Number Concentration, EC, OC and Persistent Free Radicals in DEPs

3.1.1 Diesel exhaust particulates (DEPs) distribution of 13-mode

Following the standard 13-mode driving program, Fig. 3.1 shows the concentration of ultrafine DEPs (≤ 100 nm) for individual conditions, which, in the sequential order, are cold idle, 1800 rpm/10%, 1800 rpm/25%, 1800 rpm/50%, 1800 rpm/75%, 1800 rpm/100%, warm idle-1, 3000 rpm/100%, 3000 rpm/75%, 3000 rpm/50%, 3000 rpm/25%, 3000 rpm/10% and warm idle-2. These individual driving conditions are also labeled in the x-axis of Fig. 3.1 accordingly.

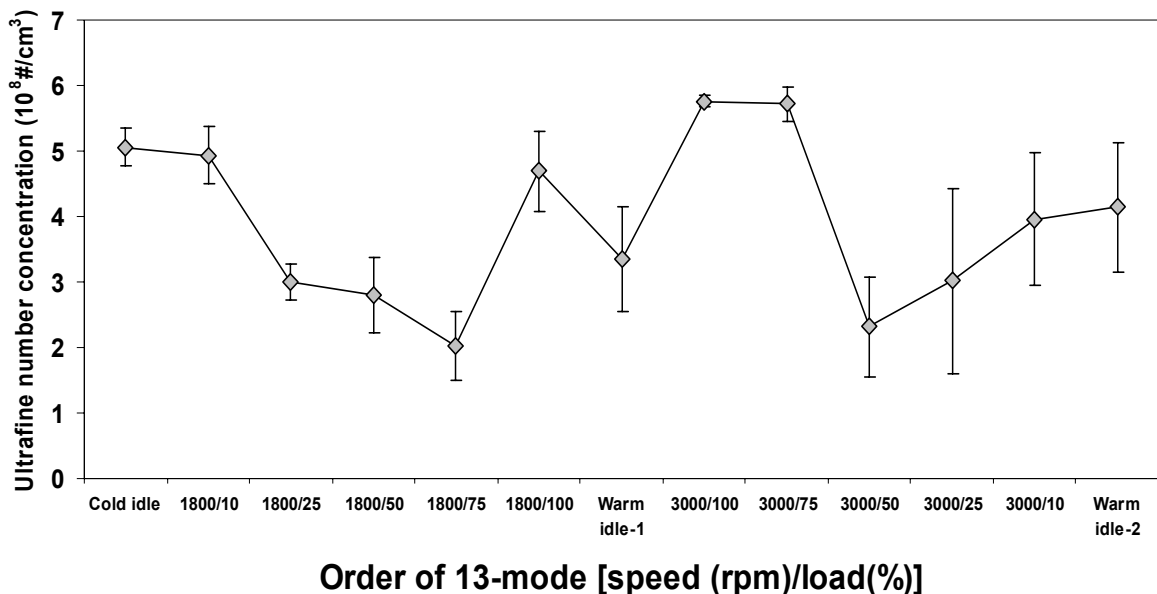


Fig. 3.1 Ultrafine number concentration of 13-mode.

It is interesting to note that under the three idling conditions, 99% of the DEPs were emitted in the ultrafine size. Among the three idle conditions, the cold idle emitted the largest amount of DEPs ($5.06 \times 10^8 \text{ \#/cm}^3$) followed by the warm idle-2 (the last testing stage, Fig. 3.1), which had a lower exhaust temperature than the 1st warm idle condition (warm idle-1, Fig. 3.1). It is expected that the warm idle-1, which had the highest exhaust temperature (156°C), generated the least ultrafine particles (UFPs) among the three idling conditions because a higher combustion temperature during idling tends to encourage the formation of smaller UFPs through homogeneous nucleation and condensation of organic vapor (Kwon et al., 2003). Although all the three idle conditions generated DEPs predominately with a size below 50 nm, the size distribution of UFPs appeared to depend on the exhaust temperatures; the peak size of the UFPs decreased from 30 nm for cold idle with an exhaust temperature of 70°C to 24 nm for the 2nd warm idle (with an exhaust temperature of 108°C), and concentrated at 20 nm for the 1st warm idle which had the highest exhaust temperature (156°C) (Fig. 3.2), agreeing with the observations of Kwon research group that an increase in the idling temperature generated smaller UFPs because of less condensation of organic vapor. Data of non-idling conditions of the 13-mode are available in Appendix G. Fig. 3.1 shows that among the non-idle conditions, the concentration trend in the UFPs emitted during both driving cycles with an engine speed of 1800 or 3000 rpm appeared to generally follow a “v” shape with the smallest concentration occurred at 1800 rpm/75% and 3000 rpm/50%, while a larger UFP concentration was observed at the highest and lowest engine loads. In the case of highest (100%) engine load, a larger pyrolysis zone and higher

combustion temperature in engine cylinders substantially promote homogeneous nucleation and condensation, contributing to an increase in UFP and larger size (>100 nm) particles (Puri, 1993; Someya, 1993).

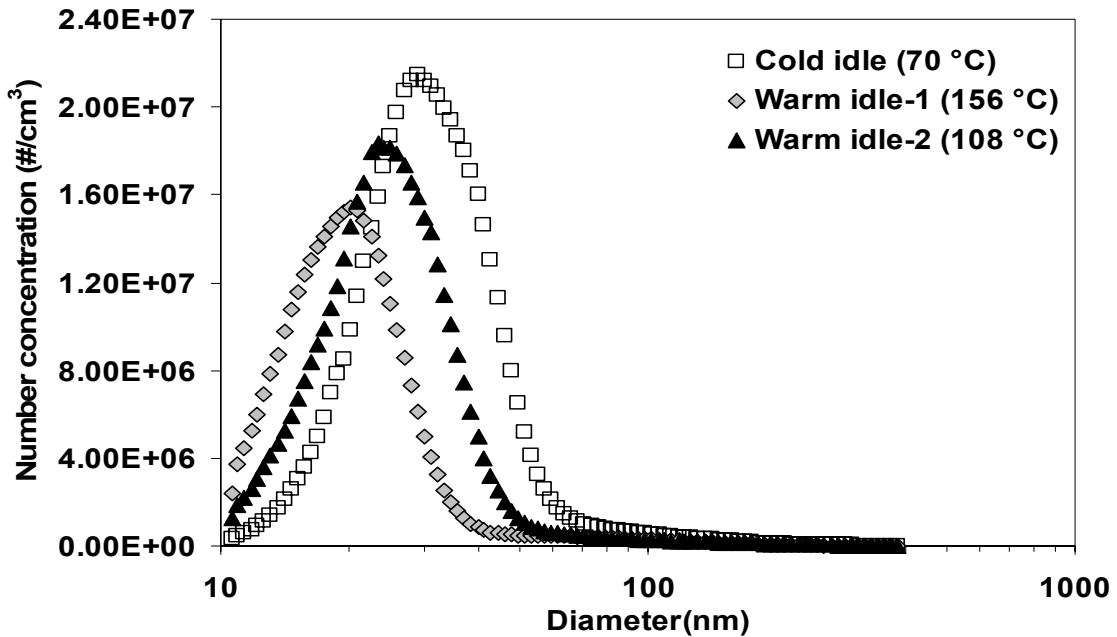


Fig. 3.2 Number-based size distributions for idling conditions of 13-mode. All data points represent an average of triplicate measurements with a standard deviation of cold idle $(0.13\text{--}205)\times 10^4 \text{ #/cm}^3$, warm idle-1 $(0.15\text{--}349)\times 10^4 \text{ #/cm}^3$, and warm-idle-2 $(0.05\text{--}525)\times 10^4 \text{ #/cm}^3$.

However, at the lowest engine load (idle condition), 99% of particulates were emitted in the UFP size due to oxygenated hydrocarbons which could act as nucleation materials of volatile UFPs. These oxygenated hydrocarbons are generated by the partial oxidation of diesel fuel within the engine cylinder under such a low engine load (Inoue et al., 2006). Since the most frequent on-road driving conditions (excluding the idle conditions) occurred with an engine load between 50% and 100% for an engine speed of 1800 or 3000 rpm (Eom et al., 2001), a highest and a medium engine loadings (100 and 60%) could be appropriate to characterize the emitted

particulates. Nevertheless, since the 13-mode test is intended for regulating exhaust emissions, this test insufficiently represents the on-road driving patterns. The subsequent tests and characterization focused on specific driving conditions, which occurred on-road most frequently.

3.1.2 Size distribution of DEPs

Fig. 3.3 shows the concentration of three exhaust gases (CO, NO_x, HC), exhaust temperature (secondary y-axis), and FTA ratio (secondary x-axis) for the four driving conditions.

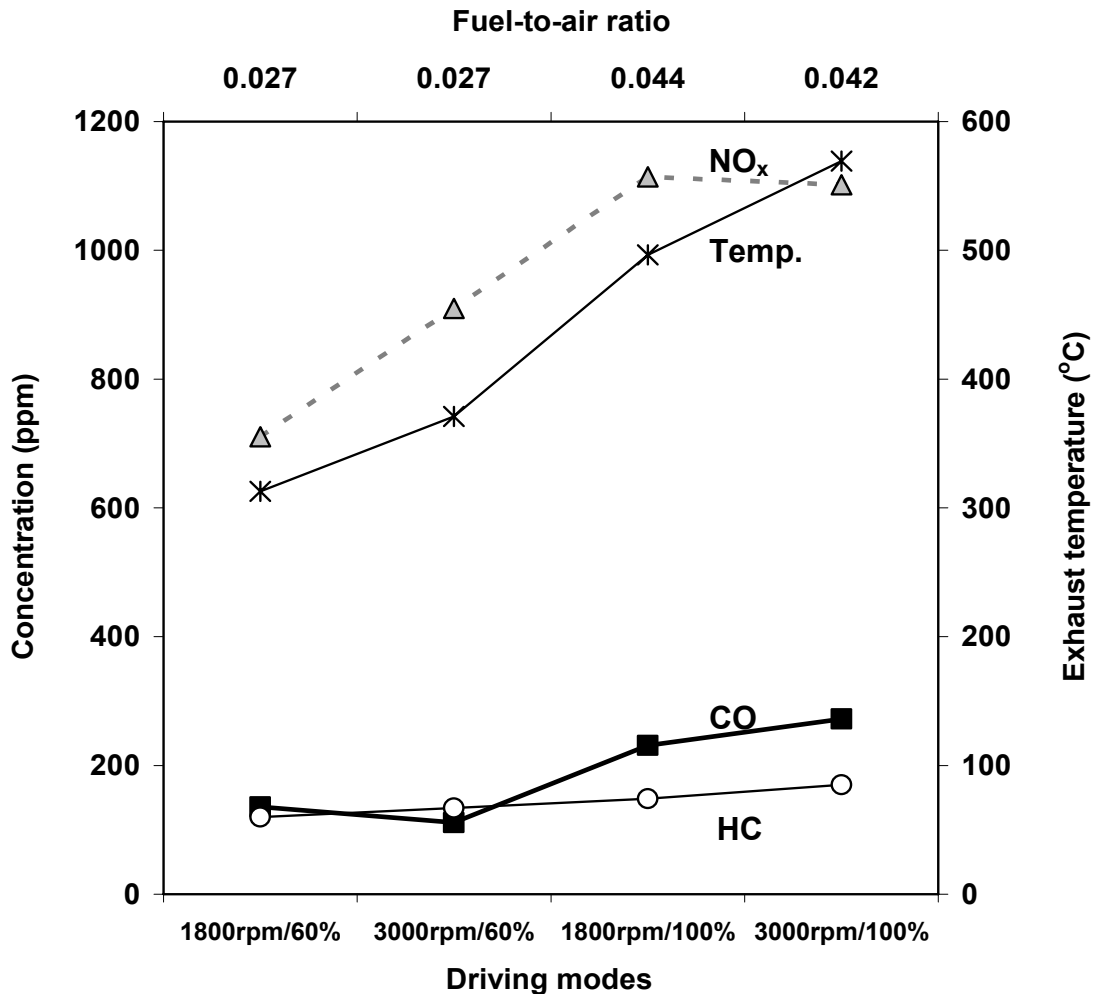


Fig. 3.3 Concentrations of exhaust gases (CO, HC, and NO_x) and temperature (corresponding to the secondary y-axis) for individual driving conditions with corresponding fuel-to-air ratio (secondary x-axis). All data points represent an average of four measurements with a standard deviation of CO (2–21) ppm, HC (0.5–24) ppm, NO_x (7–49) ppm and temperature (1–4) °C.

Compared to the driving modes with the medium engine load (60%), more CO, HC, and NO_x, along with a higher exhaust temperature (> 400°C) were emitted from the full engine load (100%). An increase in engine loads and FTA ratio tend to require stronger horse power (Dagel and Brady, 1998; Henein, 1976), which is generated from higher fuel injection pressure (Assanis et al., 2003) accompanied with a larger pyrolysis zone in combustion cylinders. This results in less complete combustion (a larger amount of CO) with higher HC, NO_x, and exhaust temperatures (Puri, 1993; Kamimoto and Kobayashi, 1991; Henein et al., 1976). Diesel engines have much higher compression ratios (15~22:1), compression pressures (30~45 kgf/cm²) and compression temperature (500~550°C) with large amount of excess oxygen than corresponding in-cylinder conditions of gasoline engines (7~11:1, 7~11 kgf/cm², and 120~140 °C). Since NO_x emissions increase mainly because of high combustion temperature, it is expected that diesel exhausts should contain higher NO_x. A larger pyrolysis zone in diesel cylinders under a full engine load could also lead to more prominent nucleation and condensation (Puri, 1993; Someya, 1993; Bockhorn, 1994). This may explain that, unlike DEPs from the medium-load operation which showed number concentrations surging at around 40–70 nm (Fig. 3.4(a) & (b)), DEPs under the full engine load (100%) exhibited distinctive bimodal distribution with a larger population in size 30–50 nm and 100–400 nm (Fig. 3.4(c) & (d)). The population of ultrafine particles (UFPs) peaked at size smaller than 50 nm indicates substantial homogeneous nucleation (Kwon et al., 2003), and the second peak between 100–400 nm could be mainly attributed to growth of DEPs through condensation.

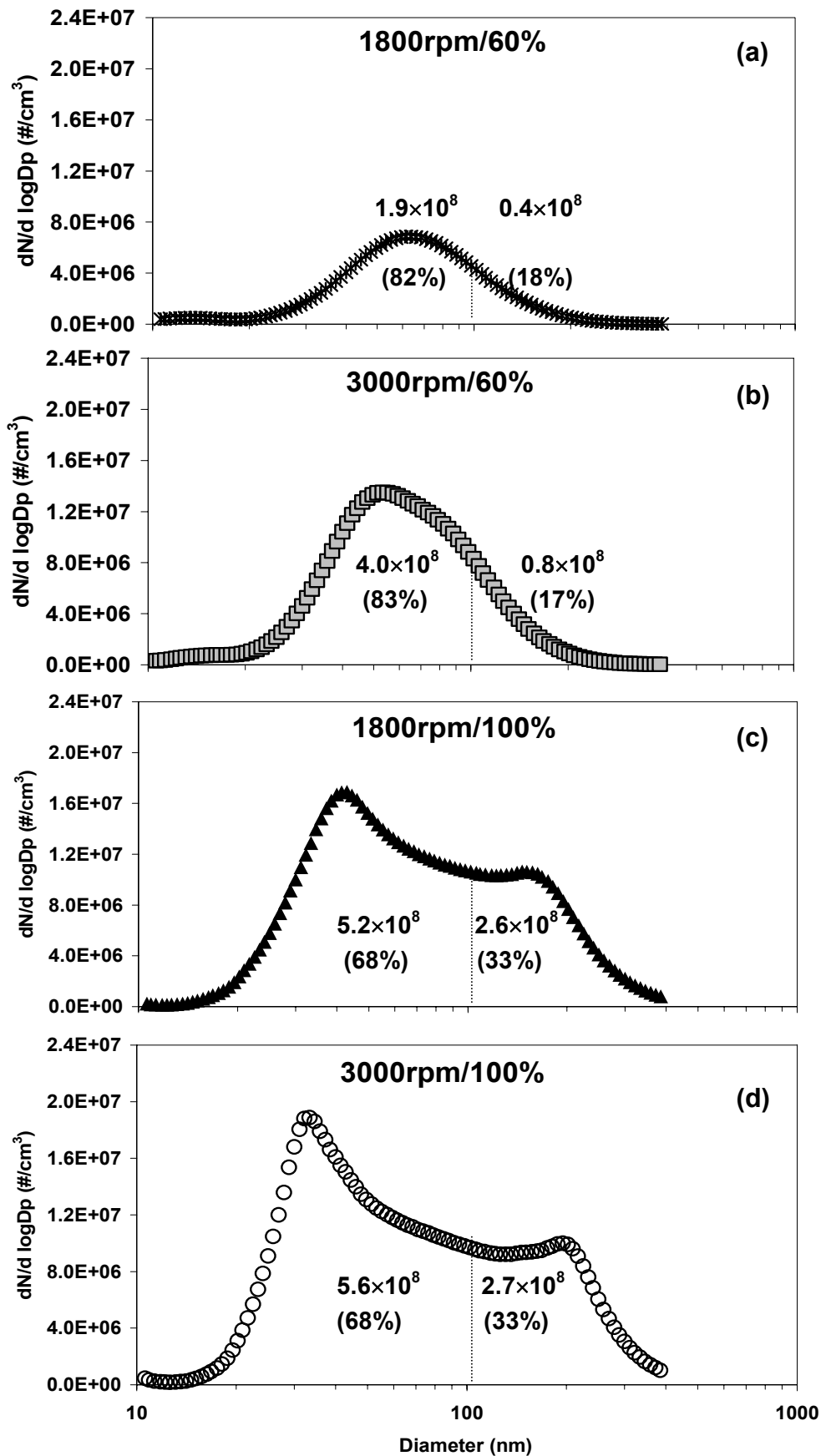


Fig. 3.4 Size distribution for individual driving conditions. All data points represent an average of twenty measurements with a standard deviation of (a) $(0.3-108) \times 10^4 \#/cm^3$, (b) $(0.3-73) \times 10^4 \#/cm^3$, (c) $(4-17) \times 10^4 \#/cm^3$, and (d) $(5-28) \times 10^4 \#/cm^3$.

Coagulation unlikely affected DEP size distribution in this study because of short residence time (about 0.1 s) in the dilution system. Sulfur in diesel fuel used in this study should contribute to nucleated UFPs since Schneider et al. (2005) reported substantially promoted nucleation (or UFPs smaller than 50 nm) when they increased the sulfur content in diesel fuel from 2 to 360 ppm. Based on TEM image, Park et al. (2003) explained that sulfur in diesel fuel would easily form H_2SO_4 vapor, which inclines to nucleate as new particles or condense onto existing particles (e.g., diesel soot). Using diesel fuel containing sulfur of around 300 ppm, Baumgard and Johnson (1996) found a surge in DEPs of 10–30 nm from a medium-duty diesel engine with an engine load of 75%. Hence, sulfur (200 ppm) in the diesel fuel used in this study should substantially contribute to DEPs peaking around 30 nm under the full engine load (Fig. 3.4(c) & (d)).

Fig. 3.4 also shows the total number concentration for UFPs and DEPs larger than 100 nm along with corresponding percentages (in terms of number concentrations). 68–83% of DEPs emitted from the four driving modes were distributed between 20 and 100 nm (Fig. 3.4), consistent with on-road measurements of DEPs generated from a heavy-duty truck (Kittleson, 2002) containing UFPs for more than 80% of numbered DEPs. This suggests that DEPs, in particular in the ultrafine mode, can contribute a large amount of surface area to carry toxic materials and to facilitate chemical reactions. It should be noted that the overall number concentrations given in Fig. 3.4 could be overestimated comparing with actual on-road number concentration of DEPs; because dilution of on-road exhausts can be up to 1000 times (Kerminen et al., 1997; Kittleson et al., 2002), the limited dilution (8.2 times) adopted in our

experiments could result in a higher concentration of DEPs due to enhanced nucleation and condensation processes.

For individual driving conditions, total DEP number concentrations, ranging from 2.3×10^8 – 8.3×10^8 #/cm³ (Fig. 3.4), increased with higher engine speeds or engine loads. Interestingly, under the medium engine load of 60%, when the engine speed increased from 1800 to 3000 rpm, DEP number concentration increased for more than 2 times, changing from 2.3×10^8 – 4.8×10^8 #/cm³ (Fig. 3.4(a) & (b)), whereas under the full engine load, an increase in the engine speed marginally affected resultant DEP number concentration (Fig. 3.4(c) & (d)). This indicates that effects of engine speeds on DEP concentration are insignificant if diesel engines were under the full load. A possible reason could be the invariance in amounts of elemental carbons (EC), which can represent soot-type of particles formed during combustion. As shown later in this chapter, amounts of EC remains insensitive to changes in engine speed under the full engine loads (Fig. 3.6), suggesting that total number of particles did not change significantly. On the other hand, an increase in engine loads substantially increased resultant DEP populations, especially when the vehicles were under a lower driving speed; a full engine load significantly enhanced DEP number concentrations from 2.3×10^8 – 7.8×10^8 #/cm³ under the engine speed of 1800 rpm, and from 4.8×10^8 – 8.3×10^8 #/cm³ under the engine operation of 3000 rpm (Fig. 3.4). In other words, decreasing the engine load from 100% to 60% decreased total DEP numbers for at least 1.7 to more than 3 times. For DEPs in ultrafine mode, Fig. 3.4 shows that increasing the engine load up to 100%, UFPs increased for more than 2.5 times (from 1.9×10^8 – 5.2×10^8 #/cm³) under the engine speed of 1800 rpm and for at least 1.4 times

under the maximum engine speed (3000 rpm). For DEPs in 100–400 nm generated under an engine speed of 1800 rpm, decreasing the engine load from 100% to 60% reduced corresponding DEPs for more than 6 times, changing from more than $2.5 \times 10^8 \text{ \#/cm}^3$ to less than $1 \times 10^8 \text{ \#/cm}^3$ (Fig. 3.4(a) & (c)). Under a high engine speed of 3000 rpm, decreasing the full engine load to the medium level (60%) effectively lowered DEPs in 100–400 nm for more than 3 times (from $2.7\text{--}0.8 \times 10^8 \text{ \#/cm}^3$) (Fig. 3.4(b) & (d)).

3.1.3 Persistent free radicals and carbon content in DEPs

Fig. 3.5 shows that concentrations of persistent free radicals in DEPs from the tested four steady-state driving conditions ranged from $4\text{--}186 \times 10^{16} \text{ \#spin/g}$, substantially depending on engine loads. Under the maximum engine load, persistent free radicals in DEPs ranged from $123\text{--}186 \times 10^{16} \text{ \#spin/g}$, more than 11 times of that under the 60% engine load ($4\text{--}11 \times 10^{16} \text{ \#spin/g}$) (Fig. 3.5). This is expected because compared to the medium engine-load condition, a higher engine load tends to induce more severe pyrolysis in combustion cylinders, which could reinforce soot formation, resulting in more abundant persistent free radicals. This can be of special concerns because the maximum engine load in this study also generated larger numbers (surface areas) of DEPs, which could facilitate more reactions of existing persistent free radicals, which could cause adverse respiratory effects (Cormier et al., 2006; Dellinger et al., 2001; Squadrito et al., 2001; Valavanidis et al., 2005). Nevertheless, simply reducing the engine load from 100% to 60% can significantly decrease persistent free radicals in DEPs for more than 16 times (under engine speed of 1800

rpm), or up to 30 times (under engine speed of 1800 rpm), in addition to lowering number concentrations.

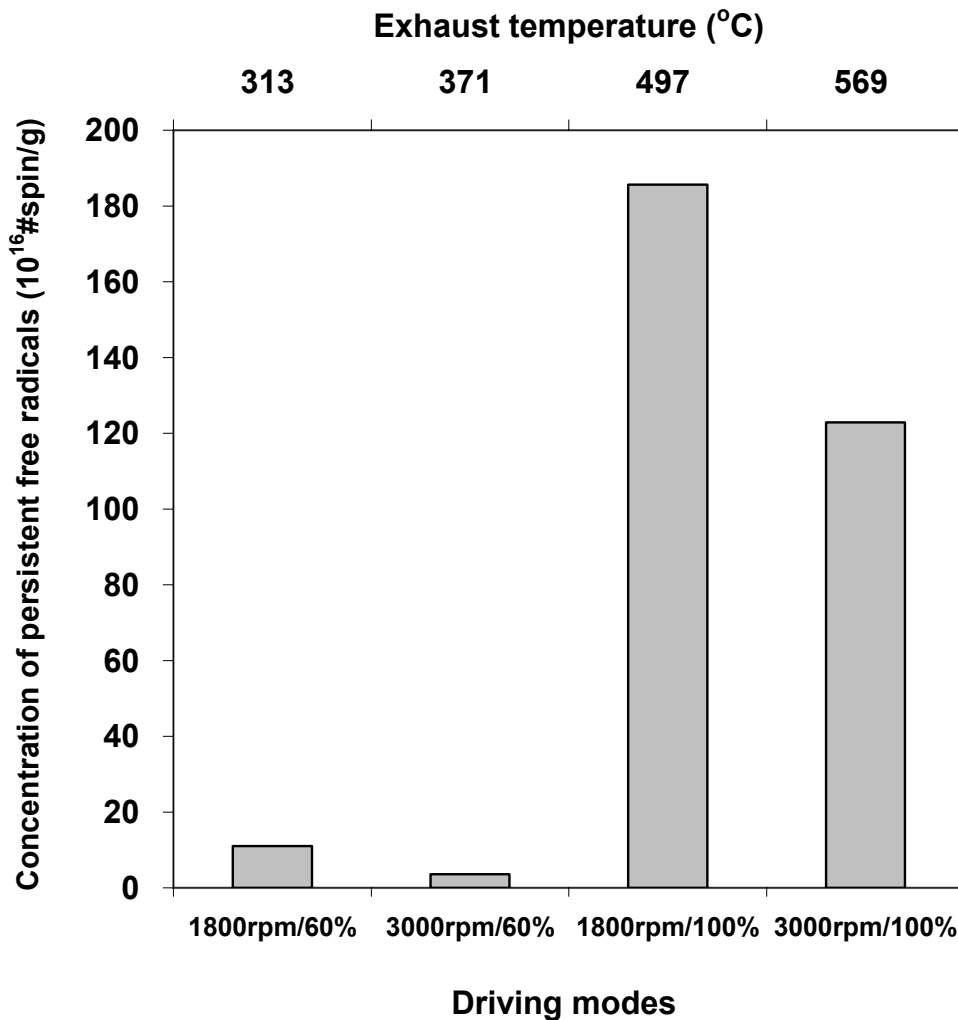


Fig. 3.5 Concentrations of persistent free radicals in DEPs of individual driving conditions.

Similar to reported persistent free radicals in DEPs retained in tailpipes (Abi-Aad et al., 2001; Yamanaka et al., 2005) and emitted from diesel-powered taxis (Valavanidis et al., 2005), identified persistent free radicals in this study exhibited a g-value of 2.0028 ± 0.0002 , corresponding to 1- to 5-ring aromatic hydrocarbon π radicals (anion), coronene (anion) or aliphatic hydrocarbon σ radicals (neutral)

(Petrakis and Grandy, 1983). The aromatic structure of the persistent free radicals found in this study could indicate nucleation and growth of soot through polymerization of polycyclic aromatic hydrocarbons (PAHs) and/or polyynes (including acetylene) (Wen et al., 2006; Richter et al., 2005; Violi et al., 1999).

Formation of aromatic-structured persistent free radicals during pyrolysis depends on combustion temperatures (Ledesma et al., 2002; Marsh et al., 2004). In spite of different fuels, four studies examining combustion of catechol fuel, tobacco and cellulose chars pyrolysis consistently observed that concentrations of aromatic-structured persistent free radicals peaked at a threshold temperature and then decreased with increasing combustion temperatures (Maskos et al., 2005; Wind et al., 1993; Ledesma et al., 2002; Marsh et al., 2004). Fig. 3.5 shows that under the full engine load, since the DEPs from the engine speed of 3000 rpm along with an exhaust temperature of 569°C (secondary x-axis) contained less persistent free radicals than that from the engine speed of 1800 rpm with an exhaust temperature of 497°C, the threshold temperature corresponding to the most abundant persistent free radicals would be lower than 569°C, resulting in the decreasing concentration of persistent free radicals with an increase in the exhaust temperature.

Fig. 3.6 shows that total particulate matter (TPM) were emitted from the individual driving conditions in an decreasing order of 3000 rpm/100% > 1800 rpm/100% > 3000 rpm/60% > 1800 rpm/60%; under the maximum engine speed and load (3000 rpm/100%), the diesel engine generated largest amounts of elemental carbons (EC) and organic carbons (OC) of 27.3 and 17.6 mg/m³, respectively.

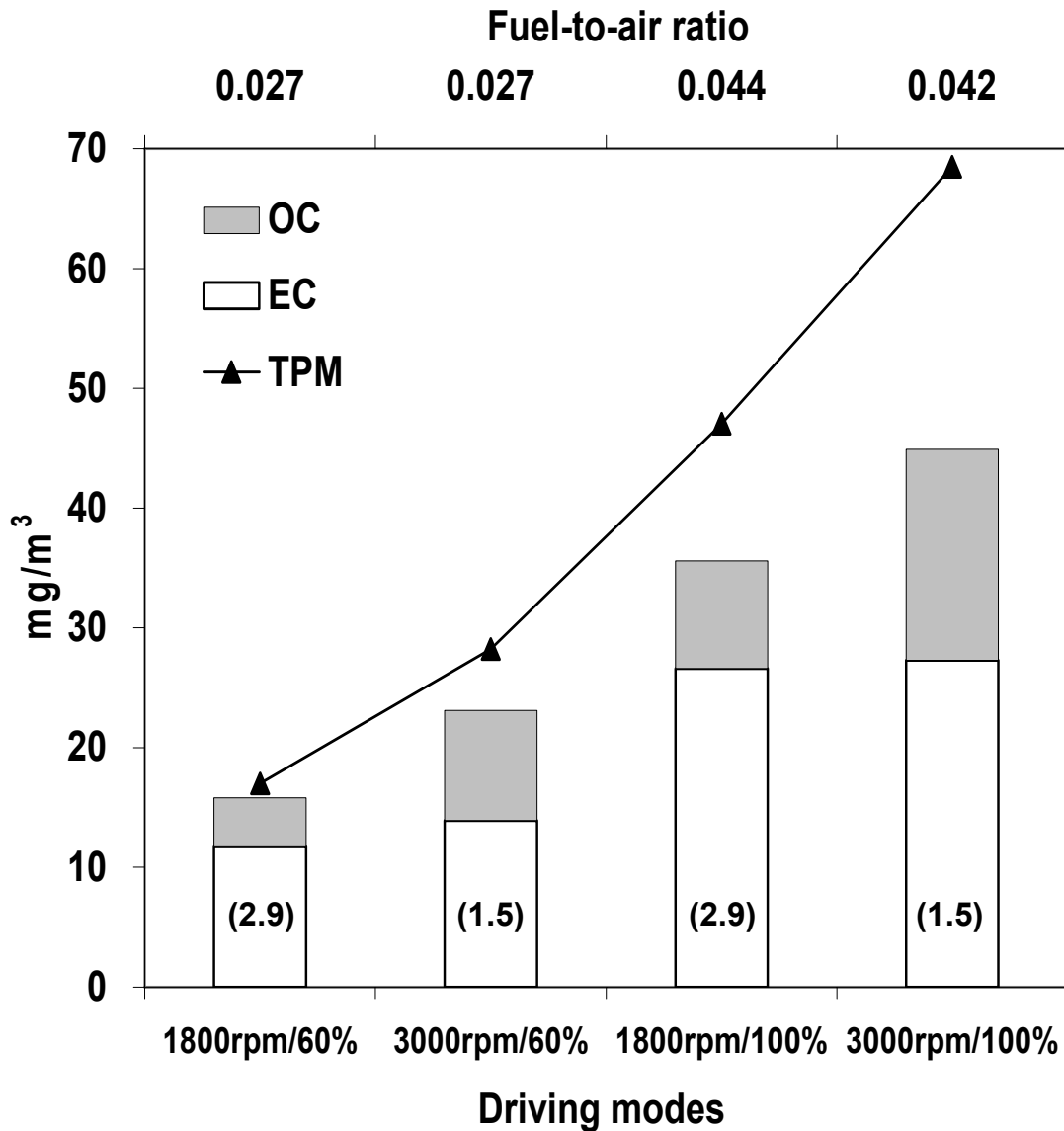


Fig. 3.6 Concentration of total DEPs (or total particulate matter, TPM), and EC, OC, and EC-OC ratio (shown in parentheses) in DEPs of individual driving conditions, with corresponding fuel-to-air ratio (the top x-axis). Each data point represents the average of triplicate measurements with corresponding standard deviations of 0.090–0.203 mg/m³ for OC and 0.090–0.235 mg/m³ for EC.

Interestingly, under a constant engine speed, when the engine load increased from 60% to 100%, EC and OC concurrently increased for about 2 times, which could be due to the higher FTA ratio (secondary x-axis, Fig. 3.6). On the other hand, an increase in the engine speed marginally affected FTA ratios and emitted EC, while enhanced

OC in DEPs for around 2 times. It should be noted that while the FTA ratio remained similar, the actual amounts of fuel and air can concurrently increase. Hence, invariant FTA ratios unnecessarily indicate similar combustion conditions. Based on concentrations of CO and hydrocarbons (HC) in exhaust, combustion conditions seem to insensitively depend on engine speed (Fig. 3.3). For example, when engine speed increased from 1800 to 3000 rpm, amounts of CO and HC changed insignificantly or marginally. Since amounts of elemental carbon depend more on combustion condition (Shi et al., 2000), it is expected that they would change little with engine speeds. On the other hand, amounts of organic carbons (OC) depend on exhaust temperatures. Since exhaust temperature increased with increasing engine speed (Fig. 3.3), it is not surprising that OC increased accordingly. Thus, relative to reduction in engine speeds, decreasing engine loads can concurrently reduce both EC and OC, which is more effective of minimizing carbonaceous materials in DEPs.

As the EC and OC trends mentioned above, parentheses in Fig. 3.6 show that an increase in the engine speed from 1800 to 3000 rpm mainly led to more OC along with invariant EC in DEPs, which consequently decreased the EC-OC ratio from 2.9 to 1.5. This is supported by Ålander et al. (2004) who tested a (direct injection) diesel engine similar to this study using a chassis dynamometer and reported a decrease in EC-OC ratios at higher engine speeds. In fact, depending on the engine speed, EC-OC ratios of DEPs from individual driving conditions in this study were either 1.5 or 2.9. This is within a wide range of values obtained from eleven types of on-road heavy-duty diesel trucks, spanning from 0.2–2.4 (Shah et al., 2004). In addition, since increasing the engine load concurrently enhanced emission of EC and OC, and

resulted in a similar EC-OC ratio of 1.5 (Fig. 3.6), EC-OC ratios reflect little on how different engine types and driving conditions affect resultant carbonaceous content of DEPs.

3.1.4 Size segregated EC and OC in DEPs

Fig. 3.7 shows size segregated EC, OC, and EC-OC ratio in DEPs smaller than 1 μm emitted from individual driving modes tested in this study. Consistent with the trend in TPM (Fig. 3.6), the EC and OC concentrations of DEPs smaller than 1 μm generally increased with increasing the engine speed or engine load, ranging from 0.20–1.37 and 0.10–0.40 mg/m^3 . However, unlike the TPM showing relatively invariant EC-OC ratios for individual driving conditions (Fig. 3.6), the EC-OC ratios of DEPs smaller than 1 μm generally increased with increasing engine loads, spanning from 1.9 to 3.1 (Fig. 3.7). This demonstrates that EC-OC ratios of TPM masked the size dependency of EC-OC ratios in the sub-micron DEPs. On the other hand, since DEPs smaller than 1 μm only contained 5% and 3% of total EC and OC in TPM, respectively, the EC-OC ratios of the TPM were mainly determined by DEPs larger than 1 μm . For DEPs below 1 μm , at 60% load, combustion temperature slightly increased from 312°C to 371°C with similar combustion condition based on amounts of CO and HC in exhausts (Fig. 3.3). Hence, EC and OC changed insignificantly when engine speed increased under the 60% engine load. On the other hand, at 100% load, an increase in engine speed substantially increased exhaust temperature from 497°C to 569°C along with more severe incomplete combustion (Fig. 3.3). The increase in temperature significantly enhanced amounts of OC, and the

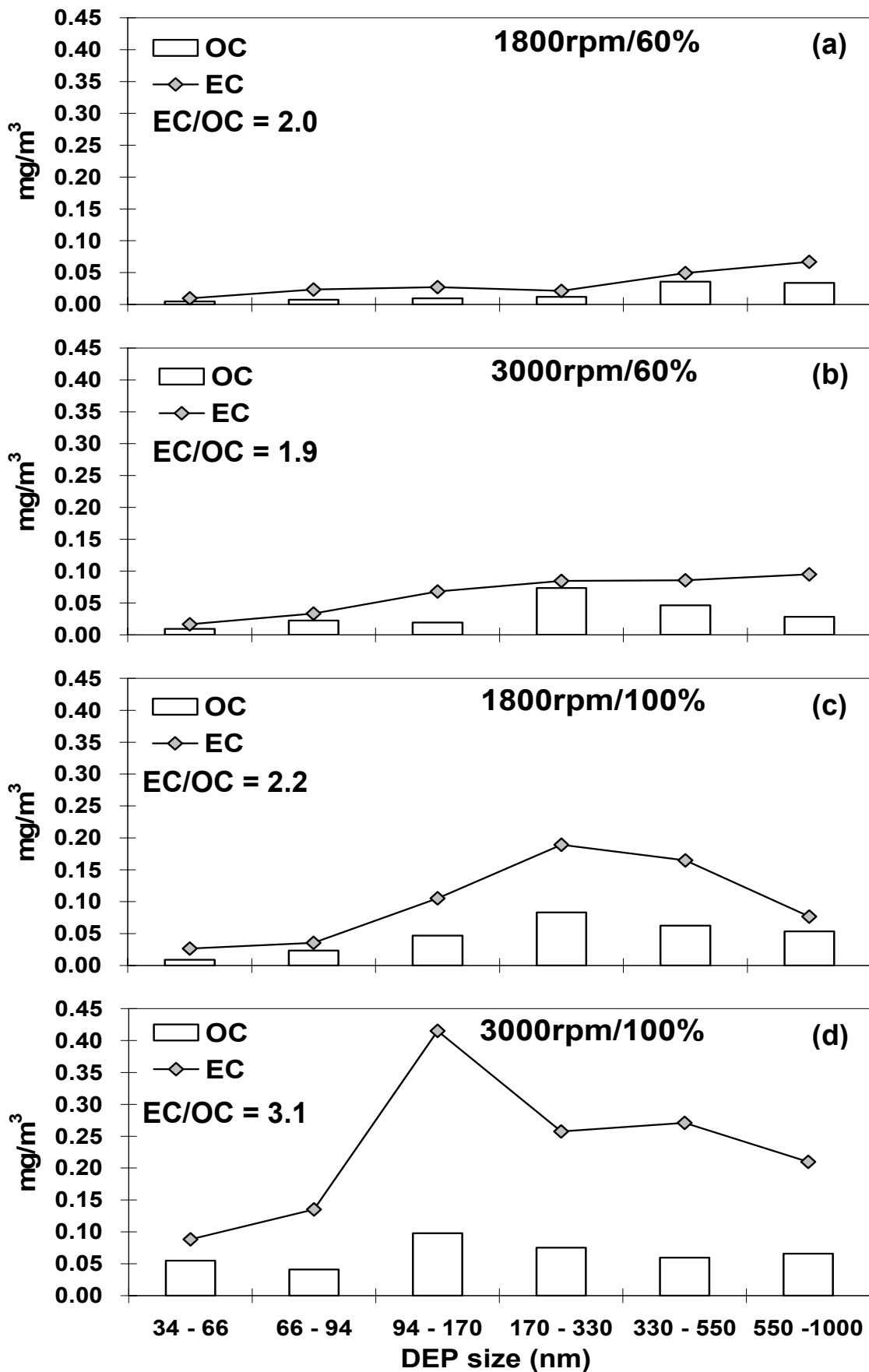


Fig. 3.7 Size distribution of EC, OC, and EC-OC ratios of DEPs (34–1000 nm). All data points represent an average of triplicate measurements with a standard deviation of <math><0.01\text{--}0.15\text{ mg/m}^3</math> for EC and <math><0.01\text{--}0.11\text{ mg/m}^3</math> for OC.

more severe incomplete combustion increased, in particular, EC (or soot process). This results in a trend that EC/OC ratio increased with engine speed at 100% load. For DEPs below 1 μm , at 60% load, combustion temperature slightly increased from 312°C to 371°C with similar combustion condition based on amounts of CO and HC in exhausts (Fig. 3.3). Hence, EC and OC changed insignificantly when engine speed increased under the 60% engine load. On the other hand, at 100% load, an increase in engine speed substantially increased exhaust temperature from 497°C to 569°C along with more severe incomplete combustion (Fig. 3.3). The increase in temperature significantly enhanced amounts of OC, and the more severe incomplete combustion increased, in particular, EC (or soot process). This results in a trend that EC/OC ratio increased with engine speed at 100% load.

For size segregated EC, Fig. 3.7(a) and (b) show that under the medium (60%) engine load, EC mildly increased with larger DEP size, whereas under the full engine load, EC peaked at size of 170–330 nm and 94–170 nm as shown in Fig. 3.7(c) and (d), respectively. Among the tested four driving conditions, the driving mode of 3000 rpm/100% exhibited the largest EC concentration for all six size groups (Fig. 3.7), with a concentration ranging from 0.09–0.42 mg/m^3 . This is consistent with previous observations of DEPs from heavy-duty diesel engines with a size cross all size or $\leq 2.5 \mu\text{m}$ that stronger formation of soot (or EC) took place at high engine speeds and high engine loads (Shah et al., 2004; Shi et al., 2000). Relative to the medium engine speed and engine load (1800 rpm/60%), the maximum engine speed/load (3000 rpm/100%) emitting EC in UFPs (34–94 nm) and in 94–1000 nm was around 7 times higher (0.22 vs. 0.03 mg/m^3 for 34–94 nm; 1.15 vs. 0.17 mg/m^3 for 94–1000 nm).

This is expected because heavier engine loads, which are often accompanied with a higher combustion temperature and larger injection of fuel (or FTA ratios), tend to encourage formation of primary soot (nonvolatile core) in size 20–50 nm (Burtscher, 1992) followed by agglomeration. While particle-cluster agglomeration may primarily contribute to DEPs in ultrafine size, cluster-cluster agglomeration could substantially result in accumulation-mode DEPs (Virtanen et al., 2004). This suggests that large EC in size of 94–170 nm (Fig. 3.7(d)) and in size of 170–330 nm (Fig. 3.7(c)) could be attributed to strong sooting under the driving condition of 3000 rpm/100%, and substantial cluster-cluster agglomeration under the driving condition of 1800 rpm/100%, respectively.

Consistent with the trend in EC, among the tested driving conditions, size-segregated OC (in DEPs smaller than 1000 nm) from the driving condition of 3000 rpm/100% showed the largest concentration for all the six size ranges, spanning from 0.04 mg/m³ (66–94 nm) to 0.10 mg/m³ (94–170 nm) (Fig. 3.7(d)). This could be due to the higher FTA ratio and stronger fuel injection pressure under this most demanding driving condition, resulting in supersaturated organic vapor available for nucleation and condensation. Less nucleation of UFPs under 1800 rpm/60% may also explain that the resultant OC in 34–94 nm was down to 0.01 mg/m³ (Fig. 3.7(a)), one tenth of corresponding OC (0.10 mg/m³) under the driving condition of 3000 rpm/100%. Interestingly, under the two driving conditions with the full engine load, OC in DEPs smaller than 1 μm mainly peaked at the accumulation mode, 170–330 nm (Fig. 3.7(c)) and 94–170 nm (Fig. 3.7(d)) for the engine speed of 1800 and 3000 rpm, respectively. Since condensation would dominate DEPs in accumulation-mode

(100–1000 nm), decreasing the engine load from 100% to 60% reduced OC in DEPs larger than 100 nm for more than 1.5 times, changing from more than 0.25 mg/m³ down to less than 0.17 mg/m³ (Fig. 3.7).

3.2 Effect of Driving Conditions on Metal Contents in DEPs

3.2.1 Effects of driving conditions, diesel fuel, and lubricants on metals in DEPs

For DEPs of 34 nm–1 μm, Fig. 3.8(a) demonstrates that the total quantified metals ranged from 6.1–7.7 μg/m³. Fig. 3.8(a) also shows that the engine speed marginally affected metal concentrations in DEPs. On the other hand, when the engine load increased from 60% to 100%, metal concentrations (μg/m³) increased for more than 16% along with higher fuel-to-air ratios (secondary x-axis), suggesting that a larger consumption of diesel fuel contributed to the increased metal content. To evaluate metal abundance per unit of DEPs (by weight), Fig. 3.8(b) shows that metal abundance significantly decreased with an increase in the engine speed or engine load, differing from the trend in Fig. 3.8(a). This is mainly because, at a higher speed or load, diesel engines tend to emit more DEPs (secondary x-axis) consisting of significant amounts of carbonaceous compounds. In particular, at the medium engine speed (1800 rpm), an increase in engine load from 60% to 100% enhanced DEP mass concentration (secondary x-axis of Fig. 3.8(b)) for at least five times, or decreased metal abundance for more than four times (Fig. 3.8(b)). Relative to Fig. 3.8(a), while metal abundance (metal content per unit of DEPs, by weight as shown in Fig. 3.8(b)) can be employed as an emission rate to facilitate modeling of source apportionments, metal concentration (mass per unit of air volume) is applicable to examine effects of

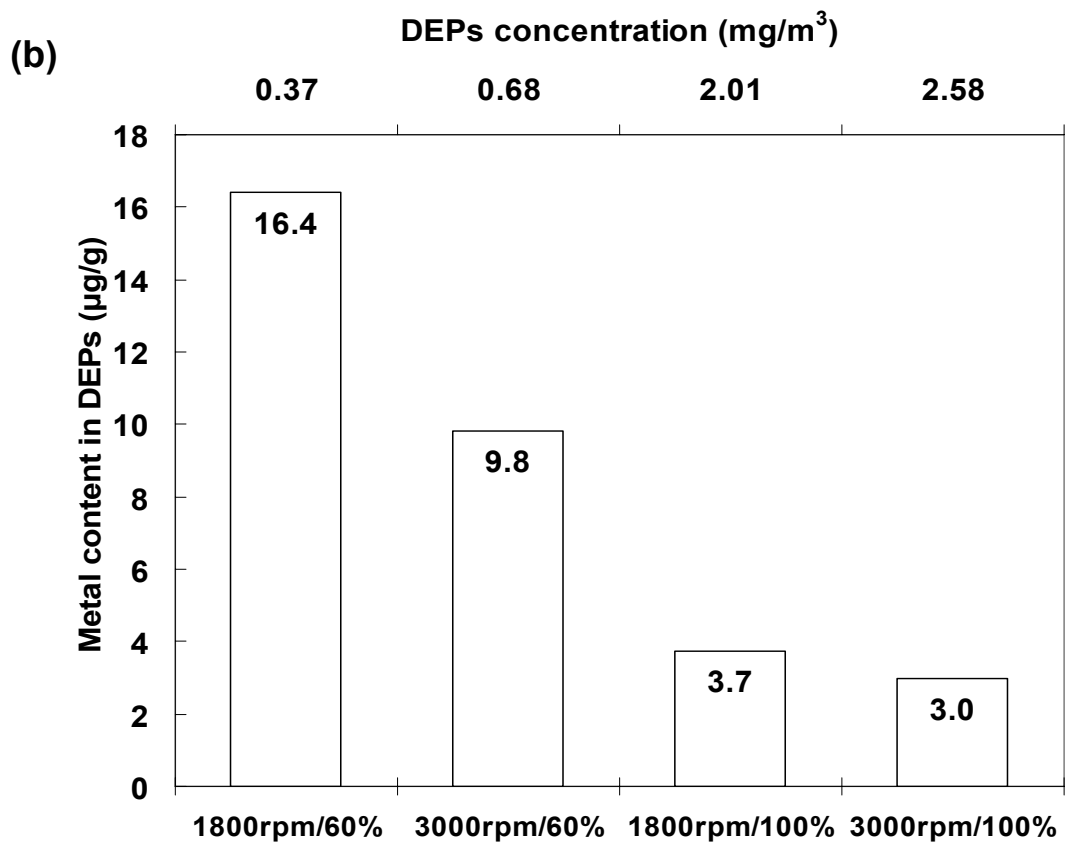
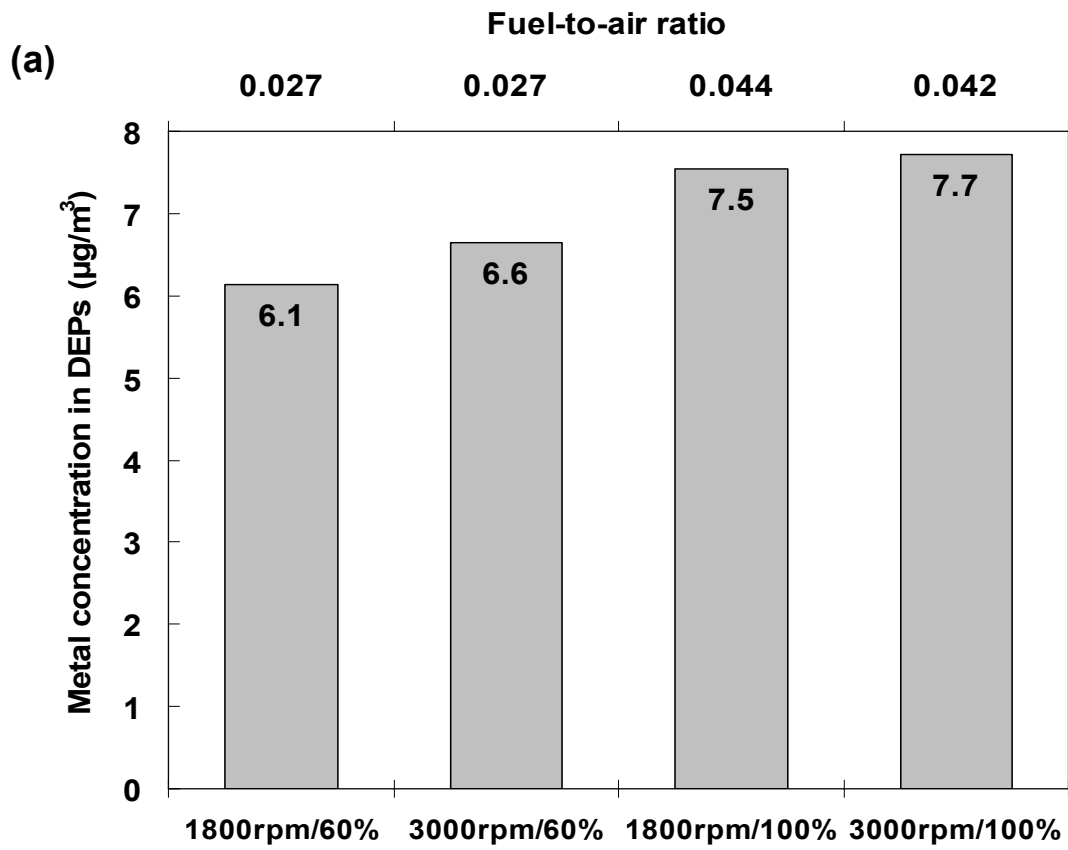


Fig. 3.8. Effect of driving conditions on metal contents in DEPs (34 nm–1 μm).

driving conditions on metal emissions without interference of concurrent changes in carbonaceous materials in DEPs. In addition, the expression of metal concentrations (mass per volume) is comparable with those in ambient environments and from primary emission sources, paving ways to assess how DEPs affect ambient air quality.

Among the identified 18 metal species, Fig. 3.9 depicts nine species with the rest nine trace metals classified into the category of “Others”, which accounted for less than 3% of total quantified metals. Because Fe is the major component in both diesel fuel and lubricant used in this study (Fig. 3.9(a) & (b)), it consistently exhibited the highest concentration in DEPs of all four driving conditions (Fig. 3.9(c)–(f)). In the diesel fuel, Fe concentration (14.7 $\mu\text{g/mL}$) is more than 60% of total quantifiable metal content, followed by Cu (14%) and Cr (12%) (Fig. 3.9(a)). While the lubricant used in this study contains quantifiable metals of 47.7 $\mu\text{g/mL}$, which is more than two times higher than diesel fuel (23.2 $\mu\text{g/mL}$), the little consumption rate of lubricants (< 60 g/hr), compared to diesel fuel (10–27 kg/hr), contributed little to resultant metals in DEPs. Hence, it is not surprising that the lubricant insignificantly affected resultant profiles of metal concentrations in DEPs (Fig. 3.9(c)–(f)) although more than 40% of quantified metals in the lubricant are attributed to Mn (17%), Ni (14%) and Mo (14%) (Fig. 3.9(b)).

Fig. 3.9(c)–(f) show Fe as the most abundant metal species (>38%) followed by Pb (5–15%), Cr (9–12%), V (9–10%) and Li (8–15%). Fe exhibited the largest concentration ranging from 2.3–3.9 $\mu\text{g/m}^3$, consistent with Wang et al. (2003), who reported Fe having the highest concentration (543 $\mu\text{g/m}^3$) among the identified 12

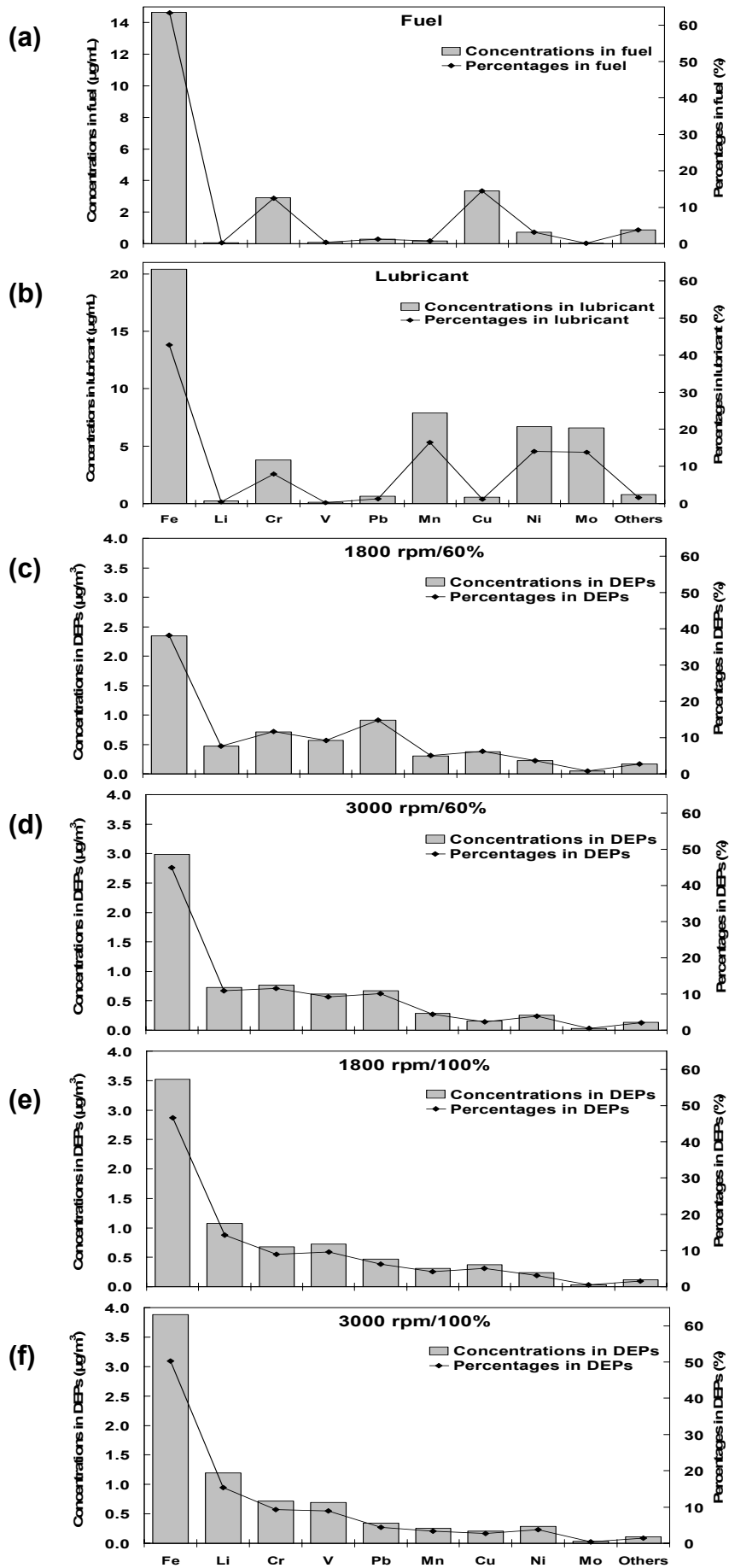


Fig. 3.9 Comparison of metal contents in DEPs (34 nm–1 μm) with diesel fuel and lubricant.

transition metals. Such a high concentration of Fe measured in total DEPs could be attributed to the high content of Fe in the used diesel fuel and the aged (1990-model) medium-duty diesel engine. In this study, Fe and Cr in DEPs were most likely originated from diesel fuel containing relatively abundant Fe, Cr, and Cu (Fig. 3.9(a)).

Pb and V could participated in DEPs mainly through engine wear since Pb is commonly used in alloys of engine bearings and in coatings of engine pistons (Denis et al., 2000); V is often incorporated in materials of cylinder liner (Vatavuk and Demarchi, 1995) and combustion chamber (Holmes et al., 1990). Similar to Pb and V, Li could be added to aluminum alloys for engine pistons (United States Patent 5169462), and is normally used as one of antirust additives (Denis et al., 2000). Hence, although less than 1% of Li was quantified in the diesel fuel and lubricant employed in this study (Fig. 3.9(a) & (b)), it can participate in combustion through engine wear where its high volatility and reactivity (Allègre et al., 2001; Sullivan, 2001) could easily facilitate formation of lithium oxide and lead to relatively large amounts of Li in DEPs (Fig. 3.9(d)–(f)). This may also explain why more Li was quantified in DEPs of driving conditions with the higher engine speed (3000 rpm) or engine load (100%) (Fig. 3.9(e) & (f)), accompanied with a higher combustion temperature, in addition to more consumption of the diesel fuel and lubricant.

3.2.2 Metal contents in size segregated DEPs

Size distribution of metals in DEPs was first evaluated in two size groups, 34–94 nm (ultrafine DEPs) and 94 nm–1 μm (accumulation-mode DEPs). Fig. 3.10(a) shows that while metal concentration of accumulation-mode DEPs (in white bars) changed

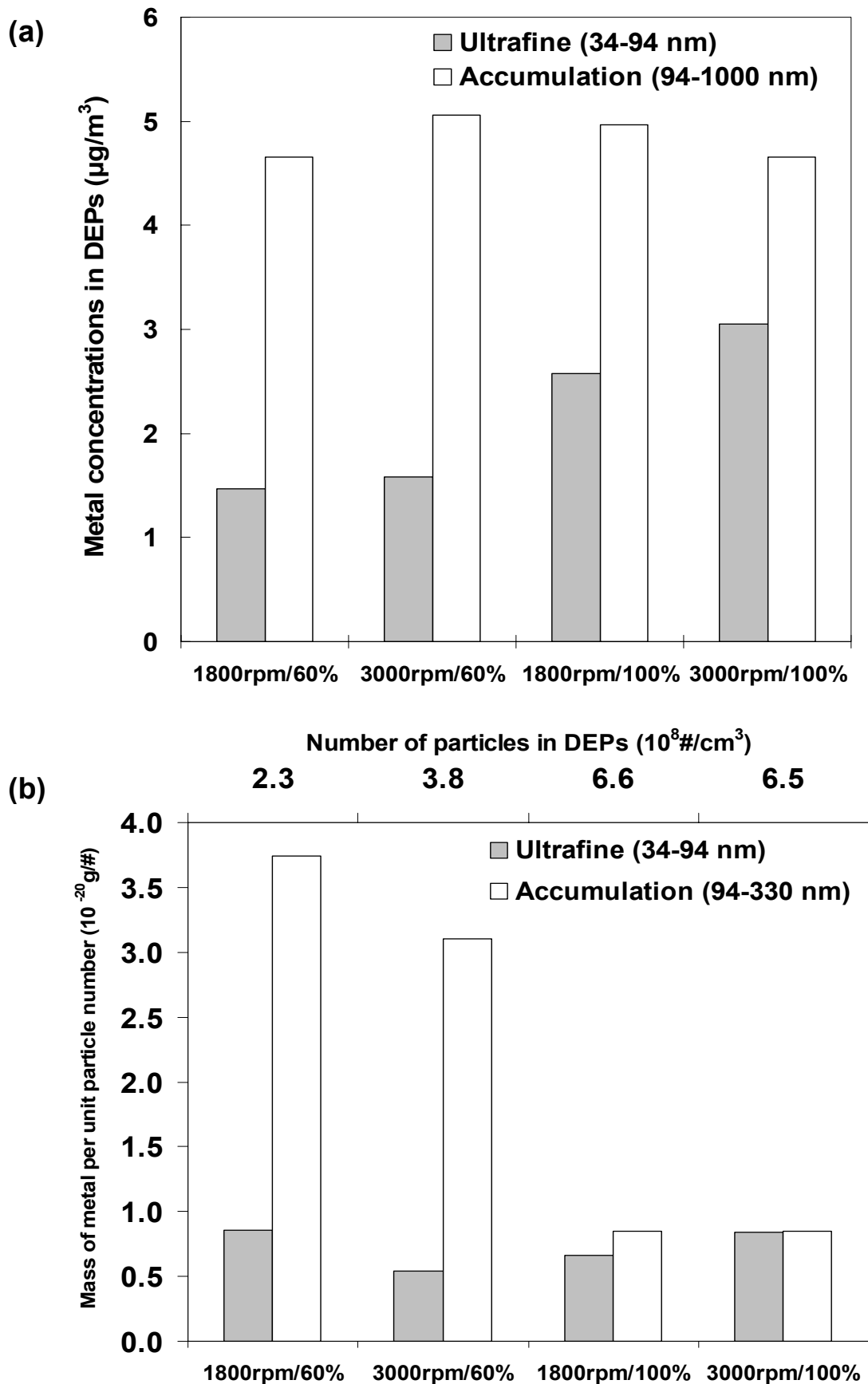


Fig. 3.10 Effect of driving conditions on size distribution of metal contents in DEPs.

marginally (by around 10%), a full engine load significantly increased metals in ultrafine DEPs (in gray bars) by 73% (from 1.5–2.6 $\mu\text{g}/\text{m}^3$) and 94% (from 1.6–3.1 $\mu\text{g}/\text{m}^3$) under the medium and maximum engine speeds, respectively. This provides insights of Fig. 3.8(a) that the increase (1.1–1.4 $\mu\text{g}/\text{m}^3$) of metals in DEPs (34 nm–1 μm) of the driving conditions under the full engine load was mainly contributed by ultrafine DEPs. Since after-treatment devices (e.g., diesel particle filters) can efficiently remove (metals in) DEPs larger than 100 nm (Mohr et al., 2006; Kittleson et al., 2006), employing after-treatment devices coupled with a restricted engine load (e.g., up to 60% as shown in Fig. 3.10(a)) can complementarily remove metals in DEPs over a wide size range, including those in ultrafine DEPs.

Fig. 3.10(a) also shows that under the maximum engine load, metals in ultrafine DEPs was more than 1.7 times of those under the 60% engine load. This may affirm the hypothesis of Lee et al. (2006) that under higher engine loads, a larger amount of diesel fuel in an engine results in supersaturated metal vapor, favoring homogeneous nucleation. Since the same group also postulated that smaller amounts of metal vapor in a combustion chamber (e.g., under a smaller engine load) could preferably undergo heterogeneous condensation onto existing carbon particulates, it is not surprising that, under the medium engine load (60%), more than 75% (by weight) of quantified metals concentrated in DEPs larger than 100 nm (Fig. 3.10(a)).

In terms of metal content in each DEP, Fig. 3.10(b) shows that under the full engine load, the amounts of metal carried by each ultrafine (34–94 nm) particle and accumulation-mode (94–330 nm) DEPs are similar ($0.7\text{--}0.9 \times 10^{-8}$ pg/particle), indicating that nucleation and condensation resulted in similar metal content per

particle. On the other hand, under the medium engine load, the amounts ($3.1\text{--}3.7\times 10^{-8}$ pg/particle) of metal concentrated in DEPs of 94–330 nm are at least 4 times more than that in ultrafine DEPs. This suggests that under a smaller engine load, metals were involved in DEPs dominantly through condensation.

To examine size distribution of metals in more detail, Fig. 3.11 shows metal concentrations in 6 size groups, ranging from 34–1000 nm. Consistent with Fig. 3.10, under the medium engine load, most metals concentrated in DEPs larger than 100 nm (Fig. 3.11(a) & (b)), whereas a full engine load elevated metal content in ultrafine DEPs, peaking at DEPs smaller than 66 nm with a concentration more than $1.5\ \mu\text{g}/\text{m}^3$ (Fig. 3.11(c) & (d)). This further supports that under higher engine loads, more metals participate in ultrafine DEPs. Interestingly, at the full engine load, metal contents showed an opposite trend to elemental carbon (EC) (Fig. 3.11(c) & (d)); when metal concentrations decreased (or increased) in individual size ranges, EC increased (or decreased) concurrently. This could be supported by Kim et al. (2005) who reported that an addition of metal additives to diesel fuel could suppress soot inception and growth because metal components can catalyze oxidation of soot in combustion chambers. The same research group also doped soot by bubbling fuel through iron pentacarbonyl prior to combustion, and observed that the iron-doped soot underwent more significant oxidation at combustion temperatures above 500°C . By using a high temperature oxidation tandem differential mobility analyzer, they also found that iron-doped soot was “shrunk” to nano size during combustion, indicating that a larger amount of metals in ultrafine DEPs shown in Fig. 3.11(c) and (d) could also be contributed by oxidation of larger DEPs at high temperatures under full engine loads.

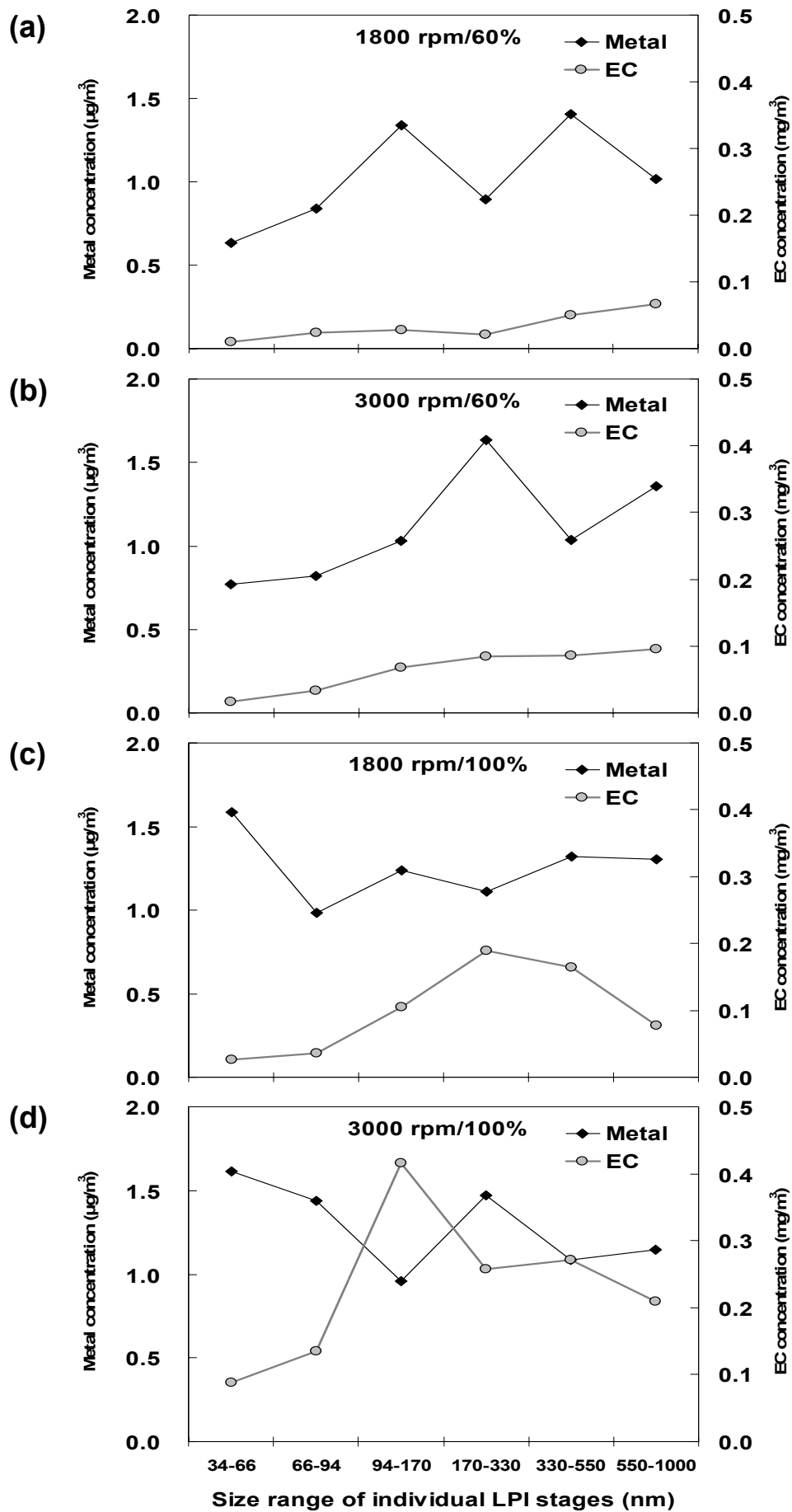


Fig. 3.11 Size distribution of metal contents and elemental carbon in DEPs.

For the driving conditions under the 60% engine load, however, indistinguishable trends between metals and EC are observed in DEPs smaller than 1 μm , which could be attributed to less soot emission resulting from less fuel consumption and lower combustion temperature ($< 500^\circ\text{C}$).

Fig. 3.12 shows the size segregation of nine metal species exhibiting relatively more substantial concentrations in DEPs. Depending on the engine loads, these metals show two general trends in their size distribution: under the engine load of 60%, individual metals concentrated more in DEPs larger than 100 nm, with an accumulated concentration in DEPs (100–1000 nm, accumulation mode) of 26 ng/m^3 (for Mo) to more than 2100 ng/m^3 (for Fe), or the metals in DEPs of accumulation mode is 2.0–6.5 times of that in ultrafine DEPs. On the other hand, under the full engine load, the amount of metals in DEPs was generally distributed more evenly among individual size ranges, compared to that of the medium engine load (Fig. 3.12); DEPs larger than 100 nm contained metals, in average, 1.7–1.9 times of ultrafine DEPs (see data in Appendix D, Table D). Interestingly, under the driving condition with the highest engine speed (3000 rpm) and engine load (100%), Cu in accumulation-mode DEPs was almost 7 times of that in ultrafine DEPs, uniquely differing from other metals with a concentration ratio ranging between 1 and 1.8 (data not shown).

For ultrafine DEPs, under the medium engine load, no more than 30% of most metals was in the ultrafine range (secondary y-axis of Fig. 3.12), whereas under the maximum engine load, the individual metals shown in Fig. 3.12 had, in average, 40% of their mass in the ultrafine DEPs. In fact, under the most strenuous driving

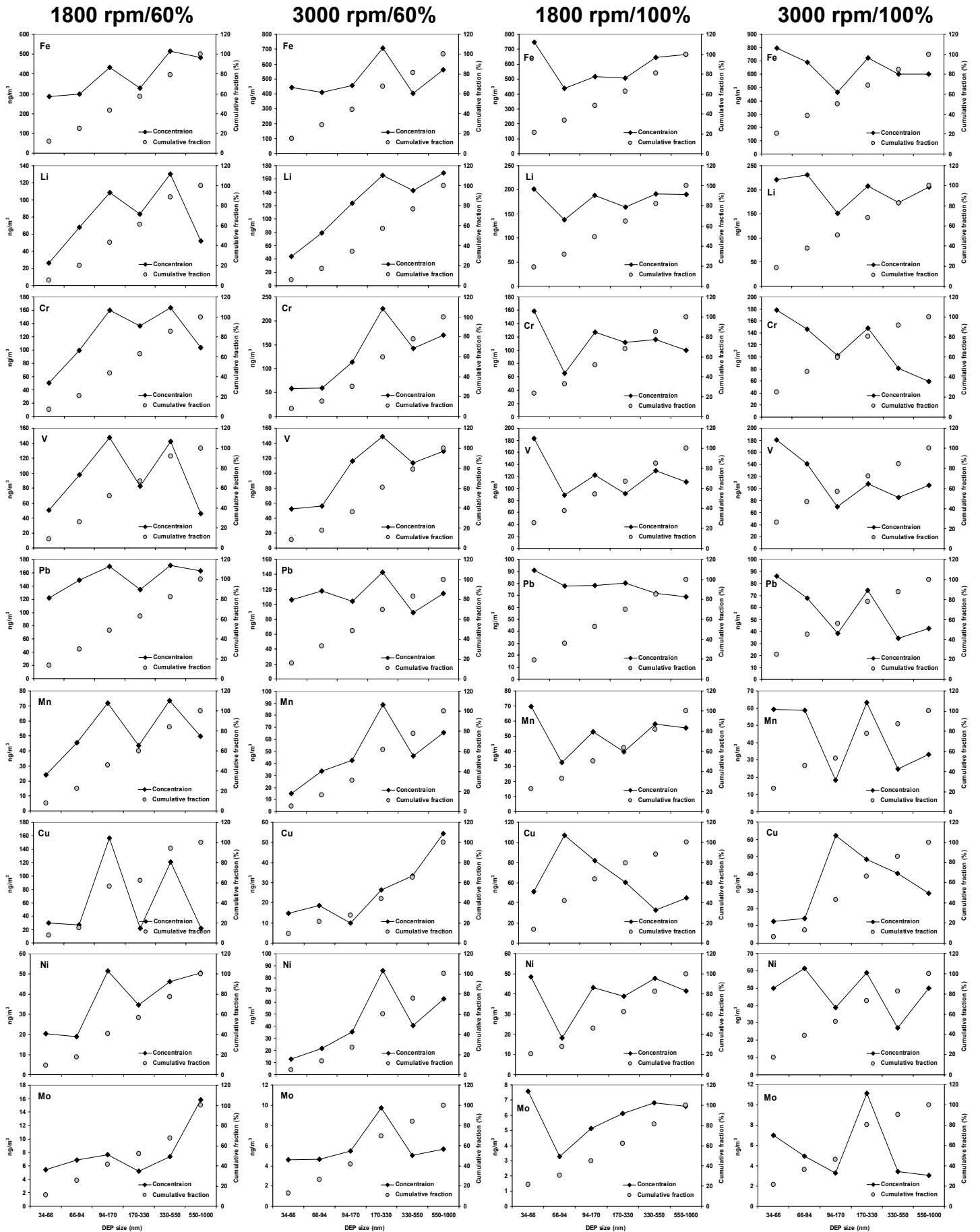


Fig. 3.12 Size distribution and cumulative fractions of 9 most abundant metals in DEPs.

condition (3000 rpm/100%), 7 out of 18 identified metals distributed 50% of their mass in ultrafine DEPs (see data in Appendix D, Table D), demonstrating that a substantial amount of metals can be carried by ultrafine DEPs.

Under the 100% engine load, metals often peaked at the smallest ultrafine DEPs (< 66 nm) with a concentration up to ~800 ng/m³ (for Fe) (Fig. 3.12). This, again, indicates the dominant involvement of metals (in particular Fe) in ultrafine DEPs under the full engine load. In addition, when the engine load increased from 60% to 100% (at the maximum engine speed of 3000 rpm), the averaged cumulative fraction of five metals Fe, Li, Cr, V and Pb increased for around 2 times (from 22% to 43%) (Fig. 3.12). This suggests that reducing the engine load can substantially decrease the amount of metals in ultrafine DEPs.

It is worthwhile to note that while roadside observations also show that a substantial amount of metals (e.g., 50% of quantified cadmium) was retained in ultrafine particles emitting mainly from diesel vehicles (Lin et al., 2005), consistent with this study, the most abundant five metals (Fe, Cr, Pb, Ni and Cd) in ultrafine (10–100 nm) particulates collected along roadsides with a substantial influence of diesel emissions (Lin et al., 2005) differ from this study (Fe, Li, Cr, V and Pb). This is not surprising because roadside measurements can vary depending on locations and on-road fleet compositions.

3.2.3 Comparison of metals-to-iron ratio with other studies

Table 3.1 summarizes concentration ratios of four metals (Cr, Ni, Cu, and Pb) to Fe, which were derived from four studies, including this work. In addition to different

Table 3.1 Metal-to-iron ratios of particulates in vehicle emissions

Types of used fuel	Diesel	Diesel	Diesel	Gasoline
Engine/vehicle	1 medium-duty engine	1 medium-duty engine	1 light-duty vehicle	24 light-duty vehicles
Driving conditions	4 steady-state modes ¹	3 constant speeds ²	Federal Test Procedure ³	Transient modes ⁴
Testing methods	Engine dynamometer	Engine dynamometer	Chassis dynamometer	Chassis dynamometer
Source	This study	Wang et al., 2003	Vilhunen et al., 1999	Cadle et al., 2001
Cr-Fe ratio	0.23±0.06	0.21±0.02	0.09±0.01	0.03±0.01
Ni-Fe ratio	0.08±0.01	0.13±0.02	0.14±0.02	0.04±0.02
Cu-Fe ratio	0.09±0.05	0.11±0.01	0.03±0.01	0.07±0.05
Pb-Fe ratio	0.21±0.13	0.03±0.00	0.01±0.01	0.04±0.03
No. of tests	4	3	3	3

¹Consisting of two engine speeds (1800 and 3000 rpm) and two engine loads (60 and 100%)

²Engine speeds of 100, 60, 40% under a maxim engine load

³3 steps of Federal Test Procedure (FTP)

⁴3 types of testing programs: (i) 3 steps FTP (ii) Unified Cycles (iii) REP05 driving cycles

types of engines and testing methods, published studies often adopt different units of metal concentrations making cross-comparison difficult. As Table 3.1 shows, by normalizing the individual metals with the Fe concentration in the same studies, these four studies, consisting of 3 studies on DEPs and 1 study of gasoline emissions, provide comparable information of metal in particulates emitting from vehicle tailpipes. Unlike other metals, Cr-to-Fe (Cr-Fe) ratio of DEPs (0.09 ± 0.01 – 0.23 ± 0.06) is at least 2 times higher than that of particulates from gasoline exhausts (0.03 ± 0.01) (Table 3.1). The higher Cr-Fe ratio in DEPs could be due to a larger amount of Cr in diesel fuels and lubricants, while Cr was hardly detected in both regular- and premium-level of gasoline fuels (in USA) since year 1998 (Ozaki et al., 2004). It should be noted that although diesel-powered cars tend to emit more Cr, gasoline-powered vehicles (in USA) of model years earlier than 1985 can emit more Cr and Fe than diesel-powered vehicles (Cadle et al., 1999); employing the Cr-Fe ratio, instead of Cr or Fe concentration individually, can objectively differentiate diesel- vs. gasoline-originated emissions. Nevertheless, adopting the abovementioned Cr-Fe ratio as a fingerprint for diesel emissions should be conditional because Cr-Fe ratios in stack emissions (such as from oil fired power plants, coke ovens, and coal power plants) and of biomass burning exhibit a Cr-Fe ratio ranging from 0.09–0.28 (Reddy et al., 2005; Wang et al., 2003; See et al., 2007), similar to that in DEPs. In addition, Cr-Fe ratios in ambient PM_{10} and $PM_{2.5}$ near a city area is smaller than 0.03 (Marcazzan et al., 2001; Singh et al., 2002), similar to that of gasoline exhausts. Hence, the Cr-Fe ratio is only applicable to identify contribution of DEPs for studies

conducted in traffic tunnels or at locations under a substantial influence of traffic emissions.

3.3 Effect of Driving Conditions on Organic Compounds in DEPs

3.3.1 Effects of driving conditions on identified organic compounds in DEPs

Fig. 3.13(a) shows that the concentration of identifiable organic compounds in DEPs ($<1 \mu\text{m}$) ranged from 12.4 to around $20 \mu\text{g}/\text{m}^3$ for individual driving conditions. The secondary x-axis shows the corresponding concentration of total organic compounds in DEPs ($<1 \mu\text{m}$), which was estimated based on experimentally measured organic carbon in DEPs ($<1 \mu\text{m}$) coupled with an organic-mass-to-organic carbon (OM-OC) ratio of 1.2 (secondary x-axis). The OM-OC ratio of 1.2 employed in the estimation is reasonable because most organics in DEPs have alkane structure.

Differing from the trend in identifiable organic compounds, when the engine speed and load increased from 1800 rpm/60% to 3000 rpm/100%, the total organic in DEPs ($<1 \mu\text{m}$) (secondary x-axis) increased for almost 4 times, changing from 0.12 up to $0.47 \text{ mg}/\text{m}^3$ (Fig. 3.13(a)), whereas no more than 10% of the organic compounds were identifiable (Fig. 3.13(b)). This indicates that more than 90% (by wt) of organics in DEPs ($<1 \mu\text{m}$) in this study could be under detection limit and/or unidentifiable by using the existing analytical techniques because they could be humic-like substances (Ghio et al., 1996). Although literature studies reporting organics in DEPs $<1 \mu\text{m}$ in detailed are unavailable for comparison, the small fraction (%) of identifiable organics observed in this study can be supported by the

measurements of Schauer et al. (1999) and Rogge et al. (1993a), who only identified around 4% and 6% of organics in total DEPs emitting from a medium-duty and a heavy-duty diesel engine, respectively.

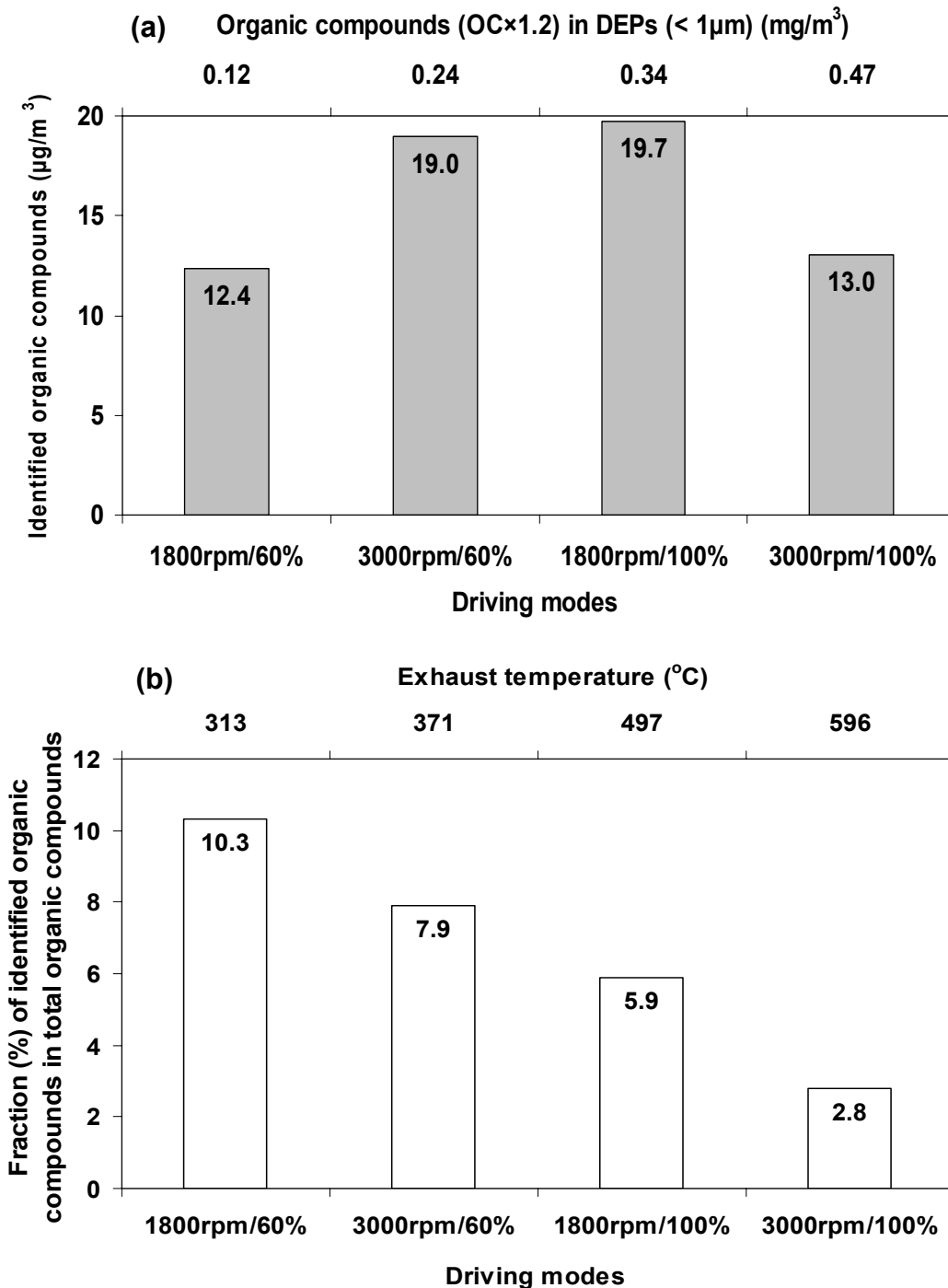


Fig. 3.13 Effect of driving conditions on identified organic compounds in DEPs (<1 µm).

When the driving conditions changed from 1800 rpm/60% to 3000 rpm/100%, Fig. 3.13(b) shows that the fraction of identifiable organics in DEPs ($<1 \mu\text{m}$) reduced for more than 3 times (from 10.3–2.8 %), indicating stronger formation of unresolved organics under more strenuous driving conditions, which were accompanied with more fuel injection and higher combustion temperature (as shown in the secondary x-axis of Fig. 3.13(b)) as well as larger pyrolysis zones in diesel engines. Such incomplete combustion could encourage formation of organics with large molecular weights, such as humic-like substances, or with complex mixture of branched and cyclic hydrocarbons, which are difficult to be resolved from analytical column (Ghio et al., 1996; Simoneit, 1984).

Table 3.2 shows that the concentration of identifiable organic compounds in DEPs of ultrafine (34–94 nm) size and accumulation (94–1000 nm) modes ranged from 2.9–5.7 $\mu\text{g}/\text{m}^3$ and 9.5–16.4 $\mu\text{g}/\text{m}^3$, respectively; a large amount (70–83%) of identifiable organics in DEPs ($<1 \mu\text{m}$) were allocated in accumulation-mode DEPs, suggesting that organic compounds in DEPs could have undergone prominent condensation. Although DEPs under the driving condition of 3000 rpm/60% and 1800 rpm/100% contained the largest concentration of identifiable organics in ultrafine (5.7 $\mu\text{g}/\text{m}^3$) and accumulation-modes (16.4 $\mu\text{g}/\text{m}^3$), respectively (Table 3.2), changes in driving conditions ambiguously correlated with the size distribution of identified organic. While aftertreatments (such as application of diesel particle filter; DPF) can effectively remove up to 99% (in terms of number) of accumulation-mode DEPs (Mathis et al., 2004), Geller et al. (2006) reported that chemical (redox) activity of DEPs unnecessarily decreased accordingly, suggesting that organic compounds in

ultrafine DEPs may contain substantial reactivity. Nevertheless, since the identifiable organics in this study are only up to 10% of total organic compounds, more understanding of size distribution and molecular structures of unresolved organics in DEPs are needed.

Table 3.2 Identifiable organic compounds in ultrafine and accumulation-mode DEPs

Driving modes	Ultrafine DEPs (34–94 nm)		Accumulation-mode DEPs (94–1000 nm)	
	Concentration ($\mu\text{g}/\text{m}^3$)	Fraction (%)	Concentration ($\mu\text{g}/\text{m}^3$)	Fraction (%)
1800 rpm/60%	2.9	23	9.5	77
3000 rpm/60%	5.7	30	13.3	70
1800 rpm/100%	3.3	17	16.4	83
3000 rpm/100%	3.0	23	10.0	77

Since organics containing hydroxyl and/or carbonyl substitutes (O-containing organics) in DEPs could provoke different oxidative stress, and cytotoxic as well as inflammatory response from aliphatic compounds and PAHs (non O-containing organics) (Shima et al., 2006; Xia et al., 2004), the identified organics were grouped as oxygen (O)-containing organics vs. non-O-containing organics. The former consists of quantifiable carboxylic acids, ester, ketones, ethers, oxygenated S-, N-containing compounds and oxygenated PAHs, and the non-O-containing organics include alkanes, alkenes, alkynes, aromatic hydrocarbons and aza arenes. The concentration of identified non-O-containing organics in DEPs ranged from 8.4–17.9 $\mu\text{g}/\text{m}^3$, 2 times more than O-containing organics (0.9–4.5 $\mu\text{g}/\text{m}^3$). Majority of both classes of identified organics were in accumulation-mode DEPs; more than 80% of O-containing organics (except DEPs of 1800 rpm/100%) and more than 60% of non-

O-containing organics were found in accumulation-mode DEPs (data not shown). Interestingly, the non-O-containing organic compounds generally show a concentration trend opposite to the O-containing organic compounds in both ultrafine (34–94 nm) and accumulation-mode (94–1000 nm) DEPs (Fig. 3.14).

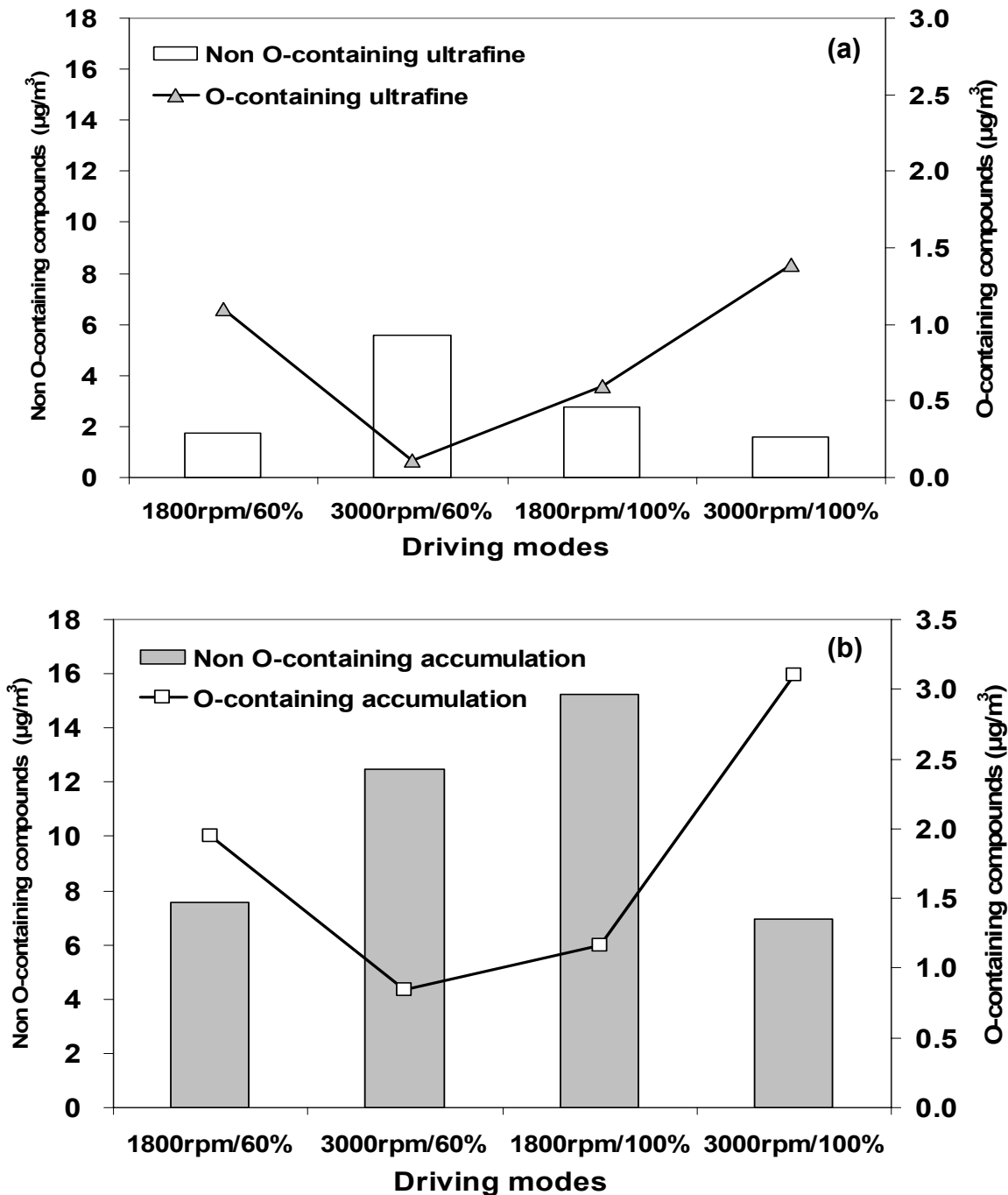


Fig. 3.14 Oxygen-containing and non-oxygen-containing organic compounds in (a) ultrafine DEPs and (b) accumulation-mode DEPs.

In ultrafine DEPs, the non-O-containing organics peaked at the driving condition of 3000 rpm/60% ($5.6 \mu\text{g}/\text{m}^3$), corresponding to the lowest concentration of the O-containing organics (Fig. 3.14(a)). Similarly, in accumulation-mode DEPs, when the non-O-containing organics exhibited a pivotal concentration ($15.2 \mu\text{g}/\text{m}^3$) under the driving condition of 1800 rpm/100%, the O-containing organics reversed a decreasing trend and peaked at the driving condition of 3000 rpm/100% with the largest concentration of $3.1 (\mu\text{g}/\text{m}^3)$ (Fig. 3.14(b)). This is consistent with observations of organics during in-cylinder diesel engine measurements that oxidative pyrolysis and partial oxidation of aliphatic hydrocarbons could increase the amount of oxygenated organic compounds (Barbella et al., 1990). Since the toxicity of O-containing compounds differ from that of non-O-containing compounds, specific molecular structure of organic compounds may provide more specific assessment of potential health problems imposed by DEPs

To better understand the potential toxicity of organic compounds in DEPs, according to molecular structure, the identified organic compounds in DEPs (34 nm to $1 \mu\text{m}$) were classified into eleven classes: alkanes, alkenes, alkynes, aromatic hydrocarbons, carboxylic acids, esters, ketones, alcohols, ethers, nitrogen (N)-containing compounds, and sulfur (S)-containing compounds.

Fig. 3.15 shows the concentration of identified compound class in DEPs ($<1 \mu\text{m}$) for individual driving conditions. Among the identified organic classes, alkane is the most abundant compound class, followed by carboxylic acids, esters, ketones and alcohols (corresponding to the secondary y-axis of Fig. 3.15).

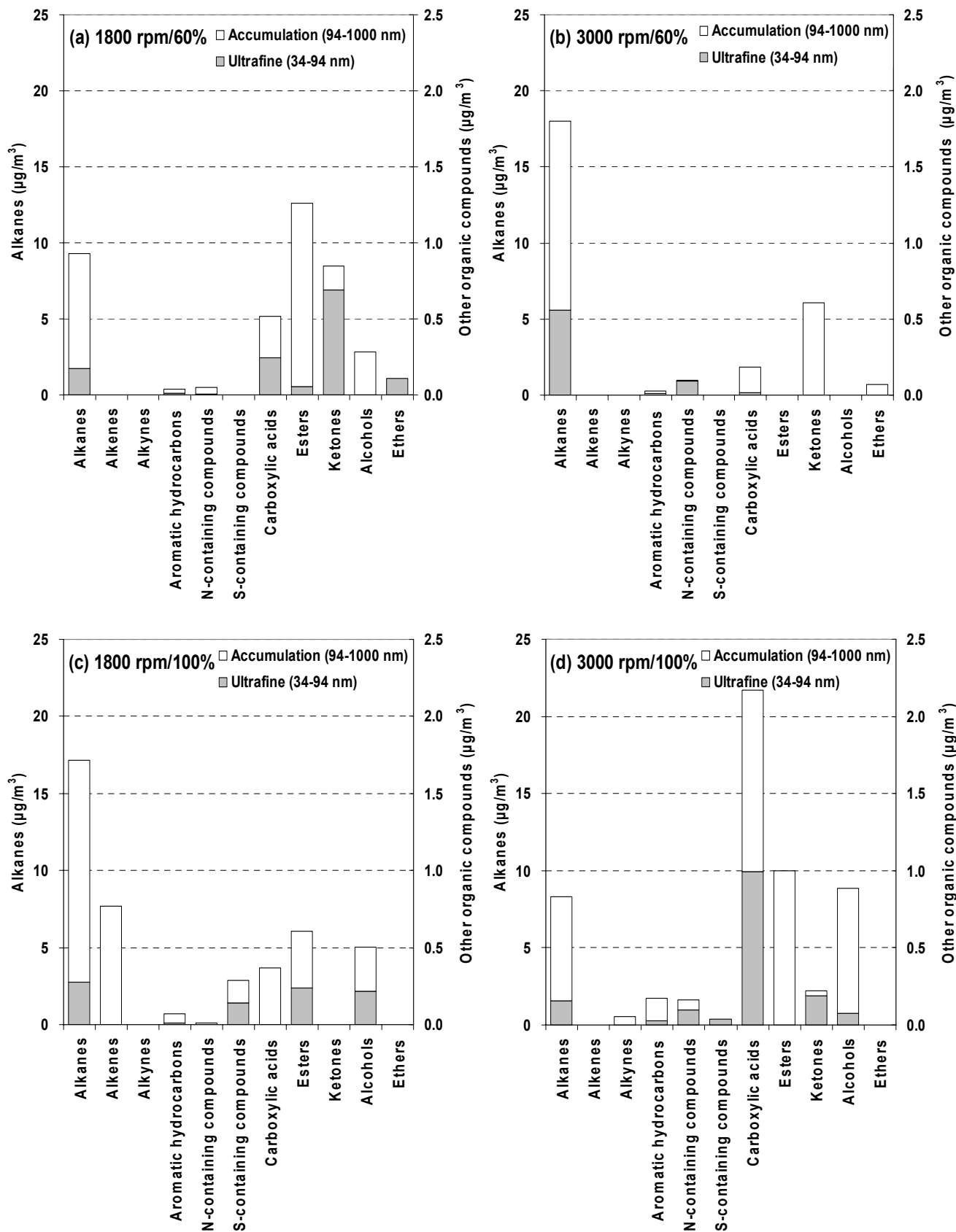


Fig. 3.15 Identified organic compound classes in DEPs (<1 µm) under four driving conditions. The concentration of non-alkane compound classes corresponds to the secondary y-axis.

Alkanes consistently exhibited the highest concentration, ranging from 8.3 $\mu\text{g}/\text{m}^3$ to 18.0 $\mu\text{g}/\text{m}^3$ (Fig. 3.15), and accounted for more than 60% (or up to 95%) of identified organics in DEPs (<1 μm) in this study. Among the tested driving conditions, DEPs of 3000 rpm/60% contained the largest alkanes (5.6 $\mu\text{g}/\text{m}^3$) in ultrafine size (grey bar, Fig. 3.15(b)), accounting for >97% of the quantified organics, and DEPs of 1800 rpm/100% contained most abundant alkanes in larger DEPs, responsible for ~88% of identifiable organics in the accumulation-mode (white bar, Fig. 3.15(c)). Abundant alkanes in DEPs found in this study are consistent with Rogge et al. (1993a) (more than 60 %). In addition, because more than 98% diesel fuel used for this study consists of alkanes (ranging from C9–C24) (Table 3.3), unburned fuel could be involved in resultant DEPs.

Table 3.3. Identifiable organic compounds in diesel fuel and lubricant employed in this study

Compound Classes	Diesel fuel	Lubricant
	Concentration ($\mu\text{g}/\text{mL}$)	
Alkanes (C9–C24)	11,067.6	-
PAHs	133.5	-
Carboxylic acids	-	482.8
Ketones	-	42.2
Oxygenated N containing compounds	-	18.8
Alcohols	-	8.3
Esters	-	6.3
PAHs	-	1.6

Consistent with the trend given in Fig. 3.14, alkanes show a concentration trend opposite to oxygenated compounds (including carboxylic acids, esters, ketones and

alcohols) (Fig. 3.15). For example, a higher concentration in oxygenated organics in DEPs of 1800 rpm/60% and 3000 rpm/100% ($3.0\text{--}4.3\ \mu\text{g}/\text{m}^3$) was accompanied with alkanes in a smaller concentration ($8.3\text{--}9.3\ \mu\text{g}/\text{m}^3$) (Fig. 3.15(a) & (d)), whereas other two driving conditions (3000 rpm/60% and 1800 rpm/100%) emitted smaller amounts of oxygenated organics along with larger amounts of alkanes ($17.1\text{--}18.0\ \mu\text{g}/\text{m}^3$) (Fig. 3.15(b) & (c)). It is worth while to note that among the four tested driving conditions, the maximum engine speed and load (Fig. 3.15(d)) emitted DEPs ($<1\ \mu\text{m}$) containing the largest amount of carboxylic acids ($2.2\ \mu\text{g}/\text{m}^3$), alcohols ($0.9\ \mu\text{g}/\text{m}^3$), N-containing compounds ($0.2\ \mu\text{g}/\text{m}^3$) and aromatic hydrocarbons ($0.2\ \mu\text{g}/\text{m}^3$), but least amount of alkanes ($8.3\ \mu\text{g}/\text{m}^3$). Although carboxylic acid is absent from diesel fuel, its abundance in the lubricant used in this study (Table 3.3) may lead to their presence in DEPs as suggested by Liang et al. (2005).

A few probable reaction pathways resulting in appearance and disappearance of organic compounds (such as carboxylic acids, esters, ketones, alcohols) in ultrafine and accumulation-mode DEPs at different driving modes could be suggested. Since chemical compositions of gas-phase compounds in diesel exhaust are unavailable, quantified organic species in particulate-phase could result from complicated pathways, including condensation and nucleation of gas-phase reactions, oxidation over particulate surfaces, etc. Hence, suggested chemical reactions based on observed concentration profiles should be taken as preliminary approximation. According to the proposed mechanisms under combustion ($\geq 800^\circ\text{C}$ with sufficient oxygen), for oxygenated organic compounds (carboxylic acids, esters, ketones, alcohols, and ethers), alcohols seemed to play a critical role determining formation of carboxylic

acids, esters, and ethers. At 1800rpm/60% driving mode, alcohols were mainly in accumulation-mode, indicating substantial condensation or particulate-phase oxidation, which could directly result in a substantial amount of esters in accumulation-mode (Fig. 3.15(a)). Ethers were solely in ultrafine-mode, which could be in expense of all alcohols in the same size of DEPs (Fig. 3.15(a)). Carboxylic acids appeared to participate evenly in ultrafine- vs. accumulation-mode DEPs. The fact that alcohols in ultrafine DEPs were negligible indicates that formation with carboxylic acids to form esters would be little as shown in (Fig. 3.15(a)). Alcohols in ultrafine DEPs could mainly be depleted by forming ethers in the same DEP mode, and hence less unavailable to react with carboxylic acids. If alcohols hold a key role of determining other classes of oxygenated compounds, it is not surprising that the disappearance of alcohols at 3000 rpm/60% was accompanied with negligible or little amounts of carboxylic acids, esters and ethers ((Fig. 3.15(b)). Interestingly, ketones showed much higher concentration in accumulation-mode at 3000rpm/60%, opposite to that at 1800rpm/60% (Fig. 3.15(a) & (b)). Since presence of ketones mainly depends on alkoxy or peroxy radicals, it is not surprising that its trend might not correlate with other oxygenated compounds in DEPs. In addition, ketones are more volatile than other oxygenated compounds; hence, they can be easily oxidized to other compounds or partition into gas-phase.

Similar to observation of Fig. 3.15(a), correlations among alcohols, carboxylic acids, esters, and ethers could be applied to the oxygenated compounds at the full engine load. In the case of 1800 rpm/100%, a relatively high concentration of alkanes (and alkenes) in accumulation-mode (Fig. 3.15(c)) indicates that condensation of

alkanes (and alkenes) dominated over oxidation of these hydrocarbons. Hence, less oxygenated organics (e.g., carboxylic acids, ketones, ethers, esters and alcohols) in both ultrafine- and accumulation-mode DEPs.

For 3000 rpm/100%, severe oxidation of alkanes and hydrocarbons could produce more carboxylic acids, esters, ketones and alcohols in ultra- and/or accumulation-mode through nucleation and condensation from gas-phase, as well as particle surface reactions. This is possible because Barbella et al. (1990) have shown that at high temperature in diesel engine cylinder, more oxidation of hydrocarbons could produce more oxygenated organics. Hence, abundant of carboxylic acids and alcohols in accumulation-mode could form dominant esters in accumulation-mode through esterification and more oxidation of alkanes in ultrafine-mode could produce relatively high ketones in ultrafine-mode.

3.3.2 Effects of driving conditions on alkanes in DEPs

Consistent with Fig. 3.15, Fig. 3.16 shows that most alkanes species concentrated in accumulation-mode DEPs of the four driving conditions; while individual alkanes in ultrafine DEPs contained a similar concentration, C19–C25 alkanes in accumulation-mode DEPs had larger concentration than other alkane species. Interestingly, after an increase in the engine speed or engine load, larger alkanes (C25–C31) decreased in concentration for more than 2 times (Fig. 3.16), which could be due to more severe thermal decomposition (Yu and Eser, 1997) since an increase in the engine speed or load in this study could enhance combustion (exhaust) temperatures for more than 200°C.

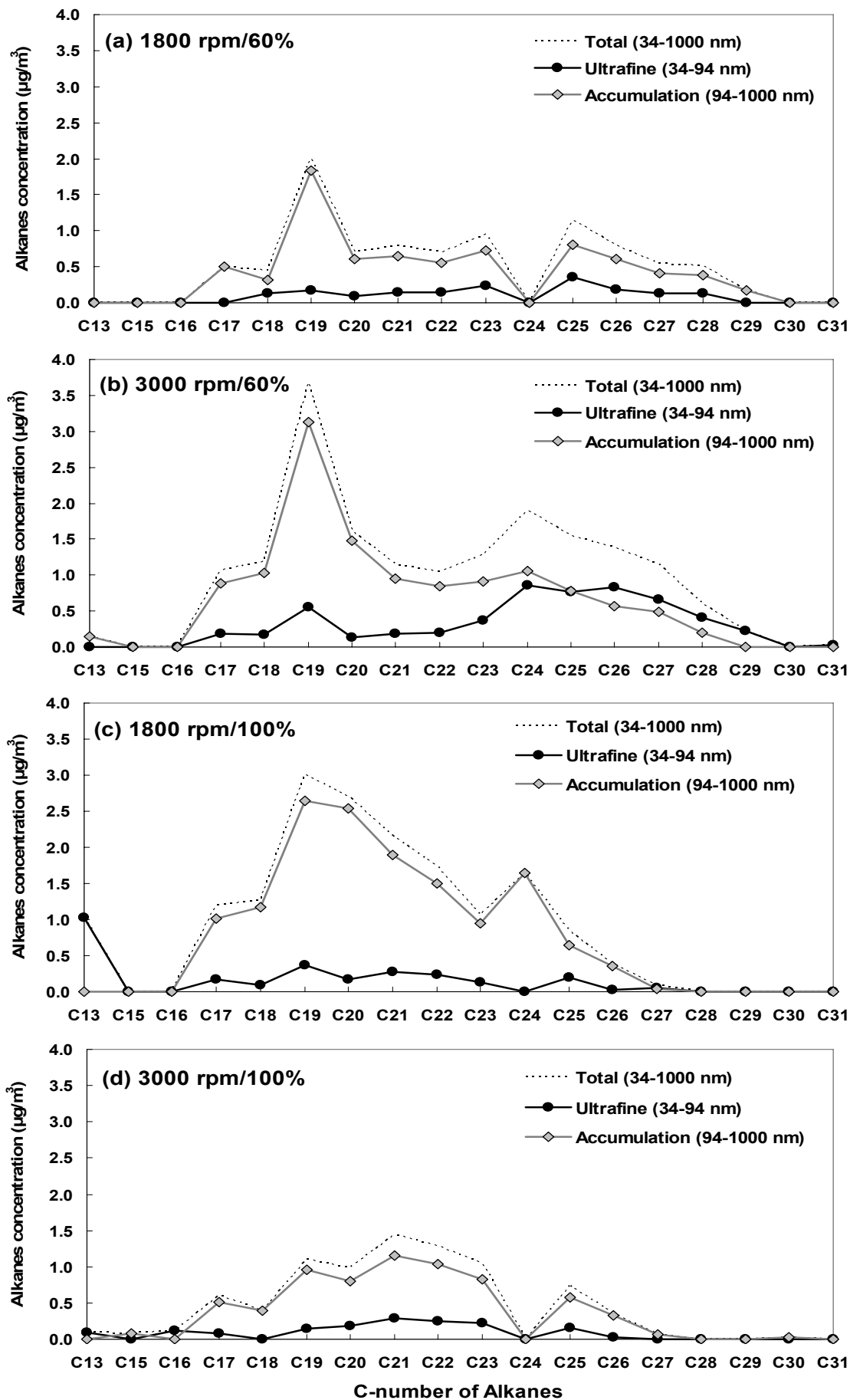


Fig. 3.16 Identified alkane species in ultrafine and accumulation-mode DEPs.

Fig. 3.16 shows that the identified alkanes in DEPs ($<1 \mu\text{m}$) (dashed lines in Fig. 4) generally peaked between C19–C25. Among the identified 17 alkane species in DEPs, C19 exhibited the highest concentration for all driving conditions, except that under the maximum engine speed and load, which peaked at C21 (Fig. 3.16(d)). While alkanes containing the highest concentration in DEPs ($<1 \mu\text{m}$) vary marginally among the individual driving conditions, a relative concentration ratios between the two most abundant alkanes may characterize effects of individual driving conditions. For example, the concentration ratios of individual driving conditions are: 1.7 (=C19/C25) for 1800 rpm/60%, 2.9 (=C19/C24) for 3000 rpm/60%, 1.8 (=C19/C24) for 1800 rpm/100%, and 2.0 (=C21/C25) for 3000 rpm/100%. This demonstrates that a ratio higher than 2 could represent DEPs of maximum engine speed. According to the data of other studies, alkanes in DEPs of a heavy-duty and a medium-duty truck operating following the Federal Test Procedure (FTP) showed a ratio of 3.0 (=C20/C25) (Rogge et al., 1993a) and 2.7 (=C20/C26) (Schauer et al., 1999), respectively. Since testing conditions, engine types, and diesel fuel used could affect emitted alkane composition and resultant ratios, the resultant ratios should be employed conditionally and may not be generalized. Nevertheless, the alkane ratio can characterize diesel- vs. gasoline-powered vehicles during tailpipe measurements because the ratio of alkanes in exhaust particulates of gasoline-powered vehicles undergoing the FTP tests were all smaller than 1.0. For gasoline-powered vehicles without and with catalytic converters, the ratio range from 0.3 (C22/C26)–0.9 (=C20/C25) and 0.7 (=C20/C25)–0.8 (C18/C25), respectively (Rogge et al., 1993a; Schauer et al., 2002). Hence, while the alkane ratio may not differentiate sources of

DEPs, it can serve as a potential fingerprint distinguish diesel-powered vs. gasoline-powered vehicles based on tailpipe measurements.

3.3.3 Effects of driving conditions on polycyclic aromatic hydrocarbons (PAHs) in DEPs

Fig. 3.17 depicts twelve identified polycyclic aromatic hydrocarbons (PAHs) in DEPs (<1 μm), according to the molecular weight, namely acenaphthylene (Acy), acenaphthene (Ace), fluorene (Flu), phenanthrene (Phe), anthracene (Ant), fluoranthene (Flt), pyrene (Pyr), chrysene (Cry), benzo(a)anthracene (BaA), benzo(b)fluoranthene (BbFt), benzo(k)fluoranthene (BkFt) and benzo(a)pyrene (BaP), with a concentration ranging from 37.9–174.8 ng/m^3 . The driving condition of 3000 rpm/100% emitted DEPs (<1 μm) containing the largest amount of PAHs, followed by 1800 rpm/100%, 1800 rpm/60% and 3000 rpm/60%. When the engine load increased from 60% to 100%, the amount of identifiable PAHs were increased for at least 2 times (under the engine speed of 1800 rpm) or for more than 5 times (under the maximum engine speed). This is expected because the higher combustion temperature and larger pyrolysis zone during the driving condition under the maximum engine load could encourage highly reactive free radicals undergoing pyrosynthesis (fusion of smaller molecules under pyrolysis conditions) to form larger and more stable PAHs (Collier et al., 1995; Mastral and Callen, 2000). Fig. 3.17 also shows the distribution of PAH in ultrafine and accumulation-mode DEPs. Similar to the alkane class, more PAHs were concentrated in the accumulation-mode DEPs (Fig. 3.15); in the ultrafine and accumulation-mode DEPs, the concentration of PAHs ranged from 10.8–23.2 ng/m^3 and 16.3–119.0 ng/m^3 , respectively.

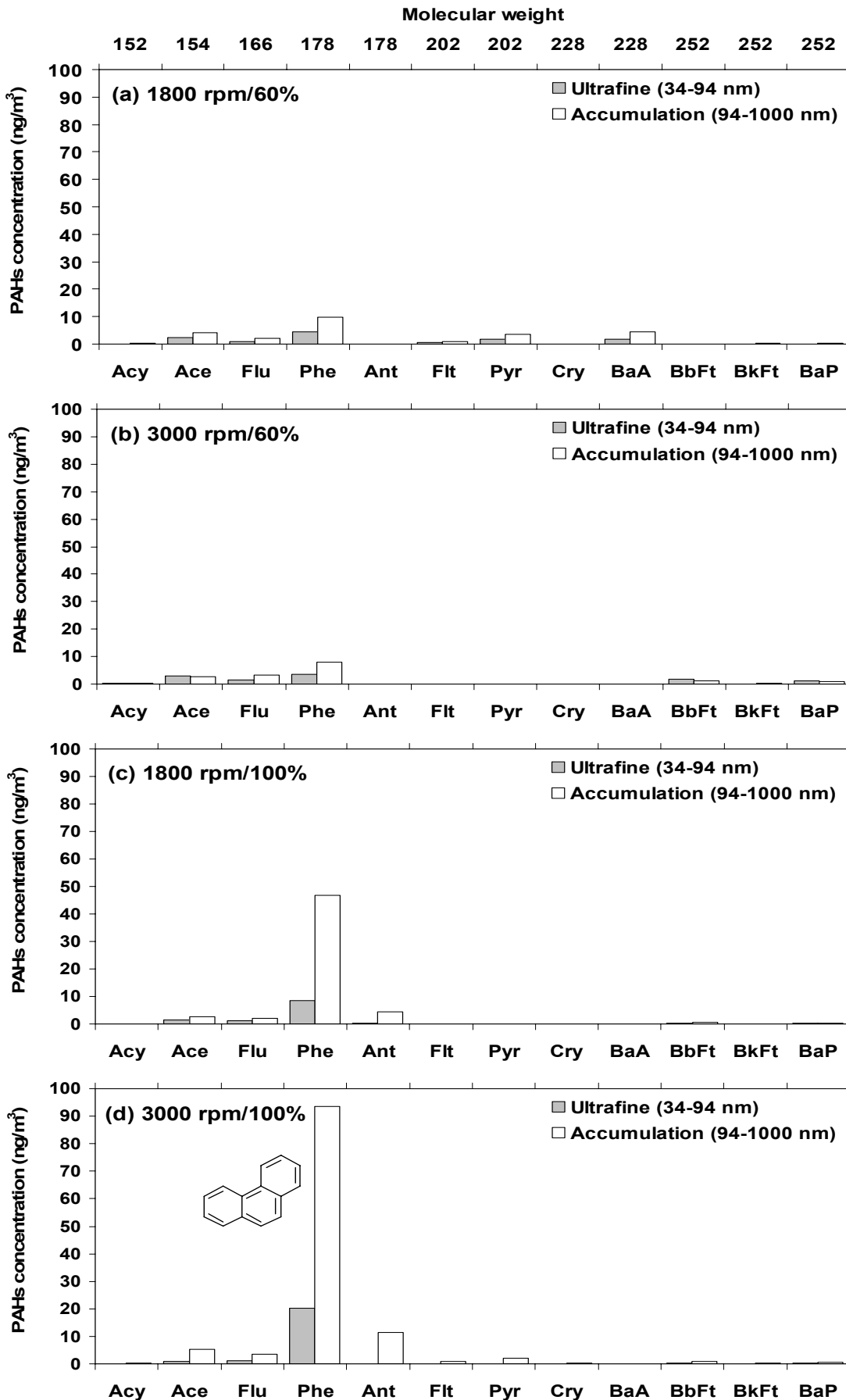


Fig. 3.17 Identified PAHs in ultrafine and accumulation-mode DEPs.

Among the identified PAHs in DEPs (<1 μm), the concentration of phenanthrene, ranging from 11.4–114.0 ng/m^3 , was the highest for the four driving conditions (Fig. 3.17). When the engine load was increased to the maximum, the concentration of phenanthrene increased up to 10 times (from 11.4–114.0 ng/m^3) (Fig. 3.17). This is consistent with other studies examining DEPs from light-duty diesel vehicles (chassis dynamometer tests) (Devos et al., 2006; Abrantes et al., 2004) and from heavy-duty diesel vehicles (Mobile Emission Laboratory tests) (Shah et al., 2005). At a bus station dedicated to only diesel-powered vehicles, phenanthrene was also the most abundant PAH (> 40% of identified PAHs) (Tavares et al., 2004), indicating that phenanthrene could fingerprint diesel emissions if its emission from other combustions sources remained insignificant. In the accumulation-mode DEPs of this study, phenanthrene is responsible for the seven-fold increase in quantified PAHs (from 16.3–119.0 ng/m^3) when the engine load increased to 100%. In other words, when the engine load increased from 60 to 100%, in accumulation-mode DEPs, the quantified PAHs increased from 16.3 up to 119.0 ng/m^3 , and phenanthrene increased from 7.9 up to 93.6 ng/m^3 accordingly (Fig. 3.17), which accounts for 83% of the increased amount in PAHs. The significant amount of phenanthrene in the accumulation-mode indicates prominent condensation onto DEPs under the most strenuous driving condition. In addition, because phenanthrene was postulated as one of the dominant intermediates during PAH growth and soot formation (Skjoth-Raamussen et al, 2004; Marinov et al, 1998) through hydrogen abstraction acetylene addition (HACA) pathways (Lombaert et al., 2006), polymerization involving prominent condensation could be important to forming DEPs in accumulation-mode.

It is also worth noting that under the maximum engine speed and engine load (3000 rpm/100%), the largest pyrolysis zone and highest combustion temperature could stimulate generation of more resonantly stabilized radicals (e.g., cyclopentadienyl radical), which can subsequently form the most abundant phenanthrene (Richer and Howard, 2000) as shown in Fig. 3.17(d). Further more, since phenanthrene (22.0 µg/mL) was one of the dominant PAHs in the diesel fuel employed for this study, more injection of diesel fuel under the maximum engine load could also contribute to the abundant phenanthrene in DEPs.

3.3.4 Effects of driving conditions on nitrogen-containing polycyclic aromatic compounds (NPACs) in DEPs

Nine NPACs were identified in DEPs (<1 µm) with a total concentration ranging from 7.0–10.3 ng/m³. Similar to the trend in quantified PAHs, the identified NPACs are more abundant in accumulation-mode DEPs of driving conditions, in particular, under the full engine load. Under the driving condition with the maximum engine speed and load (3000 rpm/100%), the stronger pyrolysis and higher combustion temperature in the diesel engine could promote pyrosynthesis between pyrolyzed PAH radicals and NO_x radicals (Ghigo et al., 2006), resulting in a larger concentration of NPACs (Fig. 3.18(d)). This appears to support the postulation of Williams et al. (1986 and 1989) that reaction of nitrogen oxides (NO_x) with PAHs in hot diesel exhausts could generate NPACs. Since NPACs were emitted during incomplete combustion of various fuels (e.g., coals and diesel) (Murahashi et al., 2003; Yu et al., 1999), they could be formed through thermal fusion under high temperatures. Rogge et al. (1993b) reported that aza arenes could be formed during

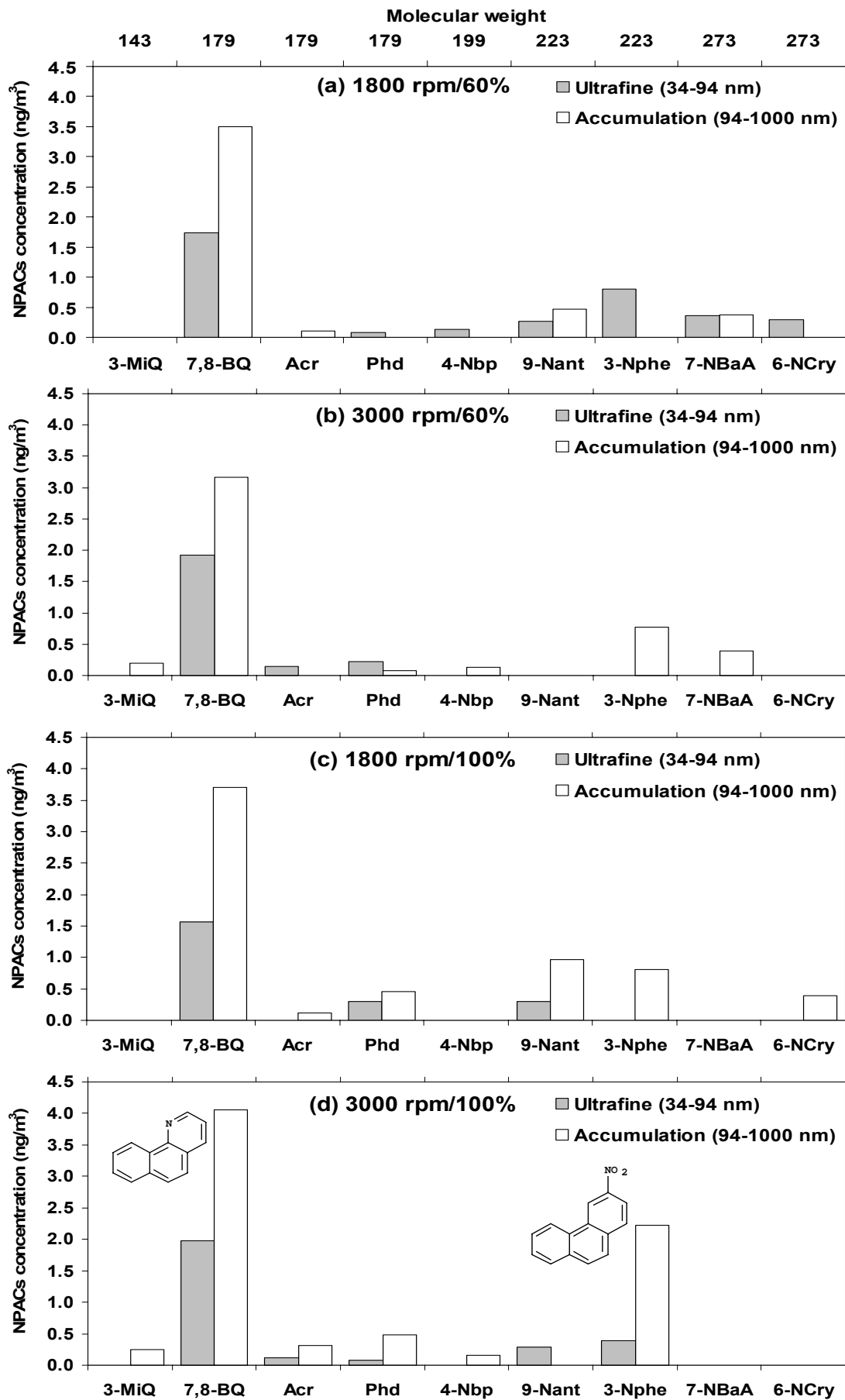


Fig. 3.18 Identified NPACs in ultrafine and accumulation-mode DEPs

the combustion of fossil fuels similar to PAH formation by incorporating N-atoms into their ring structures. Wiersum (1996) hypothesized that significant concentration of aryl radicals and NO₂ radicals could be combined to form NPACs in the pyrolysis under high temperature. In addition, Ghigo et al. (2006) suggested direct nitration of NO₂ radicals followed by H abstraction to form nitroarenes under high-temperature (1200K) combustion conditions.

The identified 9 NPACs consist of four aza arenes (nitrogen-containing heterocyclic aromatic hydrocarbons) and five nitroarenes (nitro-PAHs) with a total concentration of 5.4–7.3 ng/m³ and 1.3–3.1 ng/m³, respectively. The four aza arenes are mainly composed of 2–3 aromatic rings, including 3-methylisoquinoline (3-MiQ), 7,8-benzoquinoline (7,8-BQ), acridine (Acr), and phenanthridine (Phd). The identified five nitroarenes are 4-nitrobiphenyl (4-Nbp), 9-nitroanthracene (9-Nant), and 3-nitrophenanthrene (3-Nphe), 7-nitrobenz[a]anthracene (7-NBaA), and 6-nitrochrysene (6-NCry), which consist of 1–3 aromatic rings. According to their molecular weight, Fig. 3.18 shows the concentration of individual NPACs in DEPs (<1 μm) of individual driving conditions. For all driving conditions, 7,8-benzoquinoline (7,8-BQ) showed the highest concentration, 5.1–6.0 ng/m³, or 59–72% of the quantified NPACs. The concentration of 7,8-BQ increased with increasing engine loads with the highest concentration under the most demanding driving condition (3000 rpm/100%) (Fig. 3.18). 7,8-BQ was responsible for 66 and 63% of quantified NPACs in ultrafine and accumulation-mode DEPs, respectively. Similar to 7,8-BQ, the concentration of 3-nitrophenanthrene (3-Nphe) also peaked under the same driving condition, up to 2.6 ng/m³.

Interestingly, while 3-Nphe was particularly abundant in the accumulation-mode DEPs under 3000 rpm/100% (Fig. 3.18(d)), only under 1800 rpm/60% was it solely present in ultrafine DEPs (Fig. 3.18(a)). This indicates that 3-Nphe could mainly undergo nucleation under mild driving conditions, while the condensation became more prominent along with an increase in the engine speed and/or engine load. It is worth noting that since the most abundant PAH (phenanthrene) and NPAC (7,8-benzoquinoline and 3-nitrophenanthrene) comprise a similar molecular (3 aromatic-ring) structure (Fig. 3.18). This could evidence the formation of aza arenes (7,8-benzoquinoline) and nitro-PAHs (3-nitrophenanthrene) through respective pyrosynthesis and nitration between PAHs radicals and NO_x radicals under the most strenuous driving condition (3000 rpm/100% load). In addition, because a bay-region like structure of aromatic compounds can impose more genotoxicity and higher tumor-initiating potential compared with other type of PAHs (linear structure) (Upham et al., 1998; Rummel et al., 1999), larger amounts of phenanthrene, 7,8-benzoquinoline and 3-nitrophenanthrene, which contain the bay-region structure, suggest a higher toxic potential in DEPs generating under the largest engine speed and engine load.

Among a few studies on NPACs, Chen et al. (1998) observed strong seasonal variation of atmospheric aza arenes having a total concentration fluctuating between 0.4 and 7.6 ng/m³ in urban atmosphere. They also reported that among the identified NPAC, methylated quinoline isomers had the highest concentration with a concentration ranging from 0.01–2.29 ng/m³ and could mainly originate from combustion of fossil fuel. In addition, Rogge et al. (1993b) found aza arenes

(benzoquinoline, phenanthridine and acridine) in particulate samples collected from exhausts of natural gas combustion in a concentration of 7.4–48.4 pg/kJ. Three nitro-PAHs (9-nitroanthracene, 7-nitrobenz[a]anthracene and 6-nitrochrysene) in DEPs from the medium-duty diesel engine tested in this study were also found by Zielinska et al. (2004b), who measured 6 nitro-PAHs in DEPs by testing a light- and medium-duty diesel vehicles using a transient chassis dynamometer. This indicates that NPACs could be commonly emitted from diesel combustion. Although NPACs were also carried by particulates emitting from gasoline-powered vehicles, their concentrations are usually too low to be detected (Zielinska et al., 2004b). Since 4 of the 9 NPACs identified in this study were also reported in the abovementioned urban ambient environments, it is likely that DEPs could be one of major primary emission sources contributing to atmospheric NAPCs.

Chapter 4

CONCLUSIONS AND FUTURE WORK

4.1 Conclusions

Summary of contributions of this work

The findings of this work directly and indirectly contribute to scientific communities and government bodies, respectively as follows: (1) this study provides direct evidence that simply reducing engine loads can significantly decrease number concentrations, amounts of persistent free radicals and ultrafine-mode metals as well as carbonaceous materials in DEPs; (2) a chromium to iron ratio in DEPs can be used to differentiate emissions of gasoline- vs. diesel-powered vehicles; (3) concentration profiles of identified organics in DEPs provide the first experimental data that the evolution of phenanthrene, 7,8-benzoquinoline, and 3-nitrophenanthrene demonstrate the importance of pyrosynthesis, nitration, and soot formation in diesel engines. Chemical processes observed in coal combustions can be applicable to combustion condition of diesel engines; and (4) the systematically characterized physical and chemical properties of DEPs from on-road medium-duty diesel vehicles can provide a basis to evaluate efficiencies of aftertreatment devices and performance of alternative fuels. Comprehensive analyses of chemical composition of DEPs are particularly important because reducing numbers and mass of DEPs using aftertreatment devices, such as diesel particulate filter (DPF) and diesel oxidation catalyst (DOC), and/or

ultra low sulfur diesel (ULSD) fuel insufficiently evaluates changes in chemical properties (e.g., redox potential) of DEPs.

Specific findings of this work are classified under three components and given below:

(1) Effects of driving conditions on number concentration, EC, OC and persistent free radicals in DEPs

- The number concentration DEP (≤ 400 nm) increased with increasing engine speeds or engine loads, ranging from $2.3\text{--}8.3 \times 10^8$ #/cm³.
- Under the medium engine load (60%), the DEP population surged at around 40–70 nm. Under the full engine load (100%), DEPs showed a distinctive bimodal distribution with a large population peaking in 30–50 nm and 100–400 nm.
- Decreasing the engine load from 100% to 60% reduced (i) total DEP number concentrations for 1.7 times ($8.3\text{--}4.8 \times 10^8$ #/cm³) to >3 times ($7.8\text{--}2.3 \times 10^8$ #/cm³), (ii) DEPs in ultrafine size and 100–400 nm decreased respective 2.5 times ($5.2\text{--}1.9 \times 10^8$ #/cm³) and 6 times ($2.6\text{--}0.4 \times 10^8$ #/cm³) when the engine speed remained at 1800 rpm, (iii) At a high engine speed (3000 rpm), decreasing the engine load from 100% to 60% reduced DEPs larger than 100 nm for more than 3 times ($2.7\text{--}0.8 \times 10^8$ #/cm³), while marginally affected DEPs in ultrafine range, and (iv) significantly decrease persistent free radicals in DEPs for more than 16 times ($186\text{--}11 \times 10^{16}$ #spin/g) under an engine speed

of 1800 rpm, or more than 30 times ($123-4 \times 10^{16}$ #spin/g) under an engine speed of 3000 rpm, and (v) EC and OC in DEPs (smaller than 1 μm) were reduced for at least 3 times ($0.6-0.2 \text{ mg/m}^3$) and more than 2 times ($0.4-0.2 \text{ mg/m}^3$), respectively

- For DEPs smaller than 1 μm , at the maximum engine load, EC and OC consistently peaked at 170–330 nm DEPs of an engine speed of 1800 rpm, or 94–170 nm DEPs of an engine speed of 3000 rpm. The size distribution of EC and OC suggests strong sooting, cluster-cluster soot agglomeration, and organic condensation processes.

(2) Effects of driving conditions on metal contents in DEPs

- Total 18 metals in DEPs were quantified with a concentration ranging from 6.1–7.7 $\mu\text{g/m}^3$. Distribution of metals in ultrafine (<100 nm) and in accumulation-mode DEPs were up to 40% and 76%, respectively.
- When the engine load increased from 60% to 100%, metals in ultrafine DEPs increased from 1.5–2.6 (at the engine speed of 1800 rpm), or 1.6–3.1 $\mu\text{g/m}^3$ (at the maximum engine speed of 3000 rpm) and peaked at DEP < 66 nm. This indicates that under higher engine loads, metals may preferably participate in homogeneous nucleation.
- The opposite trends in size distribution of metals and EC in DEPs from tailpipes provide the first tailpipe evidence that metals may catalyze oxidation of DEPs during combustion.

- An increase in the engine load enhanced the averaged cumulative fraction of five most abundant metals (Fe, Li, Cr, V and Pb) in ultrafine DEPs for 1.4–1.9 times, changing from 24–34% (for 1800 rpm) and 22–42% (for 3000 rpm).
- Among the identified metals, Fe ($2.3\text{--}3.9\ \mu\text{g}/\text{m}^3$) was the most abundant species (>38%) among the total quantified metals in DEPs (34–1000 nm), followed by Pb (5–15%), Cr (9–12%), V (9–10%), and Li (8–15%), which were mainly originated from diesel fuels and through engine wear.
- Cr-to-Fe ratio (0.08–0.29) of DEPs was at least 2 times higher than that of particulates from gasoline exhaust (0.02–0.04), which could be adopted as a fingerprint differentiating diesel- vs. gasoline-emission origins at locations mainly under traffic influence.

(3) Effects of driving conditions on organic compounds in DEPs

- Concentration of the identifiable organic compounds in DEPs (<1 μm) ranged from 12.4 to around $20\ \mu\text{g}/\text{m}^3$, which accounts for 2–10% of the total organic compounds.
- When the engine speed and load increased from 1800 rpm/60% to 3000 rpm/100%, the fraction of identifiable organic compounds in DEPs (<1 μm) reduced for > 3 times, indicating stronger formation of unresolved organic compounds (such as humic like substances) under more fuel injection, higher combustion temperature and larger pyrolysis zone in diesel engines.

- For all four driving conditions, concentration of identifiable organic compounds in DEPs ultrafine (34–94 nm) and accumulation (94–1000 nm) modes ranged from 2.9–5.7 $\mu\text{g}/\text{m}^3$ and 9.5–16.4 $\mu\text{g}/\text{m}^3$, respectively; a larger amount (70–83%) of total identifiable organics in DEPs (<1 μm) were allocated in accumulation-mode DEPs.
- The identified organic compounds in DEPs (<1 μm) were classified into eleven classes: alkanes, alkenes, alkynes, aromatic hydrocarbons, carboxylic acids, esters, ketones, alcohols, ethers, nitrogen-containing compounds, and sulfur-containing compounds. The concentration of identified non-oxygen-containing organics in DEPs ranged from 8.4–17.9 $\mu\text{g}/\text{m}^3$, 2 times more than oxygen-containing organics (0.9–4.5 $\mu\text{g}/\text{m}^3$). More than 80% of oxygen-containing organics (except DEPs of 1800 rpm/100%) and more than 60% of non-oxygen-containing organics were found in accumulation-mode DEPs.
- As a function of driving conditions, the non-oxygen-containing organics exhibited a reversed concentration trend to the oxygen-containing organics in DEPs (<1 μm). The driving condition with the highest engine load and speed (3000 rpm/100%) could encourage oxidation of non-oxygen-containing organics, resulting in a larger concentration of oxygen-containing organics in DEPs, with a highest concentration of 3.1 ($\mu\text{g}/\text{m}^3$).
- For all driving conditions, alkane class consistently showed the highest concentration (8.3 $\mu\text{g}/\text{m}^3$ to 18.0 $\mu\text{g}/\text{m}^3$) among the identified organic classes in DEPs, followed by carboxylic acids, esters, ketones and alcohols. The

concentration of alkanes also accounted for more than 60% (or up to 95%) of identified organics in DEPs (<1 μm). The amount of alkanes in DEPs (<1 μm) generally peaked between C19–C25. Among the 17 alkane species identified in DEPs (<1 μm), C19 exhibited the highest concentration for all driving conditions, except that with the highest engine speed and load, which peaked at C21.

- Twelve polycyclic aromatic hydrocarbons (PAHs) in DEPs (<1 μm) were identified with a total concentration ranging from 37.9–174.8 ng/m^3 . When the engine load increased from 60% to 100%, more than 2 times of increase in the PAHs in DEPs (<1 μm) could result from stronger pyrosynthesis in diesel engines.
- Similar to the alkane class, quantified PAHs were mainly distributed in the accumulation-mode DEPs; in the ultrafine and accumulation-mode DEPs, the concentration of PAHs ranged from 10.8–23.2 ng/m^3 and 16.3–119.0 ng/m^3 , respectively.
- When the engine load was increased to the maximum, phenanthrene exhibited the highest concentration along with most substantial increase (up to 10 times). The concurrent increase in elemental carbon (relevant to soot) in DEPs (<1 μm) supports that phenanthrene is an important intermediate for PAHs growth and soot formation
- Nine NPACs were identified in DEPs (<1 μm) with a total concentration ranging from 7.0–10.3 ng/m^3 . Similar to the trend in quantified PAHs, the

identified NPACs are more abundant in accumulation-mode DEPs of driving conditions, in particular, under the full engine load. The identified NPACs are most abundant (6.4–7.5 ng/m³) in accumulation-mode DEPs from driving condition under the maximum engine load, which could encourage formation of NPACs through pyrosynthesis of PAHs and NO_x.

- The nine identified NPACs comprise four aza arenes and five nitroarenes with a respective concentration of 5.4–7.3 ng/m³ and 1.3–3.1 ng/m³. For all driving conditions, 7,8-benzoquinoline (7,8-BQ) showed the highest concentration, 5.1–6.0 ng/m³, or 59–72% of the quantified NPACs. The concentration of 7,8-BQ increased with increasing engine loads with the highest concentration under the most demanding driving condition (3000 rpm/100%). 7,8-BQ was responsible for 66 and 63% of quantified NPACs in ultrafine and accumulation-mode DEPs, respectively.
- The most abundant PAH (phenanthrene) and NPACs (7,8-benzoquinoline and 3-nitrophenanthrene) comprise a similar molecular (3 aromatic-ring) structure, which could evidence the formation of aza arenes (7,8-benzoquinoline) and nitro-PAHs (3-nitrophenanthrene) through respective pyrosynthesis and nitration between PAHs radicals and NO_x radicals under the highest engine speed and engine load (3000 rpm/100% load).

4.1 Recommended Future Work

To further understand behavior of DEPs under various driving conditions change and to evaluate effects of emissions from on-road diesel-powered vehicles on air quality, the future work expanding from the data presented in this study include:

(1) Effects of cold and warm idle condition on DEP properties

Design of on-road transportation and congested traffic conditions in urban areas easily cause on-road vehicles operating in frequent idle conditions. Since idle conditions is accompanied with unique combustion conditions, systematic characterization of DEP properties from engines under idle and transient patterns representative of on-road conditions is needed. Concurrent monitoring of gaseous pollutants will provide complimentary understanding of how gas-particle partitioning correlating with DEP properties.

(2) Effects of DEPs on air quality and public health

In addition to characterizing DEPs emitted from tailpipes, on-road sampling or near road sampling is needed to assess how primary emissions may affect air quality and public health. On-road analysis, taking substantial dilution effects into account, would provide realistic information of subsequent transport and transformation of initially emitted DEPs. This will lend information to systematically assess potential toxicity of diesel exhausts based on chemical composition in DEPs undergoing aging processes.

(3) Evaluation of removal efficiencies of aftertreatment devices

Employing the current study as the basis, removal efficiencies of various aftertreatment devices will be evaluated by comprehensively examining regulated components (such as CO, NO_x, HC and TPM) and unregulated chemical species from tailpipes. This future work could also provide important information for manufactures to advance vehicle technology and for governments to establish prospective policies. In addition, to reduce formation of soot particles, effects of amount of diesel fuel injected into engine on resultant amounts of DEPs would be evaluated.

BIBLIOGRAPHY

- Abdul-Khalek, I.S, Kittleson, D.B., Graskow, B.R., Wei, Q., Brear, F., 1998. Diesel exhaust particle size: measurement issues and trends. Society of Automotive Engineers, Warrendale, PA, 980525, 1-14.
- Abrantes, R., Assunção, J.V., Pesquero, C.R., 2004. Emissions of polycyclic aromatic hydrocarbons from light-duty diesel vehicles exhaust. *Atmospheric Environment* 38, 1631-1640.
- Abi-Aad, E., Cousin, R., Pruvost, C., Courcot, D., Noirot, R., Rigaudeau, C., Aboukaïs, A., 2001. EPR investigation and reactivity of diesel soot activated (or not) with cerium compounds. *Topics in Catalysis* 16/17, 263-268.
- Ålander, T.J.A., Leskinen, A.P., Raunemaa, T.M., Rantanen, L., 2004. Characterization of diesel particles: effects of fuel reformulation exhaust aftertreatment and engine operation on particle carbon composition and volatility. *Environmental Science and Technology* 38, 2707-2714.
- Allègre, C., Manhès, G., Lewin, E., 2001. Chemical composition of the Earth and the volatility control on planetary genetics. *Earth and Planetary Science Letters* 185, 49-69.
- Assanis, D.N., Filipi, Z.S., Fiveland, S.B., Syrimis, M., 2003. A prediction ignition delay correlation under steady-state and transient operation of a direct injection diesel engine. *Journal of Engineering for Gas Turbines and Power* 125, 450-457.
- Bamford, H.A., Backer, J.E., 2003. Nitro-polycyclic aromatic hydrocarbon concentrations and sources in urban and suburban atmospheres of the Mid-Atlantic region. *Atmospheric Environment* 37, 2077-2091.
- Barbella, R., Bertoli, C., Ciajolo, A., D'anna, A., 1990. Behavior of a fuel oil during the combustion cycle of a direct injection diesel engine. *Combustion and Flame* 82, 191-198.
- Baumgard, K.J., Johnson, J.H., 1996. The effect of fuel and engine design on diesel exhaust particle size distributions. Society of Automotive Engineers, Warrendale, PA, 960131, 37-50.
- Birch, M.E., Cary, R.A., 1996. Elemental carbon-based method for monitoring occupational exposures to particulate diesel exhaust. *Aerosol Science and Technology* 25, 221-241.
- Birch, M.E., 1998. Analysis of carbonaceous aerosols: interlaboratory comparison. *Analyst* 123, 851-857.

- Birch, M.E., Dahmann, D., Fricke, H.H., 1999. Comparison of two carbon analysis methods for monitoring diesel particulate levels in mines. *Journal of Environmental Monitoring* 1, 541-544.
- Bockhorn, H. (Eds.), 1994. Soot formation in combustion—mechanisms and models. Springer-Verlag, Heidelberg, Germany.
- Burtscher, H., 1992. Measurement and characteristics of combustion aerosols with special consideration of photoelectric charging and charging by flame ions. *Journal of Aerosol Science* 23, 549-595.
- Cachier, H., Bremond, M., Buat-ménard, P., 1989. Determination of atmospheric soot carbon with a simple thermal method. *Tellus* 41B, 379-390.
- Cadle, S.H., Mulawa, P.A., Hunsanger, E.C., Nelson, K., Ragazzi, R.A., Barrett, R., Gallagher, G.L., Lawson, D.R., Knapp, K.T., Snow, R., 1999. Composition of light-duty motor vehicle exhaust particulate matter in the Denver, Colorado area. *Environmental Science and Technology* 33, 2328-2339.
- Cadle, S.H., Mulawa, P.A., Groblicki, P.J., Laroo, C., Ragazzi, R.A., Nelson, K., Gallagher G., Zielinska B., 2001. In-use light-duty gasoline vehicle particulate matter emissions on three driving cycles. *Environmental Science and Technology* 35, 26-32.
- Cadle, S.H., Groblicki, P.J., Mulawa, P.A., 1983. Problems in the sampling and analysis of carbon particulate. *Atmospheric Environment* 17, 593-600.
- Campbell, R.M., Lee, M.L., 1984. Capillary Column Gas Chromatographic Determination of Nitro Polycyclic Aromatic Compounds in Particulate Extracts, *Analytical Chemistry* 56, 1026-1030.
- Carey, F.A. (Eds), 2006. Organic chemistry, McGraw-hill international edition, Singapore
- Cecinato, A., Marino, F., Filippo, P.D., Lepore, L., Possanzini, M., 1999. Distribution of n-alkanes, polyunclear aromatic hydrocarbons and nitrated polyunclear aromatic hydrocarbons between the fine and coarse fractions of inhalable atmospheric particulates. *Journal of Chromatography A* 846, 255-264.
- Chen, H.Y., Preston, M.R., 1998. Azaarenes in the aerosol of an urban atmosphere. *Environmental Science and Technology* 32, 577-583.
- Chen, S.J., Liao, S.H., Jian, W.J., Lin, C.C., 1997. Particle size distribution of aerosol carbons in ambient air. *Environmental International* 23, 475-488.
- Chiu, C., Miles, W., 1996. An Improved Method for Nitro-PAH Analysis, *Polycyclic Aromatic Compounds* 9, 307-314.

- Collier, A.R., Rhead, M.M., Trier, C.J., Bell, M.A., 1995. Polycyclic aromatic compound profiles from a light-duty direct-injection diesel engine. *Fuel* 74, 362-367.
- Comité des Constructeurs Français d'Automobiles (Eds.), 2006. Annual Report.
- Cormier, S.A., Lomnicki, S., Backes, W., Dellinger, B., 2006. Origin and health impacts of emissions of toxic by-products and fine particles from combustion and thermal treatment of hazardous wastes and materials. *Environmental Health Perspectives* 114, 810-817.
- Courtes, R.J., 1990. Interlaboratory analysis of carbonaceous aerosol samples. *Aerosol Science and Technology* 12, 114-121.
- Dagel, J.F., Brady, R.N. (Eds.), 1998. Diesel engine and fuel system repair. Prentice Hall, Upper Saddle River, New Jersey, Columbus, Ohio.
- Degobert, P. (Eds), 1995. Automobiles and pollution Society of Automotive Engineers, Warrendale, PA
- Dellinger, B., Pryor, W.A., Cueto, R., Squadrito, G.L., Hegde, V.H., Deutsch, A., 2001. Role of free radicals in the toxicity of airborne fine particulate matter. *Chemical Research in Toxicology* 14, 1371-1377.
- Denis, J., Briant, J., Hipeaux, J.-C. (Eds.), 2000. Lubricant properties analysis and testing. Editions Technip, Paris, France.
- Denis, M.J., Fernández, P.C., Winer, A.M., Bulter, J.W., Jesion, G., 1994. Effects of in-use driving conditions and vehicle/engine operating parameters on "off-cycle" events: comparison with federal test procedure conditions. *Journal of the Air and Waste Management Association* 44, 31-38.
- Devos, O., Combet, E., Tassel, P., Paturel, L., 2006. Exhaust emissions of PAHs of passenger cars. *Polycyclic Aromatic Compounds* 26, 69-78.
- Donaldson, K., Li, X.Y., MacNee, W., 1998. Ultrafine (nanometer) particle mediated lung injury. *Journal of Aerosol Science* 29, 553-560.
- Douce, D.S., Clench, M.R., Cooke, M., Wang, J., 1997. Evidence for the adsorption of nitro polycyclic aromatic hydrocarbons by tree bark, *Journal of Chromatography A* 786, 275-283.
- Dwivedi, D., Agarwal, A.K., Sharma, M., 2006. Particulate emission characterization of a biodiesel vs diesel-fuelled compression ignition transport engine: A comparative study. *Atmospheric Environment* 40, 5586-5595.
- Eom, M.D., Lee, Y.J., Jang, Y.G., Sunwoo, M.H., 2001. A study on the evaluation of emitted pollutants from vehicles. Final Research Report; Transportation Pollution Research Center, National Institute of Environment Research, Korea.

- European Automobile Manufacturers Association (ACEA) (Eds.), 2006. New motor vehicle registrations statistics report, European Union.
- Fleurat-Lessard, P., Pointet, K., Renou-Gonnord, M.F., 1999. Quantitative determination of PAHs in diesel engine exhausts by GC-MS. *Journal of Chemical Education* 76, 962-965.
- Geller, M.D., Ntziachristos, L., Mamakos, A., Samaras, Z., Schmitz, D.A., Froines, J.R., Sioutas, C., 2006. Physicochemical and redox characteristics of particulate matter (PM) emitted from gasoline and diesel passenger cars. *Atmospheric Environment* 40, 6988-7004.
- Ghigo, G., Causà M., Maranzana, A., Tonachini, G., 2006. Aromatic hydrocarbon nitration under tropospheric and combustion conditions. A theoretical mechanistic study. *Journal of Physical Chemistry A* 110, 13270-13282.
- Ghio, A.J., Stonehuerner, J., Pritchard, R.J., Piantadosi, C.A., Quigley, D.R., Dreher, K.L., Costa, D.L., 1996. Humic-like substances in air pollution particulates correlate with concentrations of transition metals and oxidant generation. *Inhalation Toxicology* 8, 479-494.
- Gillies, J.A., Gertler, A.W., Sagebiel, J.C., Dippel, W.A., 2001. On-road particulate matter (PM_{2.5} and PM₁₀) emissions in the Sepulveda tunnel Los Angeles California. *Environmental Science and Technology* 35, 1054-1063.
- Groose, M., Sakurai, H., Savstrom, J., Stolzenburg, M.R., Watts, Jr.W.F., Morgan, C.G., Murray, I.P., Twigg, M.V., Kittelson, D.B., McMurry, P.H., 2006. Chemical and physical properties of ultrafine diesel exhaust particles sampled downstream of a catalytic trap. *Environmental Science and Technology* 40, 5502-5507.
- Groves, J., Cain, J.R., 2000. A survey of exposure to diesel engine exhaust emissions in the workplace. *The Analysis of Occupational Hygiene* 44, 435-447.
- Guilemin, M., Cachier, H., Chini, C., Dabill, D., Dahmann, D., Diebold, F., Fischer, H.A., Fricke, H.J., Groves, A., Hebisch, R., Houpillart, M., Israel, G., Schlums, C., Sutter, E., Tucek, E., 1997. International round robin tests on the measurement of carbon in diesel exhaust particulates. *International Archives of Occupational and Environmental Health* 70, 161-172.
- Handa, T., Tsuneyuki, Y., Makoto, O., Yoshiharu, H., 1983. Detection and average content levels of carcinogenic and mutagenic compounds from the particulates on diesel and gasoline engine mufflers. *Environmental International* 9, 335-341.
- Henein, N.A., 1976. Analysis of pollutant formation and control and fuel economy in diesel engines, *Progress in Energy and Combustion Science* 1, 165-207.

- Heo, Y., Saxon, A., Hankinson, O., 2001. Effect of diesel exhaust particles and their components on the allergen-specific IgE and IgG1 response in mice. *Toxicology* 159, 143-158.
- Hering, S.V., Appel, B.R., Cheng, W., Salaymeh, F., Cadle, S.H., Mulawa, P.A., Cahill, T.A., Eldred, R.A., Surovik, M., Fitz, D., Howes, J.E., Knapp, K.T., Leonard, Turpin, B.J., Huntzicker, J.J., Zhang, X.Q., McMurry, P.H., 1990. Comparison of sampling methods for carbonaceous aerosols in ambient air, *Aerosol Science and Technology* 12, 200-213.
- Higgins, K.J., Jung, H.J., Kittleson, D.B., Roberts, J.T., Zachariah, M.R., 2003. Kinetics of diesel nanoparticle oxidation. *Environmental Science and Technology* 37, 1949-1954.
- Hildemann, L.M., Markowski, G.R., Cass, G.R., 1991. Chemical composition of emission from urban sources of fine organic aerosol. *Environmental Science and Technology* 25, 744-759.
- Hirano, S., Furuyama, A., Koike, E., Kobayashi, T., 2003. Oxidative-stress potency of organic extracts of diesel exhaust and urban fine particles in rat heart microvessel endothelial cells. *Toxicology* 187, 161-170.
- Holmén, B.A., Ayala, A., 2002. Ultrafine PM emissions from natural gas, oxidation-catalyst diesel, and particle-trap diesel heavy-duty transit buses. *Environmental Science and Technology* 36, 5041-5050.
- Holmes, D.R., Strang, A., White, C.H., 1990. Materials selection and R&D programme requirements. *Diesel Engine Combustion Chamber Materials for Heavy Fuel Operation*, Paper 4, 39-46.
- Hu, C.W., Chao, M.R., Wu, K.Y., Chang-Chien, G.P., Lee, W.J., Chang, L.W., Lee, W.S., 2003. Characterization of municipal airborne particulate metals in the surroundings of a municipal waste incinerator in Taiwan. *Atmospheric Environment* 37, 2845-2852.
- Inoue, M., Murase, A., Yamamoto, M., Kubo, S., 2006. Analysis of volatile nanoparticles emitted from diesel engine using TOF-SIMS and metal-assisted SIMS (MetA-SIMS). *Applied Surface Science* 252, 7014-7017.
- Jacobson, M.Z., 2002. Control of fossil-fuel particulate black carbon and organic matter possibly the most effective method of slowing global warming. *Journal of Geophysical Research* 107 (D19) : Art. No. 4410.
- Japar, S.M., Szkarlat, A.C., Robert, A. Gorse, Jr, 1984. Comparison of solvent extraction and thermal-optical carbon analysis methods. *Environmental Science and Technology* 18, 231-234.
- Kadkhoda, K., Pourpak, Z., Pourfathallah, A.A., Kazemnejad, A., 2004. The ex vivo study of synergistic effects of polycyclic aromatic hydrocarbon benzo(a)pyrene

- with ovalbumin on systemic immune response by oral route. *Toxicology* 199, 261-265.
- Kagawa, J., 2002. Health effects of diesel exhaust emissions—a mixture of air pollutants of worldwide concern. *Toxicology* 181-182, 349-353.
- Kamimoto, T., Kobayashi, H., 1991. Combustion process in diesel engines. *Progress in Energy and Combustion Science* 17, 163-189.
- Kelly, N.A., Groblicki, P.J., 1993. Real-world emissions from a modern production vehicle driven in Los Angeles. *Journal of the Air and Waste Management Association* 43, 1351-1357.
- Kerminen, V.M., Mäkelä, T.E., Ojanen, C.H., Hillamo, R.E., Vilhunen, J.K., Rantanen, L., Havers, N., Bohlen, A.V., Klockow, D., 1997. Characterization of the particulate phase in the exhaust from a diesel car. *Environmental Science and Technology* 31, 1883-1889.
- Kim, G.H. (Eds), 2004. *Automobile Technology*. Golden Bell, Hankuk Automobile College in Korea.
- Kim, S.H., Fletcher, R.A., Zachariah, M.R., 2005. Understanding the difference in oxidative properties between flame and diesel soot nanoparticles: The role of metals. *Environmental Science and Technology* 39, 4021-4026.
- Kim, W.S., Kim, S.H., Lee, D.W., Lee, S.H., Lim, C.S., Ryu, J.H., 2001. Size analysis of automobile soot particles using field-flow fractionation. *Environmental Science and Technology* 35, 1005-1012.
- Kim, Y.P., Moon, K.C., Lee, J.H., Baik, N.J., 1999. Concentrations of carbonaceous species in particles at Seoul and Cheju in Korea. *Atmospheric Environment* 33, 2751-2758.
- Kittelson, D.B., Watts, W.F., Johnson, J.P., 2002. Diesel aerosol sampling methodology. CRC E-43 Final Report, Coordinating Research Council, Alpharetta, GA.
- Kittelson, D.B., Watts, W.F., Johnson, J.P., 2004. Nanoparticle emissions on Minnesota highways. *Atmospheric Environment* 38, 9-19.
- Kittelson, D.B., Watts, W.F., Johnson, J.P., Rowntree, C., Payne, M., Goodier, S., Warrens, C., Preston, H., Zink, U., Ortiz, M., Goersmann, C., Twigg, M.V., Walker, A.P., Caldow, R., 2006. On-road evaluation of two diesel exhaust aftertreatment devices. *Journal of Aerosol Science* 37, 1140-1151.
- Kleeman, M.J., Schauer, J.J., Cass, G.R., 2000. Size and composition distribution of fine particulate matter emitted from motor vehicles. *Environmental Science and Technology* 34, 1132-1142.

- Korea Automobile Manufacturers Association (KAMA) (Eds), 2005. Korean automobile industry annual reports, Korea.
- Korea Ministry of Environment (Eds.), 2007. Annual Report.
- Krivácsy, Z., Gelencsér, A., Kiss, G., Mézáros, E., Molnár, Á., Hoffer, A., Mészáros, T., Sárvári, Z., Temesi, D., Varga, B., Baltensperger, U., Nyeki, S., Weinhartner, E., 2001. Study on the chemical character of water soluble organic compounds in fine atmospheric aerosol at the Jungfraujoch. *Journal of Atmospheric Chemistry* 39, 235-259.
- Kwon, S.B., Lee, K.W., Saito, K., Shinozaki, O., Seto, T., 2003. Size-dependent volatility of diesel nanoparticles: chassis dynamometer experiments. *Environmental Science and Technology* 37, 1794-1802.
- Lala, L.L., Artaxo, P., Martinelli, L.A., Camargo, P.B., Victoria, R.L., Ferraz, E.S.B., 2005. Properties of aerosols from sugar-cane burning emissions in Southeastern Brazil. *Atmospheric Environment* 39, 4627-4637
- Ledesma, E.B., Marsh, N.D., Sandrowitz, A.K., Wornat, M.J., 2002. Global kinetic rate parameters for the formation of polycyclic aromatic hydrocarbons from the pyrolysis of catechol, a model compound representative of solid fuel moieties. *Energy & Fuels* 16, 1331-1336.
- Lee, D., Miller, A., Kittleson, D., Zachariah, M.R., 2006. Characterization of metal-bearing diesel nanoparticles using single-particle mass spectrometry. *Journal of Aerosol Science* 37, 88-110.
- Liang, F., Lu, M., Keener, T.C., Liu, Z., Khang, S.J., 2005. The organic composition of diesel particulate matter, diesel fuel and engine oil of a non-road diesel generator. *Journal of Environmental Monitoring* 7, 983-988.
- Li, H., Banner, C.D., Mason, G.G., Westerholm, R., Rafter, J.J., 1996. Determination of polycyclic aromatic compounds and dioxin receptor ligands present in diesel exhaust particulate extracts. *Atmospheric Environment* 30, 3537-3543.
- Li, H., Banner, C.D., Westerholm, R., Almén, J., Grägg, K., 1994. Chemical Characterization of Exhaust Emissions Originating From the Regeneration Mode of A Diesel Particulate Trap. *Fuel* 73, 11-16.
- Li, H., Westerholm, R., 1994. Determination of mono- and di-nitro polycyclic aromatic hydrocarbons by on-line reduction and high-performance liquid chromatography with chemiluminescence detection. *Journal of Chromatography A* 664, 177-182.
- Lim, H.J., Turpin, B.J., Russell, L.M., Bates, T.S., 2003. Organic and elemental carbon measurements during ACE-Asia suggest a longer atmospheric lifetime for elemental carbon. *Environmental Science and Technology* 37, 3055-3061.

- Lin, C.C., Chen, S.J., Huang, K.L., Hwang, W.I., Chang-Chien, G.P., Lin, W.Y., 2005. Characteristics of metals in nano/ultra/fine/coarse particles collected beside a heavily trafficked road. *Environmental Science and Technology* 39, 8113-8122.
- Lingard, J.J.N., Tomlin, A.S., Clarke, A.G., Healey, K., Hay, A.W.M., Wild, C.P., Routledge, M.N., 2005. A study of trace metal concentration of urban airborne particulate matter and its role in free radical activity as measured by plasmid strand break assay. *Atmospheric Environment* 39, 2377-2384.
- Litton, C.D., 2002. Studies of the measurement of respirable coal dusts and diesel particulate matter. *Measurement Science and Technology* 13, 365-374.
- Lombaert, K., Moyne, L., Maleissye, J.T., Amouroux, J., 2006. Experimental study of PAH in engine soot by isotopic tracing. *Combustion Science and Technology* 178, 707-728.
- Lough, G.C., Schauer, J.J., Park, J.S., Shafer, M.M., Deminter, J.T., Weinstein, J.P., 2005. Emissions of metals associated with motor vehicle roadways. *Environmental Science and Technology* 39, 826-836.
- Lowenthal, D.H., Barbara, Z., Judith, C C., John, G.W., 1994. Characterization of heavy-duty diesel vehicle emissions, *Atmospheric Environment* 28,731-743.
- Marcazzan, G.M., Vaccaro, S., Valli, G., Vecchi, R., 2001. Characterisation of PM10 and PM2.5 particulate matter in the ambient air of Milan (Italy). *Atmospheric Environment* 35, 4639-4650. Marino F., Cecinato A. and Siskos P. A., Nitro-PAH in Ambient Particulate Matter in the Atmosphere of Athens, *Chemosphere*, 40, pp. 533-537. 2000.
- Marino, F., Cecinato, A., Siskos, P.A., 2000. Nitro-PAH in Ambient Particulate Matter in the Atmosphere of Athens. *Chemosphere* 40, 533-537.
- Marinov, N.M., Pitz, W.J., Westbrook, C.K., Vincitore, A.M., Castaldi, M.J., Senkan, S.M., Melius, C.F., 1998, Aromatic and polycyclic aromatic hydrocarbon formation in a laminar premixed n-butane flame. *Combustion and Flame* 114, 192-213.
- Marr, L.C., Kirchstetter, W., Harley, R.A., 1999. Characterization of Polycyclic Aromatic Hydrocarbons in Motor Vehicle Fuels and Exhaust Emissions. *Environmental Science and Technology* 33, 3091-3099.
- Marsh, N.D., Ledesma, E.B., Sandrowitz, A.K., Wornat, M.J., 2004. Yields of polycyclic aromatic hydrocarbons from the pyrolysis of catechol [ortho-dihydroxybenzene]: temperature and residence time effects. *Energy & Fuels* 18, 209-217.
- Maskos, Z., Khachatryan, L., Cueto, R., Pryor, W.A., Dellinger, B., 2005. Radicals from the Pyrolysis of Tobacco. *Energy & Fuels* 19, 791-799.

- Mastral, A.M., Callén, M.S., 2000. A review on polycyclic aromatic hydrocarbon (PAH) emissions from energy generation. *Environmental Science and Technology* 34, 3051-3057.
- Mathis, U., Kaegi, R., Mohr, M., Zenobi, R., 2004. TEM analysis of volatile nanoparticles from particle trap equipped diesel and direct-injection spark-ignition vehicles. *Atmospheric Environment* 38, 4347-4355.
- Miller, A., Ahlatrand, G., Kittelson, D., Zachariah, M., 2007. The fate of metal (Fe) during diesel combustion: Morphology, chemistry, and formation pathways of nanoparticles. *Combustion and Flame* 149 (1-2), 129-143.
- Mohr, M., Forss, A.-M., Lehmann, U., 2006. Particle emissions from diesel passenger cars equipped with a particle trap in comparison to other technologies. *Environmental Science and Technology* 40, 2375-2383.
- Molinelli, A.R., Madden, M.C., McGee, J.K., Stonehuerner, J.G., Ghio, A.J., 2002. Effect of metal removal on the toxicity of airborne particulate matter from the Utah valley. *Inhalation Toxicology* 14, 1069-1086.
- Murahashi, T., Tsuruga, F., Sasaki, S., 2003. An automatic method for the determination of carcinogenic 1-nitropyrene in extracts from automobile exhaust particulate matter. *Analyst* 128, 1346-1351.
- Na, K., Aniket, A.S., Chen, S., David, R., Cocker III, 2004. Primary and secondary carbonaceous species in the atmosphere of western riverside county, California. *Atmospheric Environment* 38, 1345-1355.
- Novakov, T., Ramanathan, V., Hansen, J.E., Kirchstetter, T.W., Sato, M., Sinton, J.E., Sathaye J.A., 2003. Large historical changes of fossil-fuel black airborne aerosols. *Geophysical Research Letters* 30, 57:1-4.
- Nygaard, U.C., Ormstad, H., Aase, A., Løvik, M., 2005a. The IgE adjuvant effect of particles: characterization of the primary cellular response in the draining lymph node. *Toxicology* 206, 181-193.
- Nygaard, U. C., Alberg, T., Bleumink, R., Aase, A., Dybing, E., Pieters, R., Løvik, M., 2005b. Ambient air particles from four European cities increase the primary cellular response to allergen in the draining lymph node. *Toxicology* 207, 241-254.
- Ohta, S., Okita, T., 1990. A chemical characterization of atmospheric aerosol in Sapporo. *Atmospheric Environment* 24A, 815-822.
- Okamura, K., Kizu, R., Toriba, A., Murahashi, T., Mizokami, A., Burnstein, K.L., Klinge, C.M., Hayakawa, K., 2004. Antiandrogenic activity of extracts of diesel exhaust particles emitted from diesel-engine truck under different engine loads and speeds. *Toxicology* 195, 243-254.

- Ozaki, H., Watanabe, I., Kuno, K., 2004. Investigation of the heavy metal sources in relation to automobiles. *Water, Air, and Soil Pollution* 157, 209-223.
- Pan, C.J., Schmitz, D., Cho, A.K., Froines, J., Fukuto, M., 2004. Inherent redox properties of diesel exhaust particles: catalysis of the generation of reactive oxygen species by biological reductants. *Toxicological Sciences* 81, 225-232.
- Park, S.S., Pancras, J.P., Ondov, J.M., Robinson, A., 2006. Application of the pseudo-deterministic receptor model to resolve power plant influences on air quality in Pittsburgh. *Aerosol Science and Technology* 40, 833-897.
- Park, S.S., Kim, Y.J., Fung, K., 2001. Characteristics of PM_{2.5} carbonaceous aerosol in the Sihwa industrial area, South Korea. *Atmospheric Environment* 35, 657-665.
- Paschke, T., Steven, B.H., David, J.M., 1992. Supercritical fluid extraction of nitrated polycyclic aromatic hydrocarbons and polycyclic aromatic hydrocarbons and polycyclic aromatic hydrocarbons from diesel exhaust particulate matter, *Journal of Chromatography* 609, 333-340,
- Petrakis, L., Grandy, D.W. (Eds.), 1983. *Free radicals in coals and synthetic fuels*. Elsevier Amsterdam, Netherlands.
- Puri, I.K. (Eds.), 1993. *Environmental implications of combustion process*. CRC Press Inc. Boca Raton, Florida, USA.
- Reddy, M.S., Basha, S., Joshi, H.V., Jha, B., 2005. Evaluation of the emission characteristics of trace metals from coal and fuel oil fired power plants and their fate during combustion. *Journal of Hazardous Materials B123*, 242-249.
- Rhead, M.M., Trier, C.J., 1992. Fuel Residues and Organic Combustion Products in Diesel Exhaust Emissions: Sources, Sampling and Analysis. *Trends in Analytical Chemistry* 11, 255-258.
- Richter, H., Granata, S., Green, W.H., Howard, J.B., 2005. Detailed modeling of PAH and soot formation in a laminar premixed benzene/oxygen/argon low-pressure flame. *Proceedings of the Combustion Institute* 30, 1397-1405.
- Richter, H., Howard, J.B., 2000. Formation of polycyclic aromatic hydrocarbons and their growth to soot—a review of chemical reaction pathways. *Progress in Energy and Combustion Science* 26, 565-608.
- Riddle, S.G., Robert, M.A., Jakobert, C., Hannigan, M.P., Kleeman, M.J., 2007. Size distribution of trace organic species emitted from heavy-duty diesel vehicles. *Environmental Science and Technology* 41, 1962-1969.
- Rogge, W.F., Hildemann, L.M., Mazurek, M.A., Cass, G.R., 1993a. Sources of fine organic aerosol. 2. Noncatalyst and catalyst-equipped automobiles and heavy-duty diesel trucks. *Environmental Science and Technology* 27, 636-651.

- Rogge, W.F., Hildemann, L.M., Mazurek, M.A., Cass, G.R., 1993b. Sources of fine organic aerosol. 5. Natural gas home appliances. *Environmental Science and Technology* 27, 2736-2744.
- Rummel, A.M., Trosko, J.E., Wilson, M.R., Upham, B.L., 1999. Polycyclic aromatic hydrocarbons with bay-like regions inhibited gap junctional intercellular communication and stimulated MAPK activity. *Toxicological Sciences* 49, 232-240.
- Salma, I., Chi, X., Maenhaut, W., 2004. Elemental and organic carbon in urban canyon and background environments in Budapest, Hungary. *Atmospheric Environment* 38, 27-36.
- Sato, H., Onose, J., Toyoda, H., Toida, T., Imanari, T., Sagai, M., Nishimura, N., Aoki, Y., 2001. Quantitative changes in glycosaminoglycans in the lungs of rats exposed to diesel exhaust. *Toxicology* 166, 119-128.
- Schauer, J.J., Kleeman, M.J., Cass, G.R., Simoneit, B.R.T., 1999. Measurement of emission from air pollution sources. 2. C₁ through C₃₀ organic compounds from medium duty diesel trucks. *Environmental Science and Technology* 33, 1578-1587.
- Schauer, J.J., Michael, J.K., Cass, G.R., Bernd, R.T.S., 2002. Measurement of emission from air pollution sources. 5. C₁-C₃₂ organic compounds from gasoline-powered motor vehicles. *Environmental Science and Technology* 36, 1169-1180.
- Schneider, J., Hock, N., Weimer, S., Borrmann, S., 2005. Nucleation particles in diesel exhaust: composition inferred from in situ mass spectrometric analysis. *Environmental Science and Technology* 39, 6153-6161.
- See, S.W., Balasubramanian, R., Rianawati, E., Karthikeyan, S., Streets, D.G., 2007. Characterization and source apportionment of particulate matter $\leq 2.5 \mu\text{m}$ in Sumatra, Indonesia, during a recent peat fire episode. *Environmental Science and Technology* 41, 3488-3494.
- Shah, S.D., Cocker III, David, R., Miller, J.W., Norbeck, J.M., 2004. Emission rates of particulate matter and elemental and organic carbon from in-use diesel engines. *Environmental Science and Technology* 38, 2544-2550.
- Shah, S.D., Ogunyoku, T., Miller, J.W., Cocker III, D.R., 2005. On-road emission rates of PAH and n-alkane compounds from heavy-duty diesel vehicles. *Environmental Science and Technology* 39, 5276-5284.
- Shi, J.P., Mark, D., Harrison, R.M., 2000. Characterization of particles from a current technology heavy-duty diesel engine. *Environmental Science and Technology* 34, 748-755.

- Shima, H., Koike, E., Shinohara, R., Kobayashi, T., 2006. Oxidative ability and toxicity of n-hexane insoluble fraction of diesel exhaust particles. *Toxicological Sciences* 91, 218-226.
- Siegl, W.O., Hammerle, R.H., Herrmann, H.M., Wenclawiak, B.W., Luers-Jongen, B., 1999. Organic Emissions Profile for A Light-duty Diesel Vehicle. *Atmospheric Environment* 33, 797-805.
- Simoneit, B.R.T., 1984. Organic matter of the troposphere-III. Characterization and sources of petroleum and pyrogenic residues in aerosols over the western united states. *Atmospheric Environment* 18, 51-67.
- Sin, D.W.M., Fung, W.H., Lam, C.H., 2002. Measurement of carbonaceous aerosols: validation and comparison of solvent extraction-gas chromatographic method and a thermal optical transmittance method. *Analyst* 127, 614-622.
- Singapore Customer Services of Land Transport Authority (Eds.), 2007. Annual Report.
- Singh, M., Jaques, P.A., Sioutas, C., 2002. Size distribution and diurnal characteristics of particle-bound metals in source and receptor site of the Los Angeles Basin. *Atmospheric Environment* 36, 1675-1689.
- Skjøth-Raamussen, M.S., Glarborg, P., Østberg, M., Johannessen, J.T., Livbjerg, H., Jensen, A.D., Christensen, T.S., 2004. Formation of polycyclic aromatic hydrocarbons and soot in fuel-rich oxidation of methane in a laminar flow reactor. *Combustion and Flame* 136, 91-128.
- Someya, T. (Eds.), 1993. *Advanced Combustion Science*. Springer-Verlag, Tokyo, Japan.
- Squadrito, G., Cueto, R., Dellinger, B., Pryor, W.A., 2001. Quinoid redox cycling as a mechanism for sustained free radical generation by inhaled airborne particulate matter. *Free Radical Biology & Medicine* 31, 1132-1138.
- Sullivan, J.B., Jr. Krieger G.R. (Eds.), 2001. *Clinical environmental health and toxic exposures*. Lippincott Williams & Wilkins, Philadelphia, USA, 2nd Edition, 987-989.
- Sullivan, J.L., Baker, R.E., Boyer, B.A., Hammerle, R.H., Kenney, T.E., Muniz, L., Wallington, T.J., 2004. CO₂ emission benefit of diesel (versus gasoline) powered vehicles. *Environmental Science and Technology* 38, 3217-3223.
- Tavares, Jr. M., Pinto, J.P., Souza, A.L., Scarminio, I.S., Solci, M.C., 2004. Emission of polycyclic aromatic hydrocarbons from diesel engine in a bus station, Londrina, Brazil. *Atmospheric Environment* 38, 5039-5044.
- Tobias, H.J., Beving, D., Ziemann, P.J., Sakurai, H., Zuk, M., McMurry, P.H., Zarling, D., Waytulonis, R., Kittleson, D.B., 2001. Chemical analysis of diesel engine

- nanoparticles using a nano-DMA/thermal deposition particle beam mass spectrometer. *Environmental Science and Technology* 35, 2232-2243.
- Upham, B.L., Weis, L.M., Trosko, J.E., 1998. Modulated gap junctional intercellular communication as a biomarker of PAH epigenetic toxicity: structure-function relationship. *Environmental Health Perspectives* 106 (Suppl 4), 975-981.
- U.S. Department of Transportation, 2006. National transportation statistics report. Bureau of transportation statistics, Washington, DC, USA.
- U.S. Diesel Technology Forum (Eds.), 2006. Statistics Report.
- Valavanidis, A., Fiotakis, K., Bakeas, E., Vlahogianni, T., 2005. Electron paramagnetic resonance study of the generation of reactive oxygen species catalysed by transition metals and quinoid redox cycling by inhalable ambient particulate matter. *Redox Report* 10, 37-51.
- Vatavuk, J., Demarchi, V., 1995. The effect of the addition of hard particles on the wear of liner and ring materials running with high sulfur fuel. *Society of Automotive Engineers*, Warrendale, PA, 950527, 79-89.
- Vilhunen, J.K., Bohlen, A., Schmeling, M., Rantanen, L., Mikkonen, S., Klockenkämper, R., Klockow, D., 1999. Trace element determination in diesel particulates by total-reflection X-ray fluorescence analysis. *Mikrochimica Acta* 131, 219-223.
- Violi, A., D'Anna, A., D'Alessio, A., 1999. Modeling of particulate formation in combustion and pyrolysis. *Chemical Engineering Science* 54, 3433-3442.
- Virtanen, A.K.K., Ristimäki, J.M., Vaaraslahti, K.M., Keskinen, J., 2004. Effect of engine load on diesel soot particles. *Environmental Science and Technology* 38, 2551-2556.
- Wang, Y.F., Huang, K.L., Li, C.T., Mi, H.H., Luo, J.H., Tsai, P.J., 2003. Emissions of fuel metals content a diesel vehicle engine. *Atmospheric Environment* 37, 4637-4643.
- Wang, Z., Fingas, M., Shu, Y.Y., Sigouin, L., Landriault, M., Lambert, P., 1999. Quantitative Characterization of PAHs in Burn Residue and Soot Samples and Differentiation of Pyrogenic PAHs from Petrogenic PAHs - The 1994 Mobile Burn Study. *Environmental Science and Technology* 33, 3100-3109.
- Wen, J.Z., Thomson, M.J., Lightstone, M.F., Rogak, S.N., 2006. Detailed kinetic modeling of carbonaceous nanoparticle inception and surface growth during the pyrolysis of C₆H₆ behind shock waves. *Energy & Fuels* 20, 547-559.
- Wiersum, U.E., 1996. The formation of polycyclic aromatic, fullerenes and soot in combustion. The mechanism and the environmental connection. *Polycyclic Aromatic Compounds* 11, 291-300.

- Williams, P.T., Abbass, M.K., Andrews, G.E., 1989. Diesel particulate emissions: the role of unburned fuel. *Combustion and Flame* 75, 1-24.
- Williams, P.T., Bartle, K.D., Andrew, G.E., 1986. The relation between polycyclic aromatic compounds in diesel fuels and exhaust particulates. *Fuel* 65, 1150-1157.
- Wilson, M.R., Lightbody, J.H., Donaldson, K., Sales, J., Stone, V., 2002. Interactions between ultrafine particles and transition metals in vivo and in vitro. *Toxicology and Applied Pharmacology* 184, 172-179.
- Wind, R.A., Li, L., Maciel, G.E., Wooten, J.B., 1993. Characterization of electron spin exchange interactions in cellulose chars by means of ESR, ¹H NMR, and dynamic nuclear polarization. *Applied Magnetic Resonance* 5, 161-176.
- Xia, T., Korge, P., Weiss, J.N., Li, N., Venkatesen, M.I., Sioutas, C., Nel, A., 2004. Quinones and aromatic chemical compounds in particulate matter induce mitochondrial dysfunction: implications for ultrafine particle toxicity. *Environmental Health Perspectives* 112, 1347-1358.
- Yamanaka, C., Matsuda, T., Ikeya, M., 2005. Electron spin resonance of particulate soot samples from automobiles to help environmental studies, *Applied Radiation and Isotopes* 62, 307-311.
- Yang, H.H., Lee, W., Mi, H.H., Wang, C., 1998. PAH Emissions Influenced by Mn-based additive and turbocharging from a heavy-duty diesel engine. *Environment International* 24, 389-403.
- Yang, H., Li, Q., Yu, J.Z., 2003. Comparison of two methods for the determination of water-soluble organic carbon in atmospheric particles *Atmospheric Environment* 37, 865-870.
- Yang, L., Lim, J., Yu, L.E., 2007. Effects of acid-washing filter treatment on quantification of aerosol organic compounds. *Atmospheric Environment* 41, 3729-3739.
- Ying, Q., Mysliwiec, M., Kleman, M.J., 2004. Source apportionment of visibility impairment using a three-dimensional source-oriented air quality model. *Environmental Science and Technology* 38, 1089-1101.
- Yu, J., Eser, S., 1997. Thermal decomposition of C10-C14 normal alkanes in near-critical and supercritical regions: product distributions and reaction mechanisms. *Industrial & Engineering Chemistry Research* 36, 574-584.
- Yu, J.Z., Joanne, W.T.T., Alan, W.M.W., Alexis, K.H.L., Louie, P.K.K., Fung, J.C.H., 2004. Abundance and seasonal characteristics of elemental and organic carbon in Hong Kong PM10. *Atmospheric Environment* 38, 11511-1521.
- Yu, L.E., Hildemann, L.M., Niksa, S., 1999. Characteristics of nitrogen-containing aromatic compounds in coal tars during secondary pyrolysis. *Fuel* 78, 377-385.

- Zheng, J., Tan, M., Shibata, Y., Tanaka, A., Li, Y., Zhang, G., Zhang, Y., Shan, Z., 2004. Characteristics of lead isotope ratios and elemental concentrations in PM10 fraction of airborne particulate matter in Shanghai after the phase-out leaded gasoline. *Atmospheric Environment* 38, 1191-1200.
- Zielinska, B., Sagebiel, J., Arnott, W.P., Rogers, C.F., Kelly, K.E., Wagner, D.A., Lighty, J.S., Sarofim, A.F., Palmer, G., 2004a. Phase and size distribution of polycyclic aromatic hydrocarbons in diesel and gasoline vehicle emissions. *Environmental Science and Technology* 38, 2557-2567.
- Zielinska, B., Sagebiel, J., McDonald, J.D., Whitney, K., Lawson, D.R., 2004b. Emission rates and comparative chemical composition from selected in-use diesel and gasoline-fueled vehicles. *Journal of the air & waste management association* 54, 1138-1150.

APPENDIX A

Table A1. Reported concentrations of EC and OC in diesel exhausts

Analytical Method	Concentration				
	$\mu\text{g}/\text{cm}^2$	mg/mile *mg/km	**mg/m ³ $\mu\text{g}/\text{m}^3$	%	mg/min
Thermal-optical (NIOSH5040)					
EC	53-310 ^a , 86.5 ^b , 1.4-151.7 ^f , 5.64-8.20 ^g , 0.07-14.90 ^h	15.35-804.76 ^c , *25.50-31.27 ^k , 175-340 ^m	**3.72-4.34 ^e , 13-122 ^j	40.5 ^c	4.1-110.7 ^m
OC	25-272 ^a , 0.5-131.8 ^f , 17.15-19.47 ^g , 1.42-21.04 ^h	51.44-407.06 ^d , *19.27-25.17 ^k , 74.7-607 ^m	**6.88-9.74 ^e , 46-125 ^j	32.6 ^c , 34.1-58.7 ⁱ , 23.6-62.7 ^l	17.0-45.5 ^m
Coulometric (ZH1/120.44)					
EC	1.6-129.1 ^f , 8.32-16.70 ^g , 0.30-17.40 ^h				
OC	0.1-131.8 ^f , 8.03-15.17 ^g , 1.20-13.70 ^h				

^aComparison of solvent extraction and thermal-optical carbon analysis methods (Japar et al., 1984)

^bInterlaboratory analysis of carbonaceous aerosol samples (Courtes, 1990)

^cChemical composition of emission from urban sources of fine organic aerosol (Hildemann et al., 1991)

^dCharacterization of heavy-duty diesel vehicle emissions (Lowenthal et al., 1994)

^eElemental carbon-based method for monitoring occupational exposures to particulate diesel exhaust (Birch, 1996)

^fInternational round robin tests on the measurement of carbon in diesel exhaust particulates (Guilemin et al., 1997)

^gAnalysis of carbonaceous aerosols: interlaboratory comparison (Birch, 1998)

^hComparison of two carbon analysis methods for monitoring diesel particulate levels in mines (Birch et al., 1999)

ⁱComposition of light-duty motor vehicle exhaust particulate matter in the Denver, Colorado area (Cadle et al., 1999)

^jA survey of exposure to diesel engine exhaust emissions in the workplace (Groves et al., 2000)

^kOn-road particulate matter (PM_{2.5} and PM₁₀) emissions in the Sepulveda tunnel, Los Angeles, California (Gillies et al., 2001)

^lIn-use light-duty gasoline vehicle particulate matter emissions on three driving cycles (Cadle et al., 2001)

^mEmission rates of particulate matter and elemental and organic carbon in-use diesel engines (Shah et al., 2004)

Table A2. Reported concentrations of EC and OC in ambient samplings

Analytical Method	Concentration	
	$\mu\text{g}/\text{cm}^2$	$\mu\text{g}/\text{m}^3$
Thermal-optical (NIOSH5040)		
EC	5.9 ^b , 6.8 ^c , 1.57-3.00 ^f	3.5 ^b , 4.86-10.7 ^g , 0.6-3.0 ^h , 1.55-3.25 ⁱ , 0.66-6.56 ^j , 1.48-3.26 ^k , 3.08-7.95 ^l , 1.5-2.5 ^m , 0.9-11 ⁿ
OC	25.4 ^b , 9.40-11.12 ^f	10.5 ^b , 7.77-14.4 ^g , 4.9-16.4 ^h , 3.24-10.8 ⁱ , 2.43- 2.46 ^j , 3.20-7.56 ^k , 6.62-14.16 ^l , 9.7-15.1 ^m , 3.5-44 ⁿ
Coulometric (ZH1/120.44)		
EC	2.30-11.25 ^f	
OC	3.97-9.60 ^f	
Carbon analyzer (CHNS, #NDIR)		
EC	#6.1-19.1 ^a	2.3-8.0 ^d , 5.05-42.8 ^e
OC (TC)	#9.9-22.6 ^a	(4.4-14.5 ^d), 1.62-70.1 ^e

^aProblems in the sampling and analysis of carbon particulate (Cadle et al., 1983)

^bComparison of sampling methods for carbonaceous aerosols in ambient air (Hering et al., 1990)

^cInterlaboratory analysis of carbonaceous aerosol samples (Courtess, 1990)

^dA chemical characterization of atmospheric aerosol in Sapporo (Ohta et al., 1990)

^eParticle size distribution of aerosol carbons in ambient air (Chen et al., 1997)

^fAnalysis of carbonaceous aerosols: interlaboratory comparison (Birch, 1998)

^gConcentrations of carbonaceous species in particles at Seoul and Cheju in Korea (Kim et al., 1999)

^hCharacteristics of PM_{2.5} carbonaceous aerosol in the Sihwa industrial area, South Korea (Park et al., 2001)

ⁱMeasurement of carbonaceous aerosols: validation and comparison of solvent extraction-gas chromatographic method and a thermal optical transmittance method (Sin et al., 2002)

^jOrganic and elemental carbon measurements during ACE-Asia suggest a longer atmospheric lifetime for elemental carbon (Lim et al., 2003)

^kComparison of two methods for the determination of water-soluble organic carbon in atmospheric particles (Yang et al., 2003)

^lAbundance and seasonal characteristics of elemental and organic carbon in Hong Kong PM₁₀ (Yu et al., 2004)

^mPrimary and secondary carbonaceous species in the atmosphere of western riverside county, California (Na et al., 2004)

ⁿElemental and organic carbon in urban canyon and background environments in Budapest, Hungary (Salma et al., 2004)

Table A3. Reported concentrations of organic compounds in diesel and gasoline exhausts*

Compound	*Medium duty diesel truck (mg/km) ^a		Compound	Light duty gasoline vehicle w/o catalyst (w/ catalyst*) (mg/km) ^b	
Resolved Semi-VOCs	12.1		Resolved Semi-VOCs	50.8 (0.94*)	
	Alkanes	4.6		Alkanes	4.1 (0.17*)
	PAHs	1.8		PAHs	43.3 (0.40*)
	Isoprenoids	2.2		Isoprenoids	(0.11*)
	Aromatic Acids	2.0		Aromatic Acids	(0.13*)
	Other Compounds	1.5		Other Compounds	3.4 (0.13*)
Resolved Particle-Phase Organic Compounds	2.28		Resolved Particle-Phase Organic Compounds	9.89 (0.05*)	
	Alkanes	0.41		Alkanes	3.3 (0.013*)
	PAHs	1.0		PAHs	4.1
	n-Alkanoic Acids	0.44		Alkylcyclohexanes	1.6
	Alkanedioic Acids	0.31		Alkanedioic Acids	(0.026*)
	Other Compounds	0.12		Other Compounds	0.89 (0.011*)
Particle EC	56		Particle EC	8.3 (0.8*)	
Particle Phase Unresolved Complex Mixture	41.4		Particle Phase Unresolved Complex Mixture	405 (1.4*)	
Semi-Volatile Gas-Phase Unresolved Complex Mixture	54		Gas-Phase Unresolved Complex Mixture	50 (7.3*)	
Gas-phase Volatile Organics	216				
	Alkanes	15.8			
	Olefins	17.3			
	Aromatics & Cyclics	22.3			
	Acetaldehyde	41.8			
	Propanal	14.0			
	Acetone	22.0			
	Crotonaldehyde	13.4			
	Other Carbonyls	55.4			

* Hot-start Federal Test Procedure

^aMeasurement of emission from air pollution sources. 2. C₁ through C₃₀ organic compounds from medium duty diesel trucks (Schauer et al., 1999)

^bMeasurement of emission from air pollution sources. 5. C₁-C₃₂ organic compounds from gasoline-powered motor vehicles (Schauer et al., 2002)

Table A4. The polycyclic aromatic compounds (PACs) found in diesel exhausts

Ring number	Main structure	PAH derivative	Nitro-PAH derivative
Two-ring PAC	naphthalene ^{a,b,c,d,p}	1-methylnaphthalene ^{c,d,p} 2-methylnaphthalene ^{c,d,p} dimethylnaphthalene ^{d,p}	1-nitronaphthalene ^{e,s} 2-nitronaphthalene ^s
	biphenyl ^b		2-nitrobiphenyl ^{f,s} 3-nitrobiphenyl ^s 4-nitrobiphenyl ^{e,f}
Three-ring PAC	phenanthrene ^{a,b,g,p}	1-methylphenanthrene ^g 2-methylphenanthrene ^g 3-methylphenanthrene ^g 4 and 9-methylphenanthrene ^g methylphenanthrene ^p dimethylphenanthrene ^p	1-nitrophenanthrene ^f 3-nitrophenanthrene ^{f,s} 4-nitrophenanthrene ^{f,s} 9-nitrophenanthrene ^{f,s}
	anthracene ^{b,g,p,q}	1-methylanthracene ^g 2-methylanthracene ^g 9-methylanthracene ^g 9,10-dimethylanthracene ^g	1-nitroanthracene ^{f,m} 2-nitroanthracene ^f 9-nitroanthracene ^{e,g,o,s} 1-nitro-2-methylanthracene ^f 2-nitro-3-methylanthracene ^f 3-nitro-1-methylanthracene ^f 2-nitrofluorene ^{f,n,o,s} 5-nitrofluorene ^f 5-nitroacenaphthene ^{e,s}
	fluorene ^{b,p}	2-methylfluorene ^g	
	acenaphthene ^{b,p} dibenzothiophene ^{b,g} acenaphthylene ^{b,c}		
	fluoranthene ^{a,c,g,h,i,j,p,q}		1-nitrofluoranthene ^{f,m,s} 2-nitrofluoranthene ^{j,s} 3-nitrofluoranthene ^{f,o,s} 7-nitrofluoranthene ^{f,s} 8-nitrofluoranthene ^{f,s}
Four-ring PAC	pyrene ^{a,c,g,h,i,j,n,p,q}	1-methylpyrene ^g 2-methylpyrene ^g	1-nitropyrene ^{d,g,i,k,l,m,n,o,r,s} 2-nitropyrene ^{i,s} 4-nitropyrene ^s dinitropyrene ^k 1,3-dinitropyrene ^s 1,6-dinitropyrene ^s 1,8-dinitropyrene ^s
	chrysene ^{b,g,h,j,n,p,q}		5-nitrochrysene ^f 6-nitrochrysene ^{o,s}
	benzo[a]anthracene ^{b,g,h,i,j,n,p,q}		7-nitrobenzo[a]anthracene ^{o,s}
More than	perylene ^{b,g,n} benzo[a]pyrene ^{b,g,h,i,j,p,q}		3-nitroperylene ^k 6-nitrobenzo[a]pyrene ^{h,s}

four-ring PAC	benzo[e]pyrene ^{g,i,j,p} benzo[ghi]pyrene ^p benzo[ghi]perylene ^{b,c,g,h,n,q} benzo[a]fluorene ^g benzofluoranthene ^p benzo[ghi]fluoranthene ^g benzo[b]fluoranthene ^{b,g,h,j} benzo[j]fluoranthene ^h benzo[k]fluoranthene ^{b,h,i,j} benzo[b+j+k]fluoranthene ^q indeno[1,2,3- cd]pyrene ^{b,g,h,i,j,q} dibenz[a,h]anthracene ^{b,i,j} dibenz[a,h+a,c]anthracene ^q benzo[b]naphtho[1,2- d]thiophene ^g cyclopenta[cd]pyrene ^g	1-nitrobenzo[a]pyrene ^s 3-nitrobenzo[a]pyrene ^s 1-nitrobenzo[e]pyrene ^s 3-nitrobenzo[e]pyrene ^s
------------------	---	--

^aQuantitative Determination of PAHs in Diesel Engine Exhausts by GC-MS (Fleurat-Lessard et al., 1999)

^bQuantitative Characterization of PAHs in Burn Residue and Soot Samples and Differentiation of Pyrogenic PAHs from Petrogenic PAHs – The 1994 Mobile Burn Study (Wang et al., 1999).

^cOrganic Emissions Profile for a Light-duty Diesel Vehicle (Siegl et al., 1999).

^dFuel residues and organic combustion products in diesel exhaust emissions: sources, sampling and analysis (Rhead and Trier, 1992).

^eEvidence for the Adsorption of Nitrated Polycyclic Aromatic Hydrocarbons by Tree Bark (Douce et al., 1997).

^fCapillary Column Gas Chromatographic Determination of Nitro Polycyclic Aromatic Compounds in Particulate Extracts (Campbell and Lee, 1984).

^gDetermination of Polycyclic Compounds and Dioxin Receptor Ligands Present in Diesel Exhaust Particulate Extracts (Li et al., 1996).

^hCharacterization of Polycyclic Aromatic Hydrocarbons on Motor Vehicle Fuels and Exhaust Emissions (Marr et al., 1999).

ⁱNitro-PAH in Ambient Particulate Matter in the Atmosphere of Athens (Marino et al., 2000).

^jDistribution of N-alkanes, Polyunuclear Aromatic Hydrocarbons and Nitrated Polyunuclear Aromatic Hydrocarbons between the Fine and Coarse Fractions of Inhalable Atmospheric Particulates (Cecinato et al., 1999).

^kDetermination of Mono- and Di-nitro Polycyclic Aromatic Hydrocarbons by On-line Reduction and High-performance Liquid Chromatography with Chemiluminescence Detection (Li and Westerholm, 1994).

^lChemical Characterization of Exhaust Emissions Originating from the Regeneration Mode of a Diesel Particulate Trap (Li et al., 1994).

^mAn Improved Method for Nitro-PAH Analysis (Chiu and Miles, 1996).

ⁿDetection and average content levels of carcinogenic and mutagenic compounds from the particulates on diesel and gasoline engine mufflers (Handa et al., 1983)

^oSupercritical fluid extraction of nitrated polycyclic aromatic hydrocarbons and polycyclic aromatic hydrocarbons and polycyclic aromatic hydrocarbons from diesel exhaust particulate matter (Paschke et al., 1992)

^pCharacterization of heavy-duty diesel vehicle emissions (Lowenthal et al., 1994)

^qComposition of light-duty motor vehicle exhaust particulate matter in the Denver, Colorado area (Cadle et al., 1999)

^rAn automatic method for the determination of carcinogenic 1-nitropyrene in extracts from automobile exhaust particulate matter (Murahashi et al., 2003)

^sDetermination and comparison of nitrated-polycyclic aromatic hydrocarbons measured in air and diesel particulate reference materials (Bamford et al., 2003)

Table A5. Reported concentrations of PAHs in diesel exhausts

Compound	Concentrations		
	(ng/m ³ of exhaust)	(µg/g of particulates)	(mg/km) *(mg/mile)
Two rings (Total)	<1200,000 ^a	-	-
Three rings (Total)	<1000,000 ^a	-	-
Four rings (Total)	<250,000 ^a	-	-
Five rings (Total)	<90,000 ^a	-	-
naphthalene	-	18-63 ^b , 59 ^c	0.19 ^d
1-methylnaphthalene	-	-	0.44 ^d , *1.42-3.85 ^j
2-methylnaphthalene	-	-	0.69 ^d , *1.65-2.90 ^j
dimethylnaphthalene	-	-	*1.88-7.47 ^j
biphenyl	-	4 ^c	-
phenanthrene	-	93-209 ^b , 94 ^c , 37.74 ^e	*0.13-0.50 ^j
1-methylphenanthrene	-	9.89 ^e	-
2-methylphenanthrene	-	19.21 ^e	-
anthracene	-	2.2 ^c , 7.15 ^e	*0.005-0.042 ^j *0.225-0.562 ^k
methylphenanthrene	-	-	*0.09-1.13 ^j
dimethylphenanthrene	-	-	*0.03-0.93 ^j
1-methylanthracene	-	10.39 ^e	-
2-methylanthracene	-	2.06 ^e	-
9-methylanthracene	-	0.1 ^e	-
9,10-dimethylanthracene	-	0.41 ^e	-
fluorene	-	12 ^c	*0.06-0.37 ^j
2-methyl-fluorene	-	0.56 ^e	-
acenaphthylene	-	2.8 ^c	-
dibenzohiophene	-	43 ^c , 2.67 ^e	-
acenaphthene	-	0.5 ^c	0.19 ^d , *0.07-0.21 ^j
fluoranthane	4.9-33.2 ^f , 1.67 ^g , 1.17 ^h	11-138 ^b , 21.1 ^d , 46.72 ^e	*0.02-0.05 ^j *0.181-0.896 ^k
pyrene	2.5-41 ^f , 1.57 ^g , 1.33 ^h	20-144 ^b , 24.3 ^d , 40.49 ^e	*0.01-0.05 ^j *0.209-1.053 ^k

1-methylpyrene	-	1.53 ^e	-
2-methylpyrene	-	3.6 ^e	-
chrysene	3.8-7.8 ^f , 2.79 ^h	27.0 ^c , 11.89 ^e , 78.9 ⁱ	*0.005-0.05 ^j *0.0238-0.153 ^k
benzo[a]anthracene	3.9-8.9 ^f , 35.0 ^g , 1.27 ^h	11.0 ^c , 7.55 ^e , 5.66 ⁱ	*0.001-0.002 ^j *0.0165-0.0768 ^k
perylene	-	0.17 ^e , 9.0 ^c , 0.05 ⁱ	-
benzo[a]pyrene	3.2-8.4 ^f , 0.61 ^g , 1.73 ^h	35.6 ^c , 1.04 ^e	*0.001-0.004 ^j *0.0108-0.0392 ^k
benzo[e]pyrene	2.8 ^h	3.06 ^e , 34.0 ^g	*0.002-0.016 ^j
benzo[ghi]pyrene	-	-	*0.001-0.006 ^j *0.0151-0.0829 ^k
benzo[a]fluorene	-	5.77 ^e	-
benzo[ghi]perylene	5.04 ^d , 1.0-8.5 ^f	76.0 ^c , 1.08 ^e , 0.22 ⁱ	-
benzofluoranthrene	-	-	*0.002-0.02 ^j
benzo[ghi]fluoranthrene	-	12.22 ^e	-
benzo[b]fluoranthrene	3.1-5.7 ^f , 4.49 ^h	29.0 ^c , 4.6 ^e	-
benzo[j]fluoranthrene	1.38 ^g	-	-
benzo[k]fluoranthrene	1.1-3.1 ^f , 0.46 ^g , 1.19 ^h	73.4 ^c	-
benzo[b+j+k]fluoranthrene	-	-	*0.0463-0.115 ^k
indeno[1,2,3-cd]pyrene	0.32-3.1 ^f , 0.23 ^g , 2.98 ^h	54.6 ^c , 0.37 ^e	*0.00797-0.0476 ^k
dibenzo[a,h]anthracene	0.24 ^g , 0.35 ^h	6.9 ^c	-
dibenzo[a,h+a,c]anthracene	-	-	*0.00145-0.0038 ^k
benzo[b]naphtho[1,2-d]thiophene	-	0.33 ^e	-
cyclopenta[cd]pyrene	-	0.19 ^e	-

^aPAH Emissions Influenced by Mn-based Additive and Turbocharging from a Heavy-duty Diesel Engine (Yang et al., 1998)

^bQuantitative Determination of PAHs in Diesel Engine Exhausts by GC-MS (Fleurat-Lessard et al., 1999).

^cQuantitative Characterization of PAHs in Burn Residue and Soot Samples and Differentiation of Pyrogenic PAHs from Petrogenic PAHs – The 1994 Mobile Burn Study (Wang et al., 1999).

^dOrganic Emissions Profile for a Light-duty Diesel Vehicle (Siegl et al., 1999).

^eDetermination of Polycyclic Compounds and Dioxin Receptor Ligands Present in Diesel Exhaust Particulate Extracts (Li et al., 1996).

^fCharacterization of Polycyclic Aromatic Hydrocarbons on Motor Vehicle Fuels and Exhaust Emissions (Marr et al., 1999).

^gNitro-PAH in Ambient Particulate Matter in the Atmosphere of Athens (Marino et al., 2000).

^hDistribution of N-alkanes, Polyunclear Aromatic Hydrocarbons and Nitrated Polyunclear Aromatic Hydrocarbons between the Fine and Coarse Fractions of Inhalable Atmospheric Particulates (Cecinato et al., 1999).

ⁱDetection and average content levels of carcinogenic and mutagenic compounds from the particulates on diesel and gasoline engine mufflers (Handa et al., 1983)

^jCharacterization of heavy-duty diesel vehicle emissions (Lowenthal et al., 1994)

^kComposition of light-duty motor vehicle exhaust particulate matter in the Denver, Colorado area (Cadle et al., 1999)

Table A6. Reported concentrations of nitro-PAHs in diesel exhausts

Compound	Concentrations		
	ng/m ³ in exhaust	µg/g, *ng/g of particulates	ng/km, *µg/km
1-nitronaphthalene	-	1.64-2.5 ^a , *13.6-86.4 ^j	-
2-nitronaphthalene	-	*37.1-238 ^j	-
2-nitrobiphenyl	-	*7-15.3 ^j	-
3-nitrobiphenyl	-	7-58.1 ^j	-
4-nitrobiphenyl	-	6.14-13.19 ^a , 5.1 ^b ,	-
1-nitrophenanthrene	-	0.5 ^b	-
3-nitrophenanthrene	-	9.3 ^b , *80.3-4350 ^j	-
4-nitrophenanthrene	-	0.7 ^b , *10.8-150 ^j	-
9-nitrophenanthrene	-	2.3 ^b , *205-510 ^j	-
1-nitroanthracene	-	4.6 ^b	-
2-nitroanthracene	-	10.1 ^b	-
9-nitroanthracene	-	4.13-9.79 ^a , 2.8 ^b , 62 ^h , *1284-6080 ^j	-
1-nitro-2-methylantracene	-	18.9 ^b	-
2-nitro-3-methylantracene	-	3.9 ^b	-
2-nitrofluorene	-	4.1 ^b , 5.52 ^g , 28 ^h , *2-46.2 ^j	-
5-nitroacenaphthene	-	2.48-12.43 ^a , *10-37.0 ^j	-
1-nitrofluoranthene	-	4.1 ^b , *48.4-274 ^j	-
2-nitrofluoranthene	0.38 ^c	*71-201 ^j	-
3-nitrofluoranthene	-	10 ^b , 11 ^h , *65.2-4301 ^j	-
7-nitrofluoranthene	-	1.6 ^b , *<2 ^j	-
8-nitrofluoranthene	-	2 ^b , *106-656 ^j	-
1-nitropyrene	12.0 ^c , 0.18 ^d	18.39-21.73 ^a , 43 ^c , 4.5-6.5 ^e , 27.7 ^g , 540 ^h , *16070-39640 ^j	0.034 ^f , *3.0 ⁱ
2-nitropyrene	0.08 ^d	*<4 ^j	-
4-nitropyrene	-	*68.2-173 ^j	-
dinitropyrene	-	0.3 ^e	-
1,3-dinitropyrene	-	*44.4-1146 ^j	-
1,6-dinitropyrene	-	*84.5-2543 ^j	-
1,8-dinitropyrene	-	*<9-3580 ^j	-
5-nitrochrysene	-	4.6 ^b	-
6-nitrochrysene	-	4 ^h , *44.4-2368 ^j	-
7-nitrobenzo[a]anthracene	-	12 ^h , *995-5300 ^j	-
3-nitroperylene	-	1.1 ^e	-
1-nitrobenzo[e]pyrene	-	*<10-1788 ^j	-

3-nitrobenzo[e]pyrene	-	*89-6857 ^j	-
1-nitrobenzo[a]pyrene	-	*<5 ^j	-
3-nitrobenzo[a]pyrene	-	*<5 ^j	-
6-nitrobenzo[a]pyrene	-	5.8 ^b , *514-1650 ^j	-

^aEvidence for the Adsorption of Nitrated Polycyclic Aromatic Hydrocarbons by Tree Bark (Douce et al., 1997).

^bCapillary Column Gas Chromatographic Determination of Nitro Polycyclic Aromatic Compounds in Particulate Extracts (Campbell and Lee, 1984).

^cDistribution of N-alkanes, Polycyclic Aromatic Hydrocarbons and Nitrated Polycyclic Aromatic Hydrocarbons between the Fine and Coarse Fractions of Inhalable Atmospheric Particulates (Cecinato et al., 1999).

^dNitro-PAH in Ambient Particulate Matter in the Atmosphere of Athens (Marino et al., 2000).

^eDetermination of Mono- and Di-nitro Polycyclic Aromatic hydrocarbons by On-line Reduction and High-performance Liquid Chromatography with Chemiluminescence Detection (Li and Westerholm, 1994).

^fChemical Characterization of Exhaust Emissions Originating from the Regeneration Mode of a Diesel Particulate Trap (Li et al., 1994).

^gDetection and average content levels of carcinogenic and mutagenic compounds from the particulates on diesel and gasoline engine mufflers (Handa et al., 1983)

^hSupercritical fluid extraction of nitrated polycyclic aromatic hydrocarbons and polycyclic aromatic hydrocarbons and polycyclic aromatic hydrocarbons from diesel exhaust particulate matter (Paschke et al., 1992)

ⁱAn automatic method for the determination of carcinogenic 1-nitropyrene in extracts from automobile exhaust particulate matter (Murahashi et al., 2003)

^jDetermination and comparison of nitrated-polycyclic aromatic hydrocarbons measured in air and diesel particulate reference materials (Bamford et al., 2003)

Table A7. Reported concentrations of metals in diesel exhausts

Elements	Concentration and Analytical Method		
	mg/mile ^{a,b} , wt % of detectable amounts ^c (XRF)	µg/m ³ (ICP-AES) ^d	mg/g of particulates *(ICP-AES) ^d
Si	0.05-1.6 ^a , 3.189 ^b , 0.63±0.04 ^c	917	20.1
P	0.07-0.35 ^a , 0.634 ^b		
S	2.59-33.33 ^a , 4.504 ^b , 0.22±0.02 ^c		
Cl	0.005-0.32 ^a , 0.139 ^b		
K	0.002-0.05 ^a		
Ca	0.03-0.96 ^a , 1.329 ^b	831	28.4
Ti	0.002-0.01 ^a	81.0	1.37
V	0.0005-0.005 ^a	20.2	0.784
Cr	0.0004-0.007 ^a	88.6	8.69
Mn	0.001-0.02 ^a	21.0	3.27
Fe	0.05-0.65 ^a , 3.151 ^b , 0.05±0.01 ^c	543	38.4
Co	0.0001-0.0006 ^a	39.3	1.45
Ni	0.0002-0.001 ^a	51.1	6.04
Cu	0.001-0.04 ^a , 0.019 ^b	55.4	3.72
Zn	0.001-1.33 ^a , 1.731 ^b , 0.07±0.01 ^c	111	3.74
Ga	0.0001-0.001 ^a		

As	0.0011-0.086 ^a		
Se	0.0008-0.059 ^a		
Br	0.0006-0.0036 ^a , 0.009 ^b		
Rb	0.0002-0.0007 ^a		
Sr	0.0002-0.0033 ^a	14.4	2.96
Y	0.0001 ^a		
Zr	0.0004-0.0039 ^a		
Mo	0.0002-0.0014 ^a	81.5	10.0
Pd	0.0034-0.0094 ^a		
Ag	0.0046-0.0229 ^a	13.7	0.865
Cd	0.0065-0.0554 ^a	10.7	0.580
In	0.0173-0.0554 ^a		
Sn	0.0319-0.0695 ^a		
Sb	0.0031-0.0107 ^a	18.8	1.44
Ba	0.0372-0.2702 ^a	23.1	0.739
La	0.0736-0.2959 ^a		
Au	0.0004-0.0013 ^a		
Hg	0.0001-0.0012 ^a		
Tl	0.0001-0.016 ^a		
Pb	0.0025-0.0085 ^a , 0.15 ^b	40.6	0.931
U	0.0003-0.0006 ^a		
Mg	0.402 ^b	138	6.16
Al	0.303 ^b	641	27.4

* Engine speed is at 100% loading condition.

^aCharacterization of heavy-duty diesel vehicle emission (Lowenthal et al., 1994)

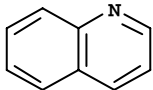
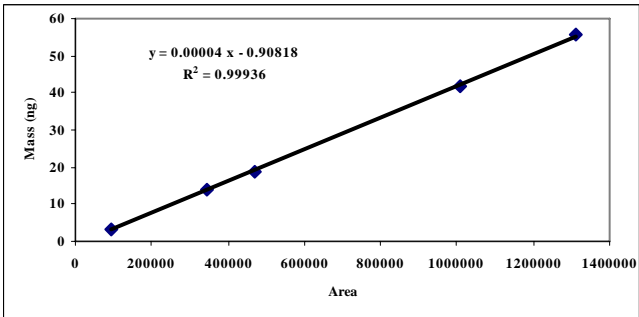
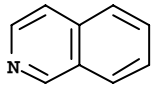
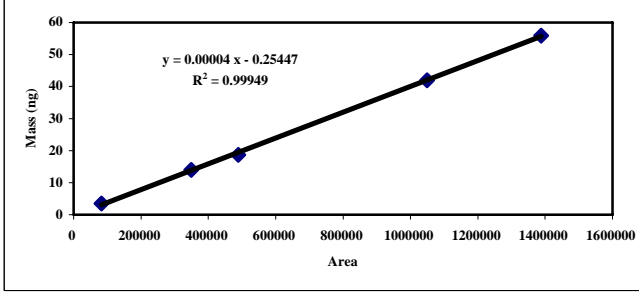
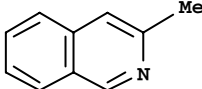
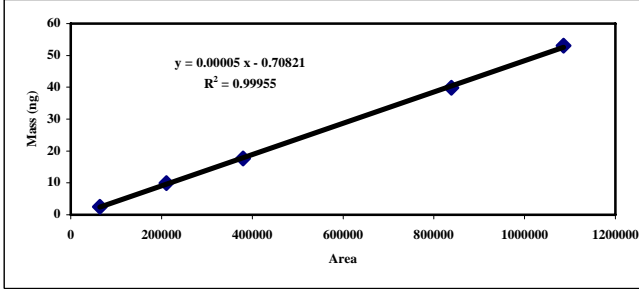
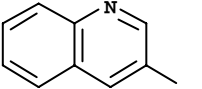
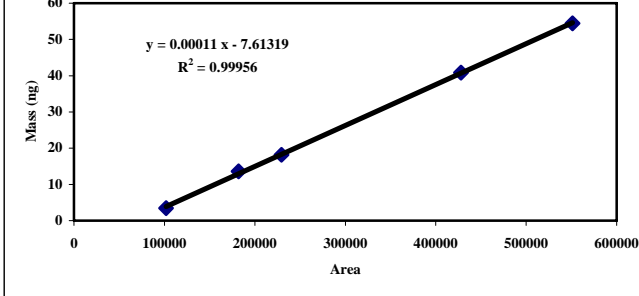
^bComposition of light-duty motor vehicle exhaust particulate matter in the Denver, Colorado area (Cadle et al., 1999)

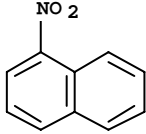
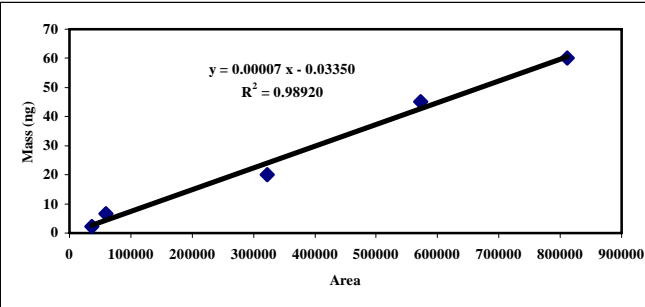
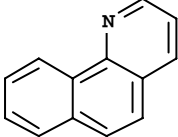
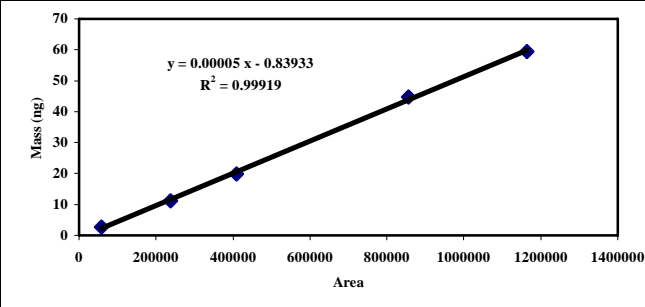
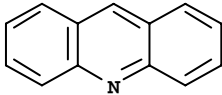
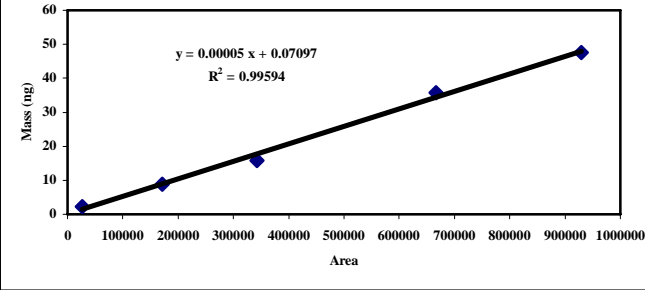
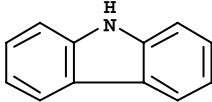
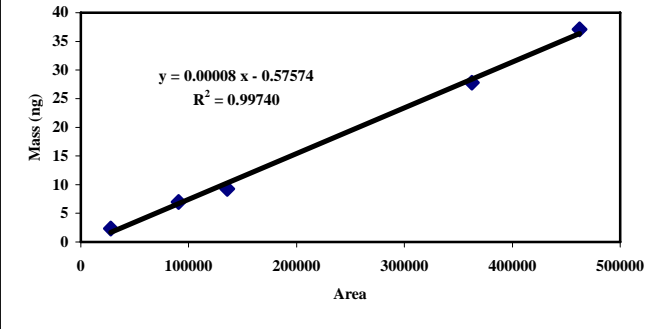
^cMeasurement of emissions from air pollution sources. 2. C₁ through C₃₀ organic compounds from medium duty diesel trucks (Schauer et al., 1999)

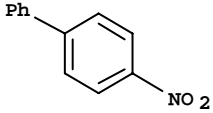
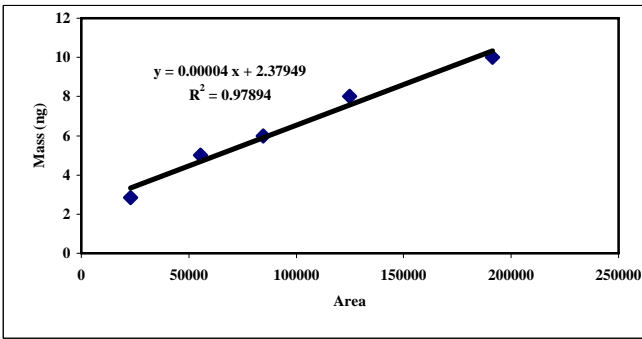
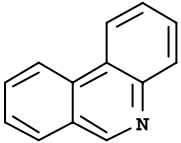
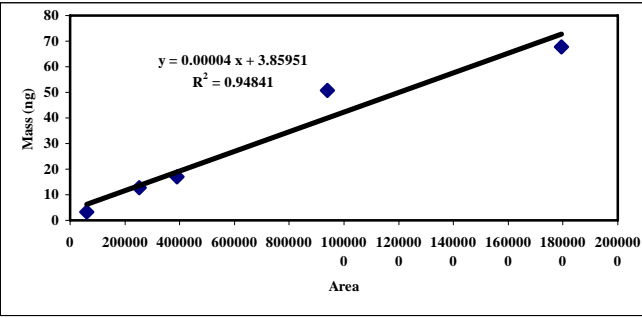
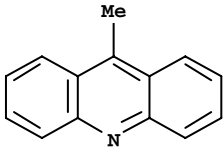
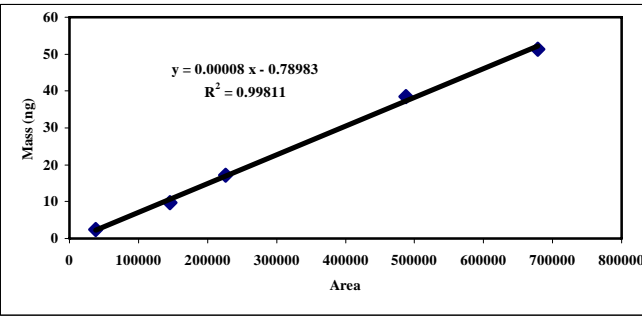
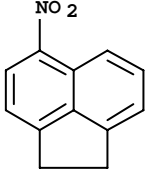
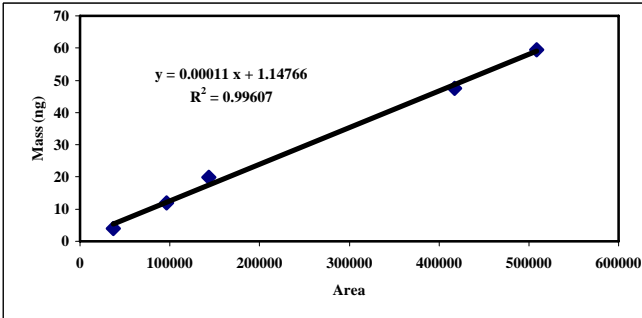
^dEmissions of fuel metals content a diesel vehicle engine (Wang et al., 2003)

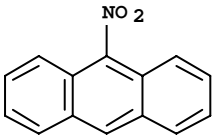
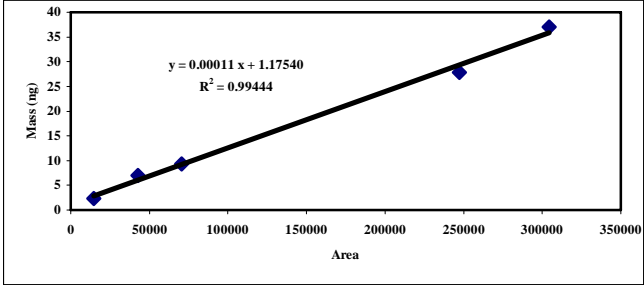
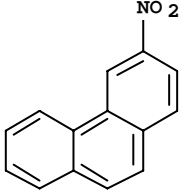
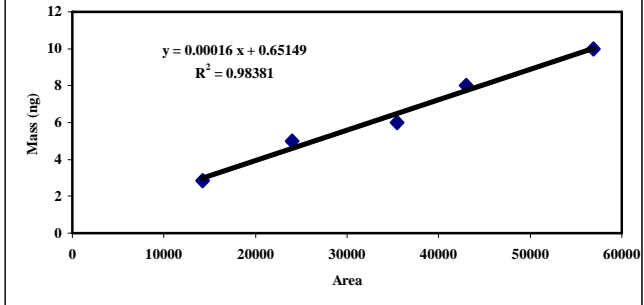
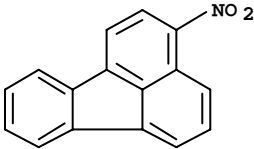
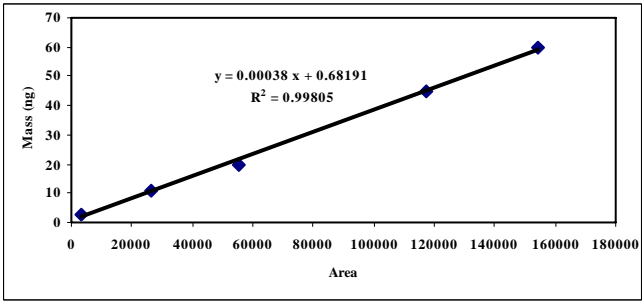
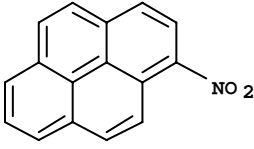
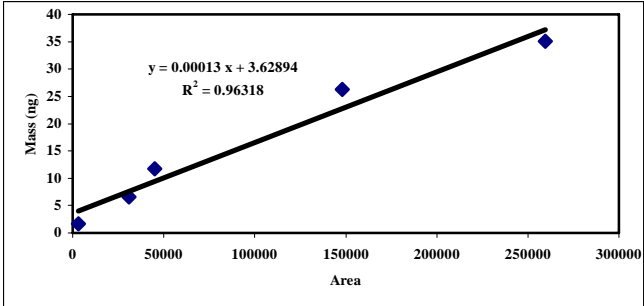
APPENDIX B

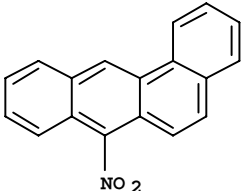
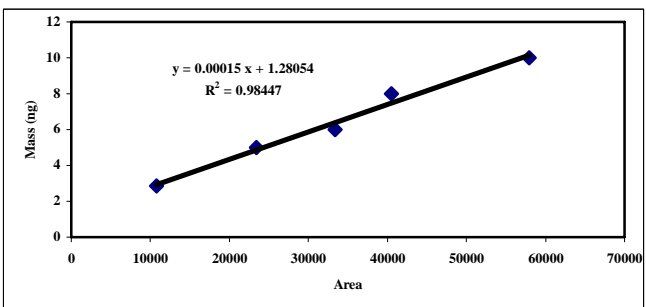
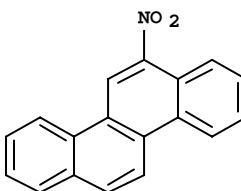
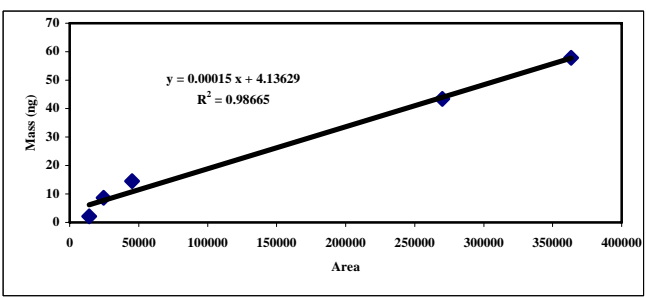
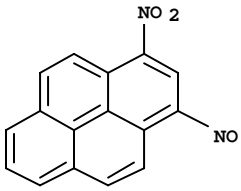
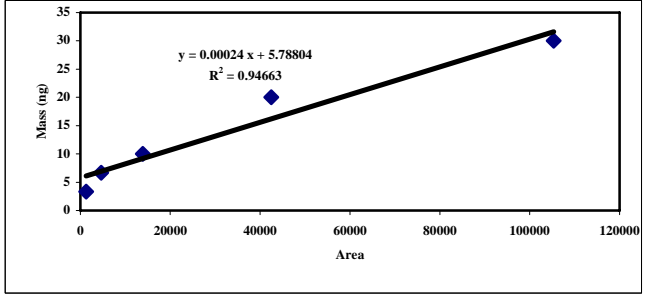
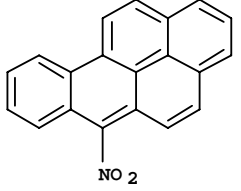
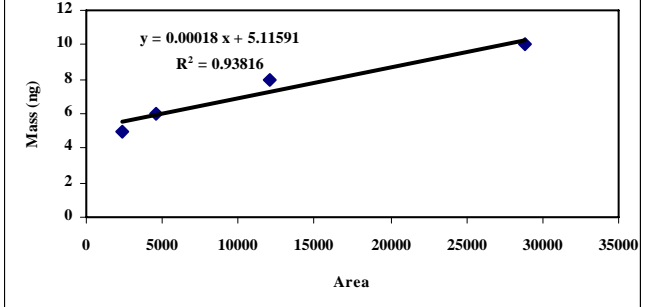
Table B1. Standard calibration plots for N-containing polycyclic aromatic compounds

Name of compound & Chemical structure	M.W.(g)	Standard calibration plot
	Average E.T.(min)	
Quinoline (C ₉ H ₇ N) 	129.161	
	10.871	
Isoquinoline (C ₉ H ₇ N) 	129.161	
	11.242	
3-Methylisoquinoline (C ₁₀ H ₉ N) 	143.188	
	12.493	
3-Methylquinoline (C ₁₀ H ₉ N) 	143.188	
	13.027	

Name of compound & Chemical structure	M.W.(g)	Standard calibration plot
	Average E.T.(min)	
1-Nitronaphthalene (C ₁₀ H ₇ NO ₂) 	173.17	
	17.173	
7,8-Benzoquinoline (C ₁₂ H ₉ N) 	179.22	
	19.944	
Acridine (C ₁₃ H ₉ N) 	179.22	
	20.116	
Carbazole (C ₁₂ H ₉ N) 	167.21	
	20.568	

Name of compound & Chemical structure	M.W.(g)	Standard calibration plot
	Average E.T.(min)	
4-Nitrobiphenyl (C ₁₂ H ₉ NO ₂) 	199.21	
	20.645	
Phenanthridine (C ₁₃ H ₉ N) 	179.22	
	20.707	
9-Methylacridine (C ₁₄ H ₁₁ N) 	193.25	
	22.496	
5-Nitroacenaphthene (C ₁₂ H ₉ NO ₂) 	199.21	
	22.838	

Name of compound & Chemical structure	M.W.(g)	Standard calibration plot
	Average E.T.(min)	
9-Nitroanthracene (C ₁₄ H ₉ NO ₂) 	223.23	
24.443		
3-Nitrophenanthrene (C ₁₄ H ₉ NO ₂) 	223.23	
25.726		
3-Nitrofluoranthene (C ₁₆ H ₉ NO ₂) 	247.25	
28.960		
1-Nitropyrene (C ₁₆ H ₉ NO ₂) 	247.25	
29.584		

Name of compound & Chemical structure	M.W.(g)	Standard calibration plot
	Average E.T.(min)	
7-Nitrobenz[a]anthracene (C ₁₈ H ₁₁ NO ₂) 	273.29	
	31.502	
6-Nitrochrysene (C ₁₈ H ₁₁ NO ₂) 	273.29	
	32.519	
1,3-Dinitropyrene (C ₁₆ H ₈ N ₂ O ₄) 	292.25	
	33.596	
6-Nitrobenzo[a]pyrene (C ₂₀ H ₁₁ NO ₂) 	297.31	
	37.702	

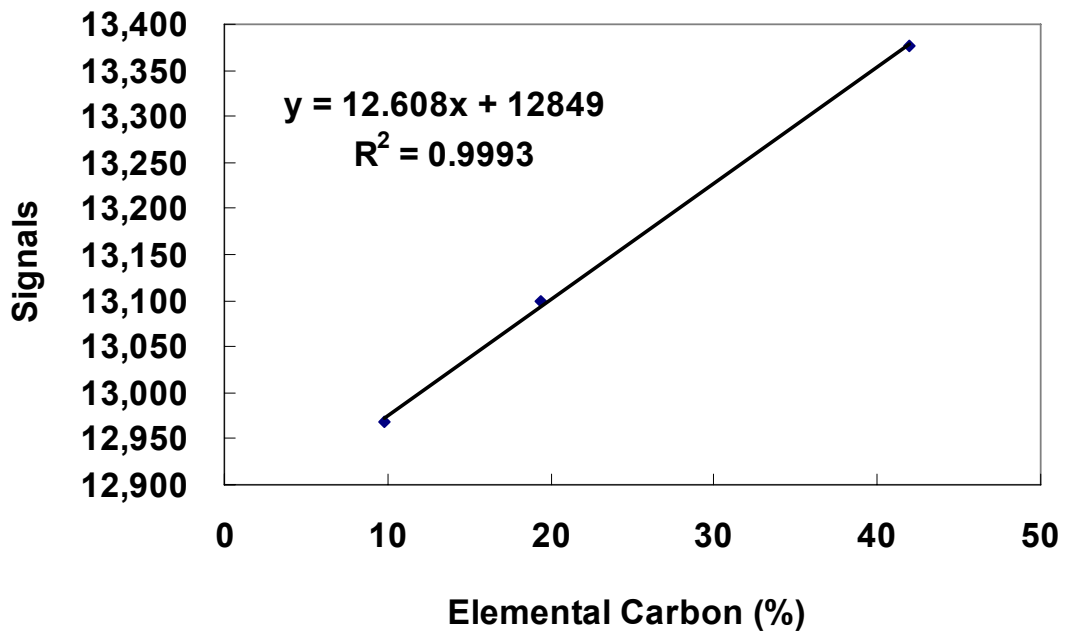
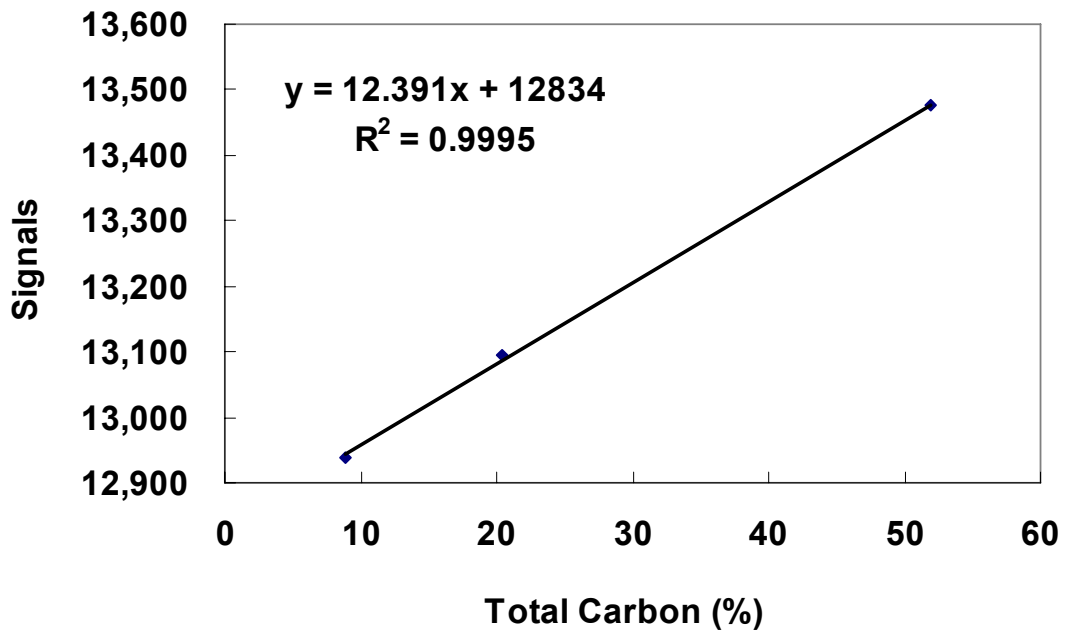


Fig. B1. Standard calibration plots for total carbon and elemental carbon

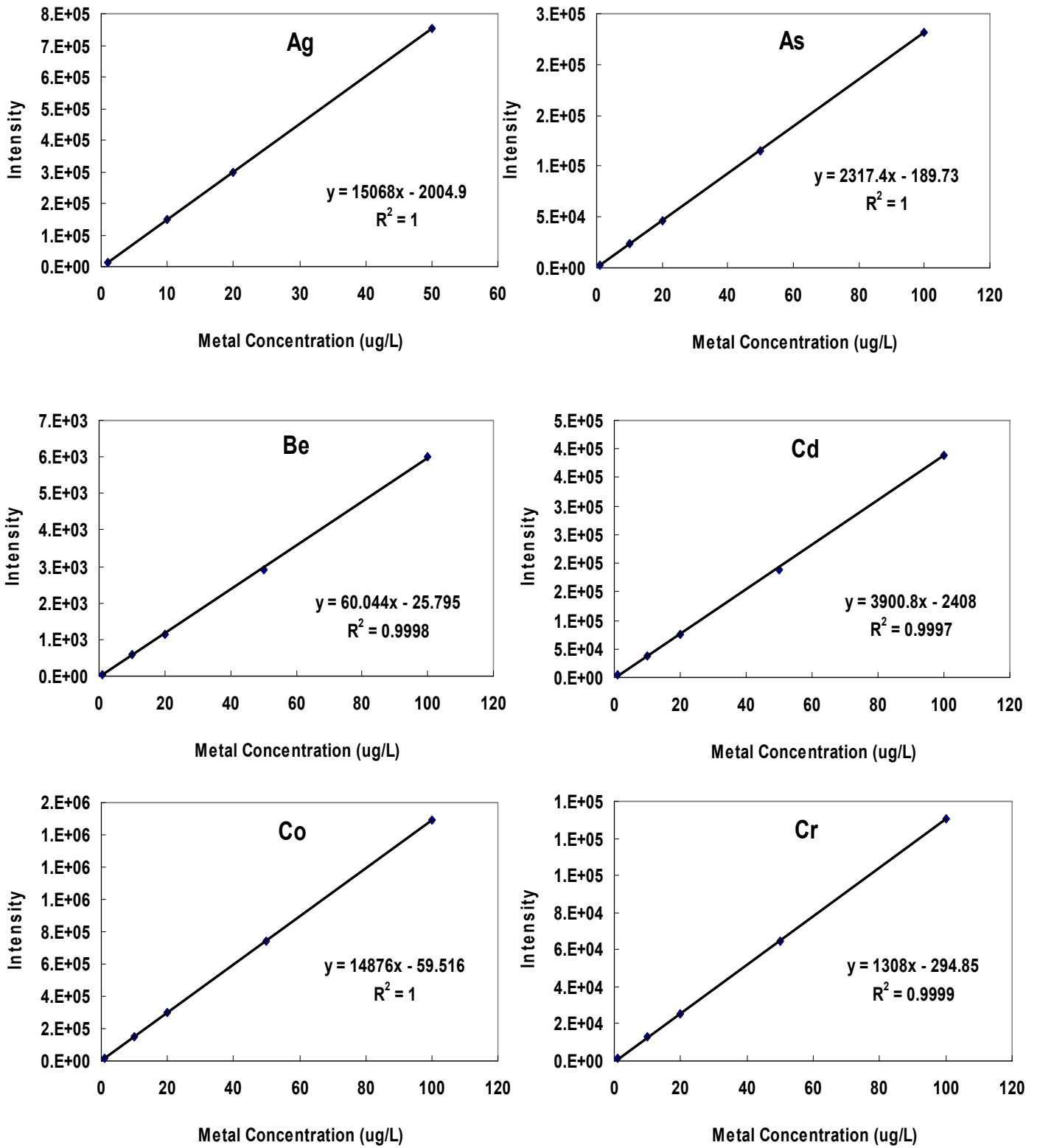


Fig. B2-1. Standard calibration plots for metals

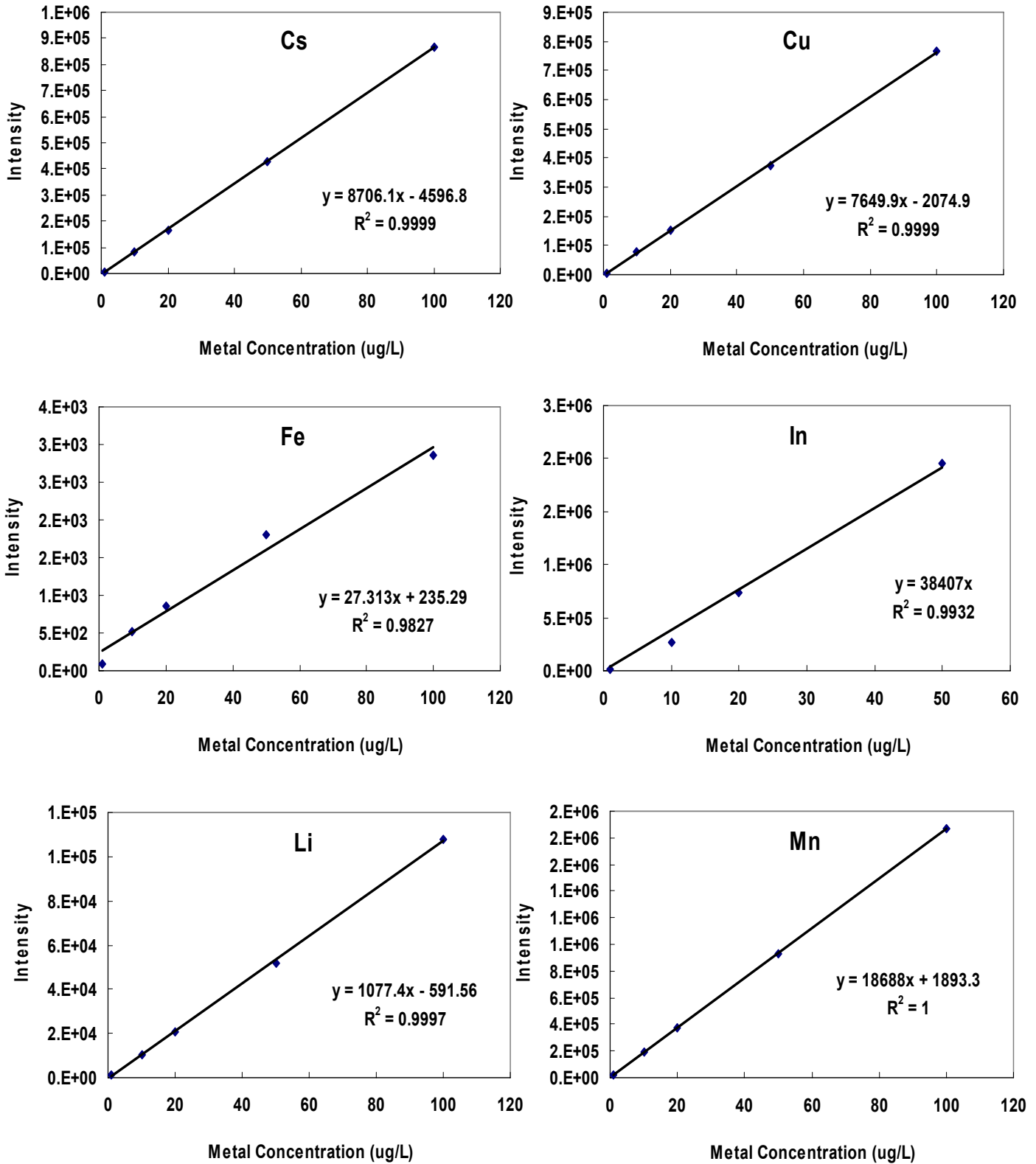


Fig. B2-2. Standard calibration plots for metals

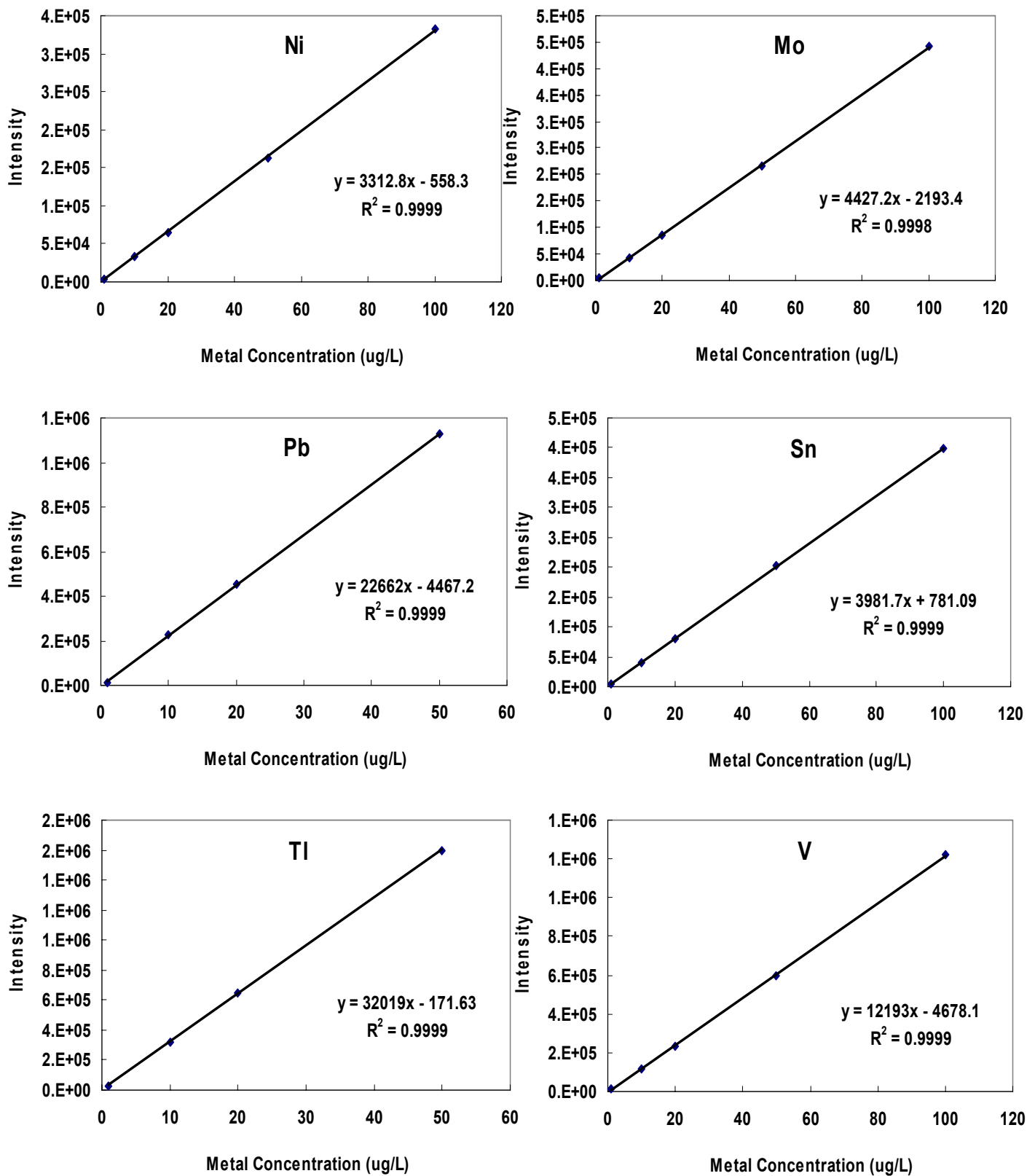


Fig. B2-3. Standard calibration plots for metals

APPENDIX C

Table C. Size segregated chemical species concentrations for 13-mode

LPI size (nm)	34-66	66-94	94-170	170-330	330-550	550-1000	Total
Carbon content (mg/m³)							
Elemental Carbon	0.10	0.16	0.20	0.27	0.38	0.27	1.38
Organic Carbon	0.02	0.03	0.04	0.07	0.08	0.04	0.28
Organic species (µg/m³)							
Alkanes	5.13	2.53	3.88	7.77	8.74	6.90	34.95
Alkenes	0.22	0.00	0.00	0.00	0.00	0.00	0.22
Polycyclic aromatic hydrocarbons	0.02	0.01	0.02	0.02	0.02	0.02	0.11
Carboxylic acids	0.05	0.15	0.00	0.10	0.25	1.67	2.21
Esters	0.00	0.13	0.00	0.10	1.06	0.43	1.71
Ketones	0.28	1.39	0.55	0.28	0.00	0.00	2.51
Alcohols	0.00	0.25	1.25	0.00	0.19	0.15	1.84
N-containing compounds	0.23	0.07	0.00	0.06	0.00	0.00	0.37
S-containing compounds	0.00	0.00	0.00	0.50	0.00	0.00	0.50
Aldehyde	0.00	0.00	0.00	0.00	0.30	0.00	0.30
Metals content (ng/m³)							
Fe	1573.29	1661.44	1461.81	1125.39	1341.21	1115.69	8278.83
Li	418.95	483.89	397.42	346.67	385.24	331.83	2364.00
V	274.39	288.87	209.17	135.94	177.03	101.90	1187.31
Cr	235.27	253.71	206.70	113.26	199.83	95.96	1104.73
Cu	25.58	80.08	126.15	284.18	64.00	29.72	609.71
Ni	70.40	82.73	64.35	45.83	54.02	87.07	404.40
Pb	79.61	110.19	72.31	18.32	43.37	9.48	333.28
Mn	76.24	102.81	65.53	18.07	49.52	8.86	321.02
As	10.49	10.56	6.96	3.94	4.52	0.91	37.39
Co	6.51	7.79	5.10	2.30	4.73	1.50	27.92
Sn	8.04	6.19	5.32	2.21	3.62	1.90	27.28
Mo	5.81	6.94	4.10	1.82	2.98	0.94	22.60
Be	4.45	3.80	2.58	3.28	2.48	3.57	20.17
Ag	3.14	2.90	1.84	0.84	1.15	1.20	11.07
Cs	1.70	2.16	1.42	0.52	0.92	0.30	7.03
Cd	0.83	1.17	0.56	0.34	0.51	0.61	4.01
Tl	0.30	0.69	0.50	0.12	0.22	0.10	1.94
In	0.29	0.33	0.20	0.06	0.12	0.07	1.08

APPENDIX D

Table D. Size distribution of metals contents in DEPs (34nm–1µm)

Driving modes (ng/m ³)	1800 rpm/60%						3000 rpm/60%						1800 rpm/100%						3000 rpm/100%					
	Size range of LPI (nm)						Size range of LPI (nm)						Size range of LPI (nm)						Size range of LPI (nm)					
	34-66	66-94	94-170	170-330	330-550	550-1000	34-66	66-94	94-170	170-330	330-550	550-1000	34-66	66-94	94-170	170-330	330-550	550-1000	34-66	66-94	94-170	170-330	330-550	550-1000
Fe	285.5	299.3	432.8	328.1	514.9	483.7	442.1	410.0	457.5	708.7	404.0	561.5	746.8	437.2	518.5	506.9	644.8	665.6	796.8	691.3	465.7	724.0	601.2	601.6
Pb	121.9	148.5	169.6	134.3	171.3	162.7	106.2	117.6	104.2	142.9	89.1	114.4	90.9	78.0	78.4	80.2	71.9	68.9	86.2	67.7	38.2	74.3	34.1	42.6
Cr	50.4	99.1	160.1	136.4	163.8	103.6	58.9	59.0	114.2	225.1	142.3	169.8	158.7	65.4	126.8	111.8	116.4	99.6	178.4	146.1	102.1	148.0	81.2	59.3
V	50.7	97.8	147.5	82.8	142.5	46.1	52.0	55.9	116.4	149.1	113.3	129.6	182.6	88.7	122.1	90.7	129.0	110.9	180.2	140.8	69.6	108.0	84.8	105.3
Li	26.0	68.2	108.8	83.5	130.3	52.2	43.6	78.8	123.6	165.5	142.8	169.0	201.1	137.2	188.0	164.1	191.3	190.6	220.9	230.8	151.0	207.9	173.9	205.2
Mn	23.9	45.4	71.8	43.7	73.4	49.6	15.0	33.5	42.5	88.6	46.2	65.4	69.5	32.5	53.0	39.7	58.0	55.5	59.4	58.7	18.3	63.2	24.8	33.2
Cu	30.1	27.0	156.9	21.9	121.1	22.0	14.7	18.7	10.0	26.3	33.5	54.4	51.0	106.9	82.0	60.4	32.6	44.7	12.5	14.3	62.0	48.3	40.3	28.9
Ni	20.2	18.8	51.5	34.6	46.1	50.6	13.0	21.7	35.4	85.8	40.7	62.8	48.5	18.1	43.1	38.8	47.7	41.6	49.9	61.5	38.9	58.9	27.0	49.9
Mo	5.4	6.8	7.7	5.2	7.4	15.8	4.6	4.7	5.5	9.8	5.0	5.6	7.6	3.3	5.1	6.1	6.8	6.6	7.0	5.0	3.3	11.1	3.4	3.1
Sn	6.4	6.6	7.1	6.8	8.9	9.8	6.0	3.9	3.7	6.2	4.6	5.9	8.0	3.9	3.0	1.6	4.0	3.9	4.6	3.8	2.7	5.3	5.8	3.8
As	4.4	8.5	11.1	6.4	10.2	4.2	4.8	4.6	7.4	9.6	6.4	7.5	9.3	5.6	6.2	5.3	5.9	5.3	7.9	6.9	2.8	4.4	3.2	4.4
Cs	2.1	2.4	2.7	2.1	2.6	2.3	1.4	1.8	1.8	2.5	1.6	1.9	1.8	1.2	1.5	1.3	1.4	1.3	1.5	1.3	0.6	1.2	0.5	0.8
Ag	2.0	2.2	2.6	1.9	2.7	2.2	3.0	2.0	2.0	3.2	1.8	2.7	3.2	1.1	1.4	1.2	1.7	1.3	1.9	1.4	0.4	0.6	0.7	1.3
Co	1.6	2.6	4.2	2.8	4.6	7.9	1.5	1.7	3.2	5.4	3.3	4.2	5.4	1.6	4.0	2.1	4.0	3.5	4.1	4.5	1.2	9.6	1.9	2.7
In	1.7	1.6	1.6	1.2	1.9	1.4	0.8	0.8	0.8	0.8	0.8	0.7	0.6	0.4	0.5	0.3	0.4	0.4	0.4	0.3	0.1	0.2	0.2	0.2
Cd	1.2	1.3	1.9	1.1	1.7	0.9	0.8	1.0	0.7	1.5	0.6	0.9	0.7	0.5	0.7	1.0	0.7	0.5	0.7	0.7	0.2	0.5	0.6	0.6
Tl	1.0	0.9	1.1	0.9	1.0	0.6	0.6	0.9	0.7	0.9	0.6	0.8	0.5	0.6	0.5	0.5	0.5	0.5	0.5	0.4	0.3	0.5	0.2	0.3
Be	0.3	0.3	0.9	0.7	1.4	0.8	0.4	1.0	1.3	1.8	1.5	1.7	1.9	1.1	1.5	1.0	1.9	2.0	2.2	2.0	1.2	2.7	1.7	1.8
Sum	635.1	837.2	1339.8	894.3	1405.8	1016.5	769.5	817.4	1030.8	1633.6	1038.0	1358.7	1588.3	983.4	1236.2	1113.0	1318.9	1302.6	1614.9	1437.6	958.5	1468.8	1085.7	1144.8
	(10%)	(14%)	(22%)	(15%)	(23%)	(17%)	(12%)	(12%)	(16%)	(25%)	(16%)	(20%)	(21%)	(13%)	(16%)	(15%)	(17%)	(17%)	(21%)	(19%)	(12%)	(19%)	(14%)	(15%)

APPENDIX E

Table E. Possible origins from fuel and/or lubricant and possible formation mechanisms during combustion^{a, b, c}

Organic compounds (Functional group)	Possible origins from fuel and/or lubricant	Possible formation mechanisms during combustion
1. Alkanes (R, C-C)	<ul style="list-style-type: none"> ▫ Fuel ▫ Lubricant (alkylated additives) 	RH (hydrocarbons) $\rightarrow R\cdot + H^+$ $R\cdot + R\cdot \rightarrow R_2$ (heavier hydrocarbons; alkanes) [chain termination]
2. Carboxylic acids (RCO_2H)	<ul style="list-style-type: none"> ▫ Lubricant additives (phenolic antioxidants; alkylsalicylates) 	$RH + O_2 \rightarrow R\cdot + HO_2\cdot$ [initiation] $R\cdot + O_2 \rightarrow RO_2\cdot$ (alkyl peroxide radical) [propagation of chain reactions] $RO_2\cdot + RH \rightarrow ROOH + R\cdot$ [propagation of chain reactions] $ROOH \rightarrow RO\cdot$ (alcoxy radical) + $HO\cdot$ [chain branching] $RCH_2OO\cdot \rightarrow RC\cdot HOOH \rightarrow RCHO$ (aldehydes) + $\cdot OH$ [formation of aldehydes -a] $RR'\cdot CHO\cdot \rightarrow RCHO$ (aldehydes) + $R'\cdot$ [formation of aldehydes -b] $RCH_2O\cdot + O_2 \rightarrow RCHO$ (aldehydes) + $HO_2\cdot$ [formation of aldehydes-c] $RCHO$ (aldehydes) $\rightarrow RCO\cdot + H^+$ $RCO\cdot$ (acyl radical) + $O_2 \rightarrow RCO_3\cdot$ (peroxide radical) $RCO_3\cdot + R'H \rightarrow RCO_3H + R'\cdot$ $RCO_3H \rightarrow RCO_2\cdot$ (carboxyl radical) + $\cdot OH$ $RCO_2\cdot + R'H \rightarrow RCO_2H$ (carboxylic acids) + $R'\cdot$ [formation of carboxylic acids -a] ROH (alcohols) + $CO \rightarrow RCO_2H$ (carboxylic acids) [formation of carboxylic acids -b]
3. Esters (RCO_2R')	<ul style="list-style-type: none"> ▫ Fuel additives (metallic additives in the form of acid salts; stearates), ▫ Lubricant additives (dispersant; succinic esters and mono- or bi-succinimides) 	RCO_2H (carboxylic acids) + $R'OH$ (alcohols) $\rightarrow RCO_2R'$ (esters) + H_2O [Fischer esterification]
4. Ketones ($RCOR'$)	<ul style="list-style-type: none"> ▫ Lubricant additives (dispersant; mono- or bi- succinimides) 	$RCHO + R'O\cdot \rightarrow RR'\cdot CHOO\cdot$ $RR'\cdot CHOO\cdot \rightarrow RC\cdot OOH R' \rightarrow RCO R'$ (ketones) + $\cdot OH$ $RR'R''\cdot COO\cdot$ (tertiary radical) $\rightarrow RCO R'$ (ketones) + $R''O\cdot$
5. Alcohols (ROH)	<ul style="list-style-type: none"> ▫ Lubricant additives (coolant; phenolic antioxidants) 	$RO\cdot + R'H \rightarrow ROH$ (alcohols) + $R\cdot$ [chain branching]

6. Nitrogen containing compounds (RN, RON, RONO, RNO ₂)	▫ Addition of nitrogen from NO _x during combustion	$O + N_2 \leftrightarrow NO + N$ $N + O_2 \leftrightarrow NO + O$ $N + OH \leftrightarrow NO + H$ $N_2 + O_2 \rightarrow 2NO$ $NO_2 + O \rightarrow NO + O_2$ $NO + H_2O \rightarrow NO_2 + OH$ $R \cdot + NO \rightarrow RON$ $R \cdot + N \rightarrow RN$ $R \cdot + NO_2 \rightarrow RONO$ (alkylnitrates) $R \cdot + NO_2 \rightarrow RNO_2$ (nitroalkanes)
7. Aromatic hydrocarbons	▫ Fuel ▫ Lubricant (alkylaryl additives)	HACA (hydrogen abstraction acetylene addition) mechanisms
8. Sulfur containing compounds (ROS)	▫ Fuel (sulfur content) ▫ Lubricant additives (extreme pressure additives; polysulphides and detergents; alkylarylsulfonates)	$SO_2 + OH \cdot \rightarrow HOSO_2 \cdot$ $HOSO_2 \cdot + O_2 \rightarrow SO_3 + HO_2 \cdot$ $SO_3 + H_2O \rightarrow H_2SO_4$ $HOSO_2 \cdot + R \rightarrow ROS + HO_2 \cdot$
9. Alkenes (R, C=C)	▫ Fuel ▫ Lubricant	H_xC-CH_x (alkanes) $\rightarrow H_{x-1}C=CH_{x-1}$ (alkenes) + H ₂ [dehydrogenation] $H-C-C-OH$ (alcohols) $\rightarrow C=C$ (alkenes) + H ₂ O [dehydration]
10. Ethers (ROR')	▫ Conversion of alcohols during combustion	$ROH + H^+ \rightarrow ROR'$ (ethers) + H ₂ O
11. Alkynes (R, C≡C)	▫ Fuel ▫ Lubricant	$H_xC=CH_x$ (alkenes) $\rightarrow H_{x-1}C \equiv CH_{x-1}$ (alkynes) + H ₂ [dehydrogenation]

^aCarey, F.A. (Eds), 2006. Organic chemistry, McGraw-hill international edition, Singapore

^bDegobert, P. (Eds), 1995. Automobiles and pollution, Society of Automotive Engineers, Warrendale, PA

^cDenis, J., Briant, J., Hipeaux, J.C. (Eds.), 2000. Lubricant properties analysis and testing. Editions Technip, Paris, France.

APPENDIX F

Table F. Size distribution of organic compounds in DEPs (34nm–1µm)

Driving modes			1800rpm/60%						3000rpm/60%						1800rpm/100%						3000rpm/100%						
			Size range of LPI (nm)						Size range of LPI (nm)						Size range of LPI (nm)						Size range of LPI (nm)						
(µg/m ³)	Formula	M.W.	34-66	66-94	94-170	170-330	330-550	550-1000	34-66	66-94	94-170	170-330	330-550	550-1000	34-66	66-94	94-170	170-330	330-550	550-1000	34-66	66-94	94-170	170-330	330-550	550-1000	
Alkanes																											
Decane, 3,3,6-trimethyl-	C13H28	184	0.00000	0.00000	0.00000	0.00000	0.00000	0.00000	0.00000	0.00000	0.00000	0.14678	0.00000	0.00000	0.00000	1.02771	0.00000	0.00000	0.00000	0.00000	0.00000	0.09516	0.00000	0.00000	0.00000	0.00000	0.00000
Undecane, 3,3-dimethyl-	C13H28	184	0.00000	0.00000	0.00000	0.00000	0.00000	0.00000	0.00000	0.00000	0.00000	0.00000	0.00000	0.00000	0.00000	0.00000	0.00000	0.00000	0.00000	0.00000	0.00000	0.00000	0.00000	0.00000	0.00000	0.00000	0.00000
Dodecane, 2,7,10-trimethyl-	C15H32	212	0.00000	0.00000	0.00000	0.00000	0.00000	0.00000	0.00000	0.00000	0.00000	0.00000	0.00000	0.00000	0.00000	0.00000	0.00000	0.00000	0.00000	0.00000	0.00000	0.00000	0.00000	0.00000	0.00000	0.07315	0.00000
Heptadecane	C17H36	240	0.00000	0.00000	0.06533	0.12176	0.18746	0.12404	0.19139	0.00000	0.10843	0.23634	0.30504	0.23367	0.07009	0.10752	0.25646	0.24889	0.24735	0.26670	0.00000	0.08460	0.19713	0.14438	0.17549	0.00000	0.00000
9-Octadecene, (E)-	C18H36	252	0.00000	0.00000	0.00000	0.00000	0.00000	0.00000	0.00000	0.00000	0.06511	0.07972	0.00000	0.05994	0.00000	0.00000	0.00000	0.00000	0.00000	0.00000	0.00000	0.00000	0.00000	0.00000	0.00000	0.00000	0.00000
5-Octadecene, (E)-	C18H36	252	0.00000	0.00000	0.00000	0.00000	0.16020	0.00000	0.00000	0.00000	0.00000	0.00000	0.00000	0.00000	0.00000	0.00000	0.00000	0.00000	0.00000	0.00000	0.00000	0.00000	0.00000	0.00000	0.00000	0.00000	0.00000
1-Octadecene	C18H36	252	0.07448	0.06038	0.00000	0.00000	0.00000	0.00000	0.16586	0.00000	0.00000	0.00000	0.07583	0.00000	0.00000	0.00000	0.00000	0.00000	0.00000	0.00000	0.00000	0.00000	0.00000	0.00000	0.00000	0.00000	0.00000
Octadecane	C18H38	254	0.00000	0.00000	0.00000	0.10698	0.00000	0.05104	0.00000	0.00000	0.10399	0.27346	0.36578	0.00000	0.08556	0.00000	0.22625	0.32976	0.33664	0.28079	0.00000	0.00000	0.00000	0.11135	0.19384	0.00000	0.00000
Tetradecane, 1,1-dimethoxy-	C16H34O2	258	0.00000	0.00000	0.00000	0.00000	0.00000	0.00000	0.00000	0.00000	0.00000	0.00000	0.00000	0.00000	0.00000	0.00000	0.00000	0.00000	0.00000	0.00000	0.00000	0.11407	0.00000	0.00000	0.00000	0.00000	0.00000
Pentadecane, 2,6,10,14-tetramethyl-	C19H40	268	0.00000	0.00000	0.21260	0.27190	0.40513	0.14647	0.21760	0.17260	0.07326	0.53906	0.68670	0.54498	0.02154	0.14728	0.20761	0.23034	0.27188	0.23210	0.00000	0.00000	0.14801	0.00000	0.00000	0.00000	0.06887
Nonadecane	C19H40	268	0.08612	0.08271	0.10818	0.20015	0.29609	0.19421	0.07764	0.08177	0.09671	0.35358	0.45330	0.38349	0.07511	0.12464	0.30801	0.52038	0.43337	0.44035	0.04657	0.09411	0.20950	0.25947	0.15186	0.12403	0.00000
Hexadecane, 2,6,10-trimethyl-	C20H42	282	0.00000	0.00000	0.00000	0.00000	0.00000	0.00000	0.00000	0.00000	0.00000	0.00000	0.00000	0.00000	0.00000	0.00000	0.00000	0.00000	0.00000	0.00000	0.00000	0.00000	0.00000	0.00000	0.00000	0.00000	0.00000
Hexadecane, 2,6,10,14-tetramethyl-	C20H42	282	0.00000	0.00000	0.00000	0.00000	0.00000	0.00000	0.00000	0.00000	0.00000	0.24190	0.00000	0.30422	0.00000	0.00000	0.13471	0.21331	0.16650	0.16395	0.00000	0.00000	0.00000	0.00000	0.00000	0.00000	0.00000
Eicosane	C20H42	282	0.03712	0.05862	0.05646	0.15829	0.22670	0.16799	0.07388	0.05942	0.07454	0.28765	0.33742	0.23267	0.05855	0.11637	0.34751	0.65568	0.45523	0.39770	0.05915	0.12203	0.26873	0.23942	0.15973	0.13678	0.00000
Hexadecane, 1,1-dimethoxy-	C18H38O2	286	0.00000	0.00000	0.00000	0.00000	0.00000	0.00000	0.00000	0.00000	0.00000	0.00000	0.00000	0.00000	0.00000	0.00000	0.00000	0.00000	0.00000	0.00000	0.00000	0.00000	0.09181	0.00000	0.00000	0.00000	0.00000
Heptadecane, 2,6,10,14-tetramethyl-	C21H44	296	0.00000	0.00000	0.00000	0.00000	0.00000	0.00000	0.00000	0.10039	0.00000	0.00000	0.00000	0.00000	0.00000	0.00000	0.00000	0.00000	0.00000	0.00000	0.00000	0.00000	0.00000	0.00000	0.00000	0.00000	0.00000
Heneicosane	C21H44	296	0.04993	0.09923	0.09668	0.19944	0.22203	0.12283	0.00000	0.08655	0.06290	0.32128	0.37000	0.20223	0.09221	0.18211	0.38328	0.68148	0.46564	0.35807	0.09361	0.19208	0.34255	0.36223	0.23348	0.22124	0.00000
Docosane	C22H46	310	0.07347	0.07605	0.07143	0.18219	0.19184	0.10502	0.12953	0.06866	0.07739	0.31793	0.26272	0.18633	0.08471	0.15153	0.33756	0.54625	0.33114	0.29127	0.08836	0.16593	0.34235	0.33070	0.20053	0.15735	0.00000
Nonadecane, 2,6,10,14-tetramethyl-	C23H48	324	0.00000	0.00000	0.00000	0.00000	0.00000	0.00000	0.00000	0.00000	0.00000	0.00000	0.00000	0.00000	0.02180	0.00000	0.00000	0.00000	0.00000	0.00000	0.07115	0.00000	0.00000	0.00000	0.00000	0.00000	0.00000
Tricosane	C23H48	324	0.12913	0.10693	0.14825	0.20816	0.20726	0.15646	0.26630	0.10676	0.09621	0.32265	0.28063	0.21276	0.00000	0.10806	0.19177	0.39090	0.20859	0.15003	0.00000	0.15196	0.27286	0.22720	0.19206	0.13953	0.00000
Tricosane, 2-methyl-	C24H50	338	0.00000	0.00000	0.00000	0.00000	0.00000	0.00000	0.00000	0.00000	0.00000	0.00000	0.00000	0.00000	0.00000	0.00000	0.00000	0.00000	0.00000	0.00000	0.00000	0.00000	0.00000	0.00000	0.00000	0.00000	0.00000
Tetracosane	C24H50	338	0.00000	0.00000	0.00000	0.00000	0.00000	0.00000	0.85521	0.00000	0.00000	0.58390	0.00000	0.46792	0.00000	0.00000	0.36889	0.48318	0.34113	0.32859	0.00000	0.00000	0.00000	0.00000	0.00000	0.00000	0.00000
Heptadecane, 9-octyl-	C25H52	352	0.00000	0.00000	0.00000	0.00000	0.00000	0.00000	0.00000	0.00000	0.00000	0.00000	0.00000	0.00000	0.00000	0.11232	0.00000	0.00000	0.00000	0.00000	0.00000	0.00000	0.00000	0.00000	0.00000	0.00000	0.00000
Pentacosane	C25H52	352	0.21164	0.13908	0.19029	0.20257	0.15577	0.25167	0.70283	0.06630	0.08787	0.20051	0.19508	0.29279	0.07872	0.00000	0.15062	0.24186	0.13345	0.12154	0.07734	0.08213	0.26730	0.16797	0.08387	0.05784	0.00000
Docosane, 9-butyl-	C26H54	366	0.00000	0.00000	0.00000	0.00000	0.00000	0.00000	0.00000	0.00000	0.00000	0.00000	0.00000	0.00000	0.00000	0.00000	0.00000	0.00000	0.00000	0.00000	0.00000	0.00000	0.00000	0.00000	0.00000	0.00000	0.00000
Docosane, 11-butyl-	C26H54	366	0.00000	0.00000	0.00000	0.00000	0.00000	0.00000	0.00000	0.00000	0.00000	0.00000	0.00000	0.00000	0.00000	0.00000	0.00000	0.00000	0.00000	0.00000	0.00000	0.00000	0.00000	0.00000	0.00000	0.00000	0.00000
Hexacosane	C26H54	366	0.16908	0.01638	0.13785	0.11429	0.05875	0.29184	0.78587	0.04091	0.05643	0.18605	0.03916	0.28223	0.00000	0.02507	0.10395	0.18001	0.06704	0.00214	0.00000	0.02676	0.20393	0.11764	0.00000	0.00000	0.00000
Heptacosane	C27H56	380	0.12162	0.01070	0.09703	0.14399	0.00984	0.15879	0.65765	0.00000	0.00000	0.13987	0.06474	0.28028	0.00000	0.05552	0.00000	0.03367	0.00000	0.00000	0.00000	0.00000	0.05483	0.00528	0.00000	0.00000	0.00000
Octacosane	C28H58	394	0.10027	0.02888	0.07745	0.16378	0.00000	0.14185	0.40797	0.00000	0.00000	0.03702	0.00000	0.15947	0.00000	0.00000	0.00000	0.00000	0.00000	0.00000	0.00000	0.00000	0.00000	0.00000	0.00000	0.00000	0.00000
Nonacosane	C29H60	408	0.00000	0.00000	0.05542	0.09228	0.00000	0.03050	0.22149	0.00000	0.00000	0.00000	0.00000	0.00000	0.00000	0.00000	0.00000	0.00000	0.00000	0.00000	0.00000	0.00000	0.00000	0.00000	0.00000	0.00000	0.00000
2,6,10,14,18,22-Tetracosahexaene, 2,6,10,15,19,23-hexamethyl-, (all-E)-	C30H50	410	0.00000	0.00000	0.00000	0.00000	0.00000	0.00000	0.00000	0.00000	0.00000	0.00000	0.00000	0.00000	0.00000	0.00000	0.00000	0.00000	0.00000	0.00000	0.00000	0.00000	0.00000	0.00000	0.00000	0.00000	0.02315
Heneicosane, 11-decyl-	C31H64	436	0.00000	0.00000	0.00000	0.00000	0.00000	0.00000	0.02479	0.00000	0.00000	0.00000	0.00000	0.00000	0.00000	0.00000	0.00000	0.00000	0.00000	0.00000	0.00000	0.00000	0.00000	0.00000	0.00000	0.00000	0.00000

Driving modes	(µg/m ³)	Formula	M.W.	1800rpm/60%						3000rpm/60%						1800rpm/100%						3000rpm/100%					
				Size range of LPI (nm)						Size range of LPI (nm)						Size range of LPI (nm)						Size range of LPI (nm)					
				34-66	66-94	94-170	170-330	330-550	550-1000	34-66	66-94	94-170	170-330	330-550	550-1000	34-66	66-94	94-170	170-330	330-550	550-1000	34-66	66-94	94-170	170-330	330-550	550-1000
N containing compounds	Formula	M.W.	34-66	66-94	94-170	170-330	330-550	550-1000	34-66	66-94	94-170	170-330	330-550	550-1000	34-66	66-94	94-170	170-330	330-550	550-1000	34-66	66-94	94-170	170-330	330-550	550-1000	
Undecanone, 2-methyl oxime	C12H25NO	199	0.00000	0.00000	0.00000	0.00000	0.03936	0.00000	0.08902	0.00000	0.00000	0.00000	0.00000	0.00000	0.00000	0.00000	0.00000	0.00000	0.00000	0.00000	0.00000	0.00000	0.00000	0.00000	0.00000	0.00000	
Isoquinoline, 1-(2,2-dimethylpropyl)-	C14H17N	199	0.00000	0.00000	0.00000	0.00000	0.00000	0.00000	0.00000	0.00000	0.00000	0.00000	0.00000	0.00000	0.00000	0.00000	0.00000	0.00000	0.00000	0.00000	0.00000	0.00000	0.00000	0.00000	0.00000	0.00000	
Butanoic acid, 4-nitrophenyl ester	C10H11NO4	209	0.00000	0.00000	0.00000	0.00000	0.00000	0.00000	0.00000	0.00000	0.00000	0.00000	0.00000	0.00000	0.00000	0.00000	0.00000	0.00000	0.00000	0.00000	0.00000	0.00000	0.00000	0.00000	0.00000	0.00000	
2-Tridecanone, o-methylloxime	C14H29NO	227	0.00000	0.00000	0.00000	0.00000	0.00000	0.00000	0.00000	0.00000	0.00000	0.00000	0.00000	0.00000	0.00000	0.00000	0.00000	0.00000	0.00000	0.00000	0.00000	0.00000	0.00000	0.05616	0.00000	0.00000	
2-Nonadecanone, O-methylloxime	C20H41NO	311	0.00000	0.00000	0.00000	0.00000	0.00000	0.00000	0.00000	0.00000	0.00000	0.00000	0.00000	0.00000	0.00000	0.00000	0.00000	0.00000	0.00000	0.00000	0.00000	0.00000	0.00000	0.00000	0.00000	0.00000	
3-Methylisoquinoline	C10H9N	143	0.00000	0.00000	0.00000	0.00000	0.00000	0.00000	0.00000	0.00000	0.00000	0.00020	0.00000	0.00000	0.00000	0.00000	0.00000	0.00000	0.00000	0.00000	0.00000	0.00000	0.00000	0.00024	0.00000	0.00000	
7,8-Benzoquinoline	C13H9N	179	0.00094	0.00079	0.00087	0.00095	0.00061	0.00106	0.00094	0.00099	0.00078	0.00084	0.00079	0.00075	0.00080	0.00077	0.00117	0.00088	0.00085	0.00079	0.00092	0.00105	0.00109	0.00102	0.00105	0.00090	
Acridine	C13 H9N	179	0.00000	0.00000	0.00010	0.00000	0.00000	0.00000	0.00014	0.00000	0.00000	0.00000	0.00000	0.00000	0.00000	0.00000	0.00000	0.00000	0.00000	0.00011	0.00000	0.00011	0.00000	0.00020	0.00000	0.00011	
Phenanthridine	C13 H9N	179	0.00000	0.00008	0.00000	0.00000	0.00000	0.00000	0.00000	0.00022	0.00000	0.00000	0.00008	0.00000	0.00000	0.00000	0.00011	0.00015	0.00010	0.00009	0.00000	0.00008	0.00000	0.00029	0.00000	0.00019	
4-Nitrophenyl	C12 H9NO2	199	0.00000	0.00013	0.00000	0.00000	0.00000	0.00000	0.00000	0.00000	0.00000	0.00013	0.00000	0.00000	0.00000	0.00000	0.00000	0.00000	0.00000	0.00000	0.00000	0.00000	0.00016	0.00000	0.00000	0.00000	
9-Nitroanthracene	C14 H9NO2	223	0.00027	0.00000	0.00000	0.00047	0.00000	0.00000	0.00000	0.00000	0.00000	0.00000	0.00000	0.00000	0.00000	0.00030	0.00000	0.00046	0.00000	0.00050	0.00000	0.00029	0.00000	0.00000	0.00000	0.00000	
3-Nitrophenanthrene	C14 H9NO2	223	0.00037	0.00043	0.00000	0.00000	0.00000	0.00000	0.00000	0.00000	0.00038	0.00000	0.00039	0.00000	0.00000	0.00000	0.00043	0.00037	0.00000	0.00000	0.00038	0.00128	0.00094	0.00000	0.00000	0.00000	
7-Nitrobenz[a]anthracene	C18H11NO2	273	0.00035	0.00000	0.00037	0.00000	0.00000	0.00000	0.00000	0.00000	0.00000	0.00000	0.00039	0.00000	0.00000	0.00000	0.00000	0.00000	0.00000	0.00000	0.00000	0.00000	0.00000	0.00000	0.00000	0.00000	
6-Nitrochrysene	C18H11NO2	273	0.00000	0.00030	0.00000	0.00000	0.00000	0.00000	0.00000	0.00000	0.00000	0.00000	0.00000	0.00000	0.00000	0.00000	0.00039	0.00000	0.00000	0.00000	0.00000	0.00000	0.00000	0.00000	0.00000	0.00000	
Aromatic hydrocarbons	Formula	M.W.	34-66	66-94	94-170	170-330	330-550	550-1000	34-66	66-94	94-170	170-330	330-550	550-1000	34-66	66-94	94-170	170-330	330-550	550-1000	34-66	66-94	94-170	170-330	330-550	550-1000	
9H-Fluoren-9-one (Fluorenone)	C13H8O	180	0.00000	0.00000	0.00000	0.00000	0.00000	0.00000	0.00000	0.00000	0.00000	0.00000	0.00000	0.00000	0.00000	0.00000	0.00000	0.00000	0.00000	0.00000	0.00000	0.00375	0.00812	0.00806	0.00000	0.00328	
Naphthalene, decahydro-1,8a-dimethyl-7-(1-methylethyl)-, 1R-(1.alpha.,4a)	C15H28	208	0.00000	0.00000	0.00000	0.00000	0.00000	0.00000	0.00000	0.00000	0.00000	0.00000	0.00000	0.00000	0.00000	0.00000	0.00000	0.00000	0.00000	0.00000	0.00000	0.00000	0.00000	0.00000	0.00000	0.00584	
7,8-Diphenylbicyclo[4.2.1]nona-2,4,7-triene	C21H18	270	0.00000	0.00000	0.00000	0.00000	0.00000	0.00000	0.00000	0.00000	0.00000	0.00000	0.00000	0.00000	0.00000	0.00000	0.00000	0.00000	0.00000	0.00000	0.00000	0.00353	0.00000	0.00000	0.00000	0.00000	
Acenaphthylene	C12H8	152	0.00003	0.00009	0.00005	0.00007	0.00012	0.00007	0.00013	0.00009	0.00015	0.00005	0.00001	0.00004	0.00004	0.00000	0.00003	0.00000	0.00003	0.00004	0.00001	0.00006	0.00006	0.00008	0.00005	0.00007	
Acenaphthene	C12H10	154	0.00004	0.000235	0.000091	0.00234	0.00040	0.00046	0.00126	0.00167	0.00079	0.00073	0.00045	0.00070	0.00081	0.00075	0.00071	0.00025	0.00078	0.00093	0.00041	0.00049	0.00062	0.00064	0.00341	0.00063	
Fluorene	C13H10	166	0.00034	0.00060	0.00079	0.00038	0.00077	0.00003	0.00057	0.00087	0.00128	0.00081	0.00035	0.00083	0.00056	0.00063	0.00065	0.00008	0.00056	0.00075	0.00045	0.00082	0.00094	0.00106	0.00086	0.00077	
Phenanthrene	C14H10	178	0.00183	0.00251	0.00106	0.00399	0.00268	0.00193	0.00144	0.00201	0.00114	0.00220	0.00175	0.00285	0.00432	0.00433	0.01678	0.00375	0.01114	0.01505	0.00504	0.01533	0.03027	0.02695	0.01804	0.01830	
Anthracene	C14H10	178	0.00000	0.00000	0.00000	0.00000	0.00000	0.00000	0.00000	0.00000	0.00000	0.00000	0.00000	0.00000	0.00036	0.00000	0.00000	0.00000	0.00429	0.00000	0.00000	0.00000	0.01134	0.00000	0.00000		
Fluoranthene	C16H10	202	0.00016	0.00029	0.00029	0.00033	0.00023	0.00018	0.00000	0.00000	0.00000	0.00000	0.00000	0.00000	0.00000	0.00000	0.00000	0.00000	0.00000	0.00000	0.00000	0.00038	0.00021	0.00016	0.00025		
Pyrene	C16H10	202	0.00063	0.00109	0.00129	0.00099	0.00085	0.00041	0.00000	0.00000	0.00000	0.00000	0.00000	0.00000	0.00000	0.00000	0.00000	0.00000	0.00000	0.00000	0.00000	0.00046	0.00061	0.00049	0.00047		
Chrysene	C18H12	228	0.00000	0.00000	0.00000	0.00000	0.00000	0.00000	0.00000	0.00000	0.00000	0.00003	0.00000	0.00000	0.00000	0.00000	0.00000	0.00000	0.00000	0.00000	0.00000	0.00001	0.00003	0.00003	0.00008		
Benzo(a)anthracene	C18H12	228	0.00071	0.00107	0.00094	0.00124	0.00109	0.00106	0.00000	0.00000	0.00000	0.00000	0.00000	0.00000	0.00000	0.00000	0.00000	0.00000	0.00000	0.00000	0.00000	0.00000	0.00000	0.00000	0.00000	0.00000	
Benzo(b)fluoranthene	C20H12	252	0.00003	0.00006	0.00006	0.00004	0.00002	0.00001	0.00151	0.00011	0.00006	0.00031	0.00011	0.00061	0.00017	0.00016	0.00019	0.00008	0.00007	0.00016	0.00011	0.00021	0.00034	0.00023	0.00012	0.00023	
Benzo(k)fluoranthene	C20H12	252	0.00002	0.00005	0.00006	0.00012	0.00009	0.00006	0.00000	0.00004	0.00000	0.00013	0.00005	0.00006	0.00001	0.00000	0.00004	0.00000	0.00002	0.00007	0.00001	0.00002	0.00005	0.00005	0.00003	0.00005	
Benzo(a)pyrene	C20H12	252	0.00002	0.00009	0.00007	0.00019	0.00011	0.00006	0.00105	0.00000	0.00004	0.00022	0.00008	0.00049	0.00011	0.00015	0.00015	0.00003	0.00008	0.00015	0.00006	0.00016	0.00028	0.00018	0.00015	0.00004	
S containing compounds	Formula	M.W.	34-66	66-94	94-170	170-330	330-550	550-1000	34-66	66-94	94-170	170-330	330-550	550-1000	34-66	66-94	94-170	170-330	330-550	550-1000	34-66	66-94	94-170	170-330	330-550	550-1000	
3-Methyl-1-(phenylthio) Butan-2-one	C11H14OS	194	0.00000	0.00000	0.00000	0.00000	0.00000	0.00000	0.00000	0.00000	0.00000	0.00000	0.00000	0.00000	0.14123	0.00000	0.00000	0.00000	0.00000	0.00000	0.00000	0.00000	0.00000	0.00000	0.00000	0.00000	
Butyric acid, thio-, S-decyl ester	C14H28OS	244	0.00000	0.00000	0.00000	0.00000	0.00000	0.00000	0.00000	0.00000	0.00000	0.00000	0.00000	0.00000	0.00000	0.00000	0.02642	0.04302	0.07369	0.0364							

APPENDIX G

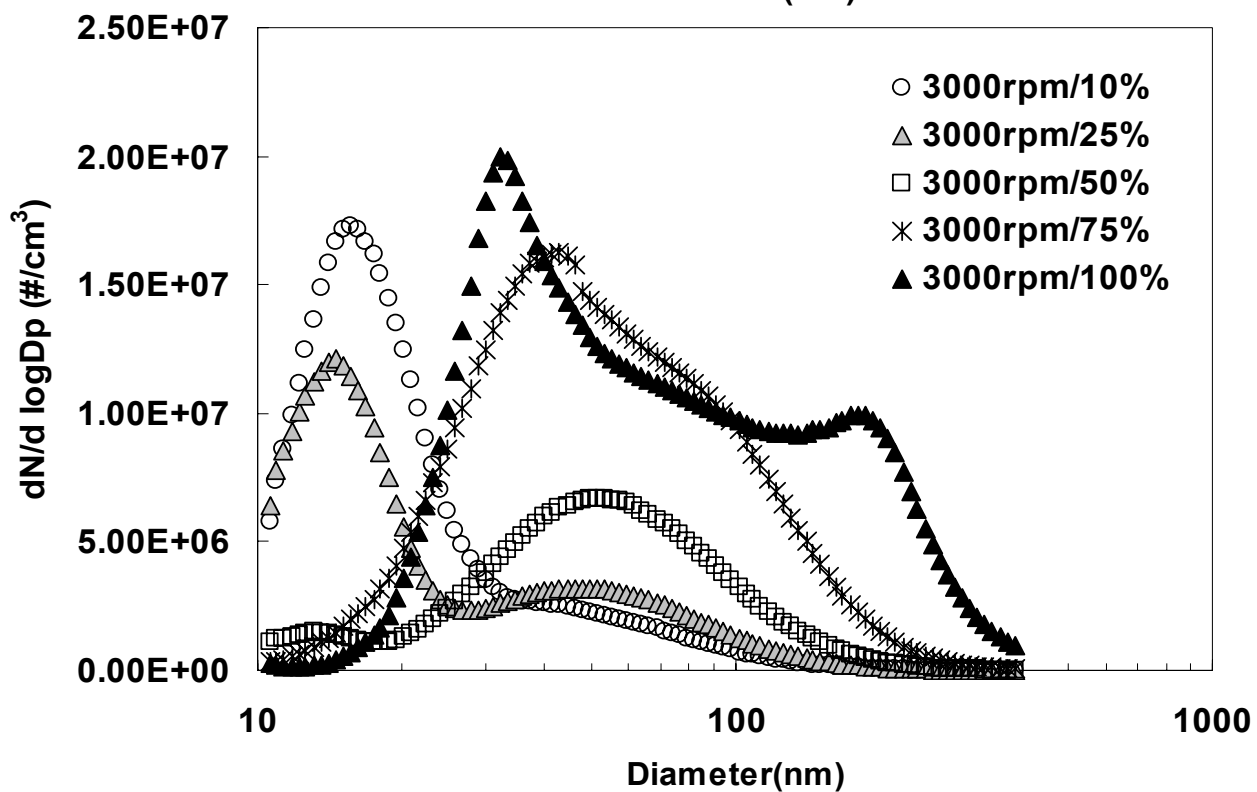
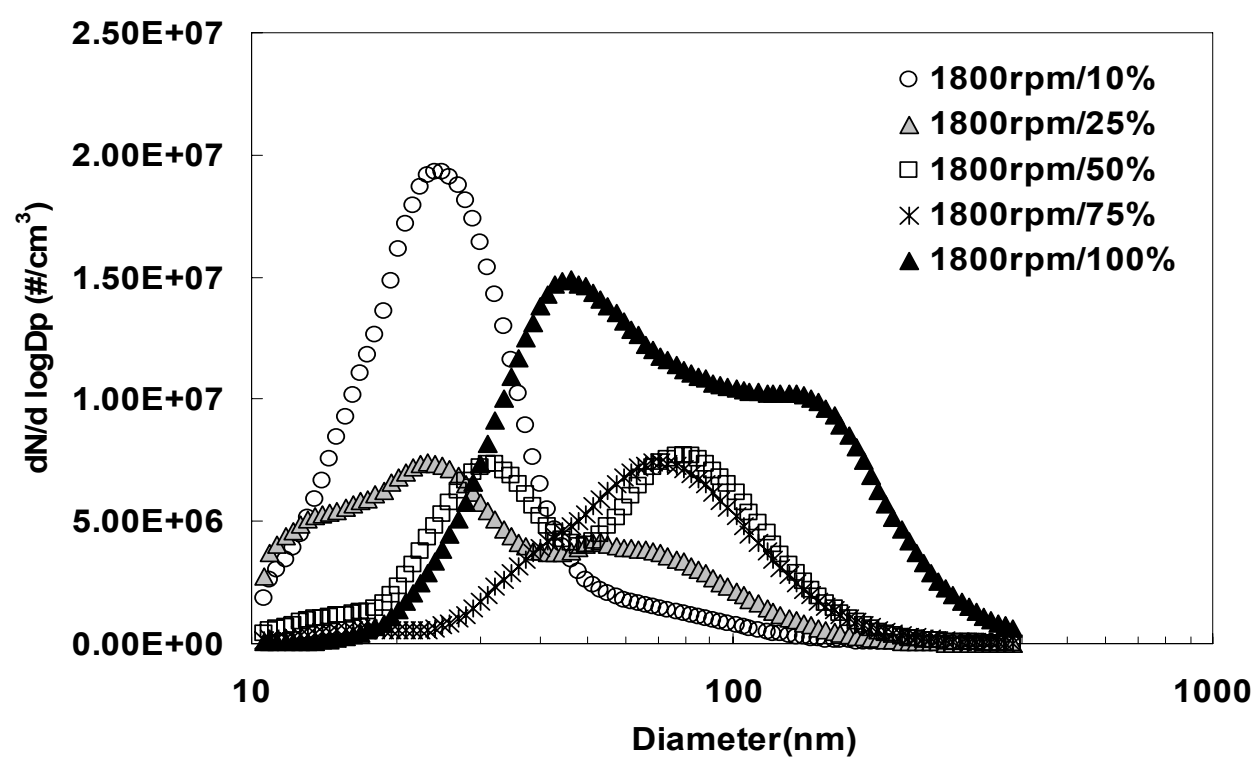


Fig.G. Size distribution for non-idling conditions of 13-mode.